APOLLO

Final Report

ER 12017 JUNE 1961

Aerodynamics

MARTIN

Apollo: Aerodynamics ----------Doc 1 of 1-
19740073600 N (74N71539)
Unclassified (Unrestricted - Publicly Available)

TI: Apollo: Aerodynamics [Final Report]
RN: NASA-CR-136719/ER-12017
CN: NAS5-303
DT: Technical Report
LA: English
OS: Martin Co. (Baltimore, MD, United States)
FS: NASA (United States) [NASA]
PB: United States
PD: Jun 01, 1961
AV: Hardcopy - A05 CASI A05 (78p)
AVNT: Unavail. Microfiche
AVSUP: Administrative -
SC: 34 (GENERAL)
CTMJ: AERODYNAMIC CONFIGURATIONS/APOLLO PROJECT/SPACECRAFT REENTRY
CTMN: AERODYNAMIC STABILITY/HYPERSONIC REENTRY
----------Line 1:18 of 19-
CTRL-E Explain/Help CTRL-F First Menu CTRL-P Previous Screen ENTER Pick
NXT-REC DN-PAGE OUTPUT FORMAT
PRV-REC UP-PAGE REQUEST-DOC
Move to the NEXT RECORD within the current search set.

N-97856

CLASSIFICATION CHANGE

TO UNCLASSIFIED
By Authority of per CASI printout + E.O. 11652
Changed by DKM Date 8/03

FOR REFERENCE

NOT TO BE TAKEN FROM THIS ROOM

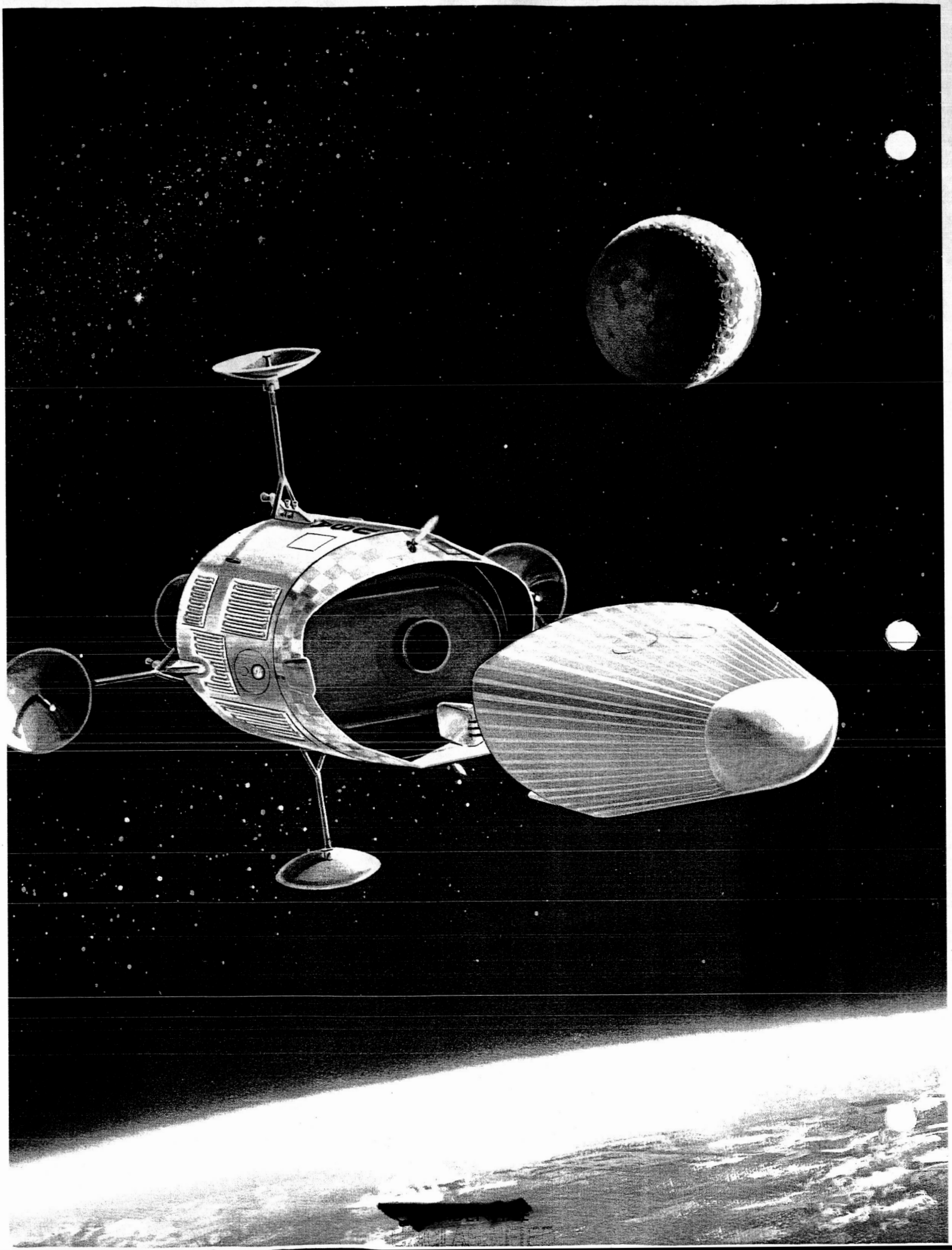

APOLLO

Final Report

Submitted to: NASA Space Task Group.
Contract NAS 5-303, Exhibit A, Item 1.2

Aerodynamics

ER 12017 JUNE 1961

MARTIN

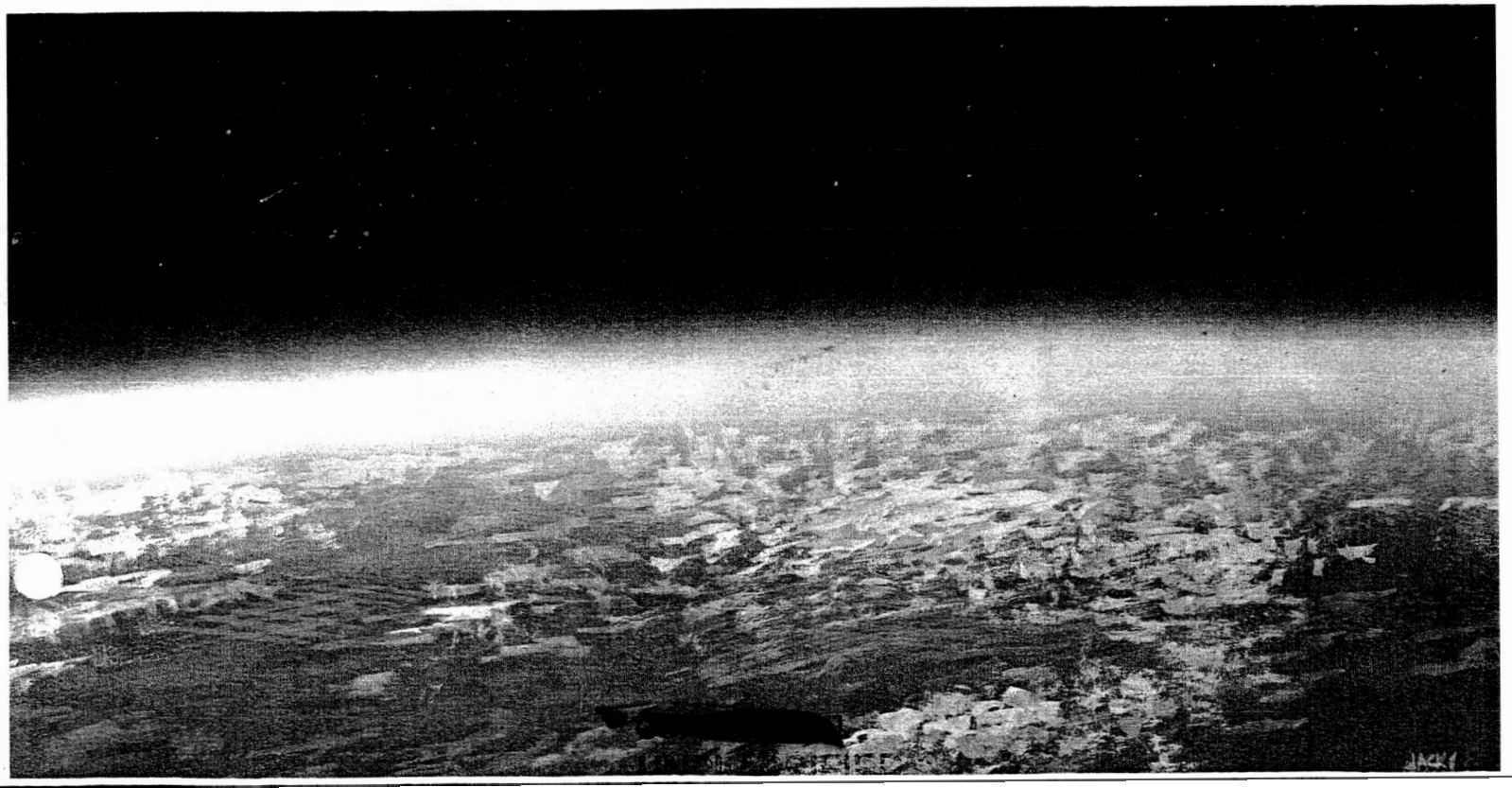

MODEL 410 — THE SYSTEM AND ITS OPERATION

*A BRIEF DESCRIPTION**

Model 410 is the spacecraft system recommended by Martin for the Apollo mission. Its design satisfies the guidelines stated in NASA RFP–302, as well as a more detailed set of guidelines developed by Martin during the Apollo design feasibility study.

We conceive the ultimate Apollo mission to be a manned journey to the lunar surface, arrived at by the preliminary steps of earth orbit, circumlunar and lunar orbit flights. Operational procedures proved out in the early steps will be carried over into the advanced steps, thus establishing a high level of confidence in the success of the lunar flights. With the recommended system, manned lunar orbit missions can be made as early as 1966.

Operational Features

For a circumlunar flight when the moon is at its most southerly declination (Fig. p–1) the launch operation proceeds southeast from Cape Canaveral and down the Atlantic Missile Range. The Saturn C–2 third stage shuts down when orbital velocity is reached at an altitude of 650,000 feet. What follows is a coasting orbit passing over the southern tip of Africa, the Indian Ocean and up the Pacific Missile Range. In this interval the crew checks out all onboard equipment, which has just passed through the accelerations, noise and vibration of the boost phase. If the pilot-commander is satisfied that all systems are working properly, the third stage is restarted and the spacecraft is injected at parabolic velocity northwest of Hawaii. If the pilot-commander is dissatisfied with the condition of the vehicle or crew, he separates from the Saturn S–IV, starts the mission abort engine, re-enters at the point shown in Fig. p–1 and lands at Edwards AFB.

Continuing translunar flight from the point of injection, the trajectory trace swings down over the Caribbean and then west over South America. This particular trajectory passes within 240 naut mi of the moon, then turns back for a direct re-entry some six days after launch. Re-entry occurs southwest of Hawaii some 3300 naut mi from the Edwards AFB landing site.

Tracking. The range coverage provided by present and planned facilities is shown in Fig. p–1 for this trajectory and for a second return trace representing the case when the moon is at the most northerly declination. This second trajectory establishes the 10000-naut mi re-entry range requirement for Apollo to meet the guidelines of operation on every day of the lunar month and of operation into a single landing site.

*For more complete descriptions, see ER 12000 or ER 12001.

Abort. During the critical launch and checkout phase, abort will be possible at any time : at the crew's discretion, automatically or by ground command. Up to nine minutes after launch (from Canaveral), the abort landing is restricted to the AMR for a circumlunar flight. Beyond this point the pilot has the option of continuing to any point along the AMR, PMR or into Edwards AFB through the use of the mission abort propulsion system and the inherent downrange maneuverability of the Model–410.

The Selected Spacecraft

The Apollo space vehicle (Model 410 spacecraft plus launching vehicle) is shown in Fig. p–2. The spacecraft—that portion of the space vehicle which makes the flight to the moon—consists of these three modules:

(1) Command module, housing the three crew members during all thrusting periods, e.g., launch from earth, any corrections to the flight path during flight in space, during re-entry and, ultimately, during landing and launch from the moon. It is the operating center from which all control of the flight is made.

(2) Propulsion and equipment module, containing all the propulsion units which operate between the point of final booster separation and re-entry after the lunar flight. It is separated from the command module at 200 naut mi from the earth on the return trip. It is designed with tankage for lunar takeoff and will be offloaded for less ambitious missions.

(3) Mission module—contained within the outer frame of the propulsion and equipment module—providing space during the lunar voyage for scientific observations and crew living functions.

Command Module

With its lifting capability, the Apollo command module represents a step forward in technology over ballistic vehicles, Mercury and (to the best of our knowledge the *Boctók* (*Vostok*). The lift results from the capsule's shape—a blunted cone flattened on the top (see Fig. p–3).

Heating and radiation protection. The Model 410 is shaped conservatively for aerodynamic heating in addition to its relatively high L/D (0.77). By accepting the large convective heat load of a nose radius smaller than that of the Mercury type, the Model 410 shape tends to minimize radiative heat transfer which is less well understood and harder to protect against. The thermal protection system provides excellent protection for the crew from the large aerodynamic heat loads, from space radiation (including solar flares) and from meteorites.

The normal mission radiation dose will not exceed the five rem limit defined by NASA. If the crew should encounter a solar event as severe as that following the May 10, 1959 flare, they would receive a dose of only 67 rem—well within the 100 rem dose limit set by Martin as tolerable during an emergency.

Thermal protection for re-entry is provided by a composite shield of deep charring ablator (nylon phenolic) bonded to superalloy honeycomb panels which are set off and insulated from the water-cooled pressure shell. The control flaps are protected from the high initial heat rate by an ablator bonded directly to the flap. The long-time, lower heating rates are handled by re-radiation from the backside. The aft bulkhead is protected by a fiberglas phenolic honeycomb panel with a foamed polyurethane insulation.

Crew provisions. The crew has access to all electronic and electrical equipment in the command module for maintenance and replacement. Both pilots have two-axis sidestick and foot controllers as well as a manual guidance mode used with the computers inoperative for deep space and re-entry operations.

Cabin pressure is maintained at the equivalent of 5000 feet altitude ("shirt sleeve" environment). Protective suiting is donned only for launching and landing, but need not be inflated except in emergency.

Guidance. The guidance system consists of both automatic and manual star tracking equipment, as well as two inertial platforms and two general purpose digital computers. Two windows, with ablative heat shield covers, are provided for use with tracking instruments.

Flight control. Pitch and yaw attitude control within the atmosphere is provided by flaps driven by hot gas servos. Outside the atmosphere dual reaction controls are used. Roll is controlled at all times by a dual reaction system.

Communications. Communications equipment includes a K_u band for re-entry, a C-band for the pre-reentry and both HF and VHF rescue beacons for landing and recovery.

Landing system. The landing system consists of a steerable parachute, retrorocket combination, enabling the M–410 to avoid local obstacles, trim out wind drift and reduce sinking speed to a nominal three feet per second—low enough for safe landing on any kind of terrain or in very rough seas. In the event of retrorocket failure, accelerations on the crew will not exceed 20 G.

Launch escape propulsion system (LEPS). LEPS is a thrust-vector-controlled, solid rocket system which separates the command module from the rest of the space vehicle in the event of an emergency during launch pad operations or during boost through the atmosphere. In an off-the-pad abort, it lifts the command module to an altitude of more than 4000 feet. During a normal boost trajectory, LEPS is jettisoned at 300,000 feet.

Propulsion and Equipment Module

The propulsion and equipment module (shown in Fig. p–3) contains propulsion devices and equipment which are not necessary for re-entry. Its outer skin serves both as a load carrying structure and as a meteorite shield for the propellant tanks, mission module and other equipment.

Propulsion devices. The mission engine, used for trajectory correction and abort, is a high preformance, modified LR–115 (Pratt & Whitney), developing 15,600 pounds of thrust. A total of 10,450 pounds of liquid hydrogen and liquid oxygen propellants may be carried, sufficient for lunar takeoff.

Four vernier engines, with 300 pounds of thrust each, are used for midcourse correction, ullage impulse to settle the mission engine propellants and for thrust vector control during operation of the mission engine. In addition there are two sets of six control jets which provide 30 pounds of thrust for roll, pitch and yaw control.

Power sources. Spacecraft equipment is powered by fuel cells (2 kw) which under normal conditions, use the boiloff from the mission propulsion system. A supply of independent reactants is provided for emergencies. Battery power is used during re-entry.

Communications. Four large antennas fold out to provide S-band communications and X-band radar altimeter information. VHF communications gear is also provided.

Mission Module

The mission module provides 400 cubic feet of living space during the lunar voyage. It serves as a midcourse work-rest area, providing freedom of movement and privacy. For operations on the lunar surface it will be a base of scientific investigations, and will serve as an airlock. The same "shirt sleeve" environment at 12.2 psi is maintained as in the command module.

The mission module provides the space and flexibility required for effective lunar reconnaissance and scientific experimentation. An Eastman-Kodak camera-telescope has been selected, for example, which has one-meter resolution at lunar orbit altitude of 50 naut mi.

MODEL 410 WEIGHT SUMMARY

Mission	Circumlunar	Lunar Orbit	Lunar Takeoff
Command Module	6954	6954	6954
Propulsion and Equipment Module	7372	13,192	15,618
Launch Escape Propulsion System	185	185	0
Adapter	489	489	0
Effective Launch Weight	15,000	20,820	22,572

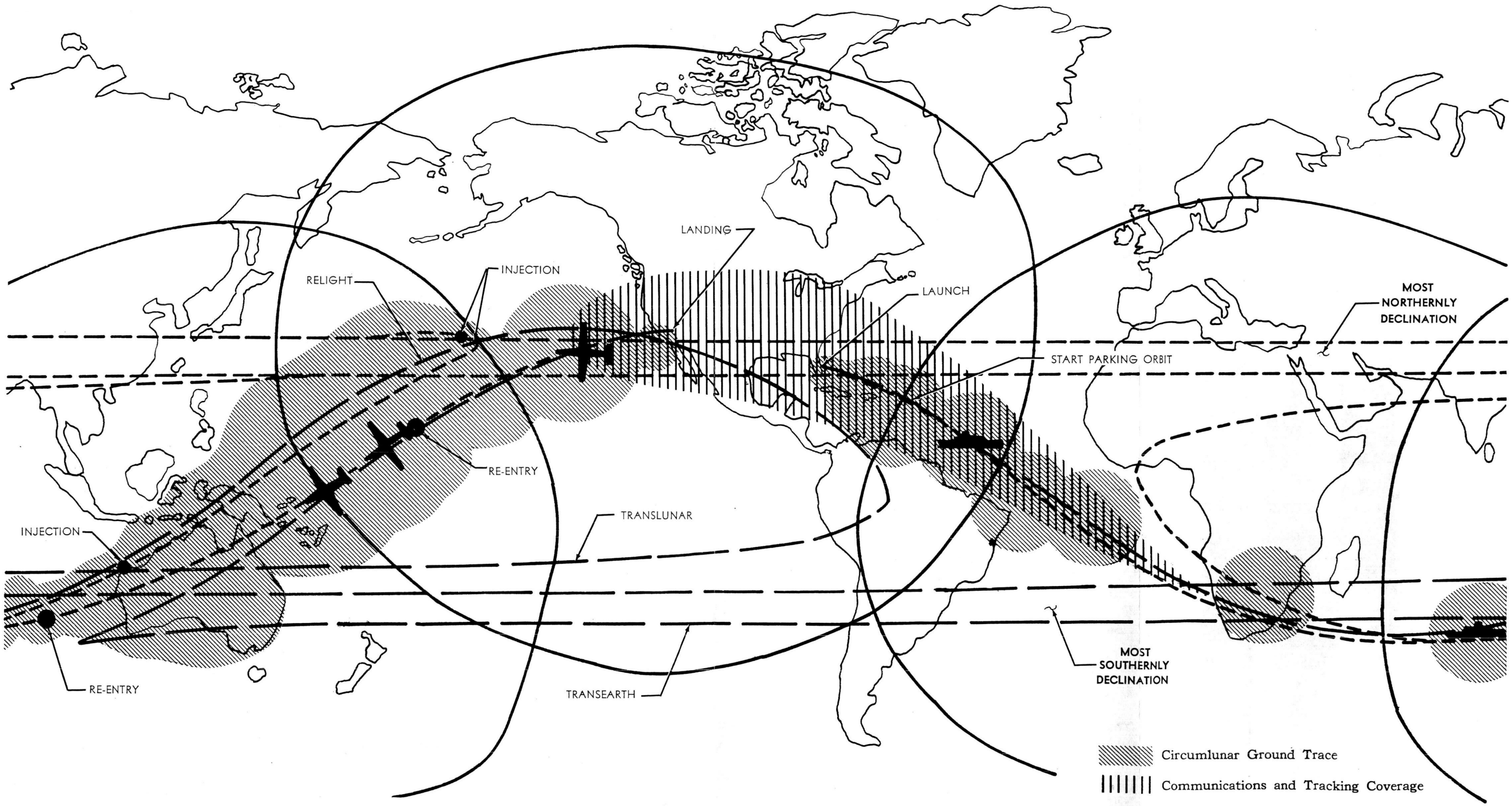

Fig. p–1 Model 410 Circumlunar Trajectory and Range Coverage

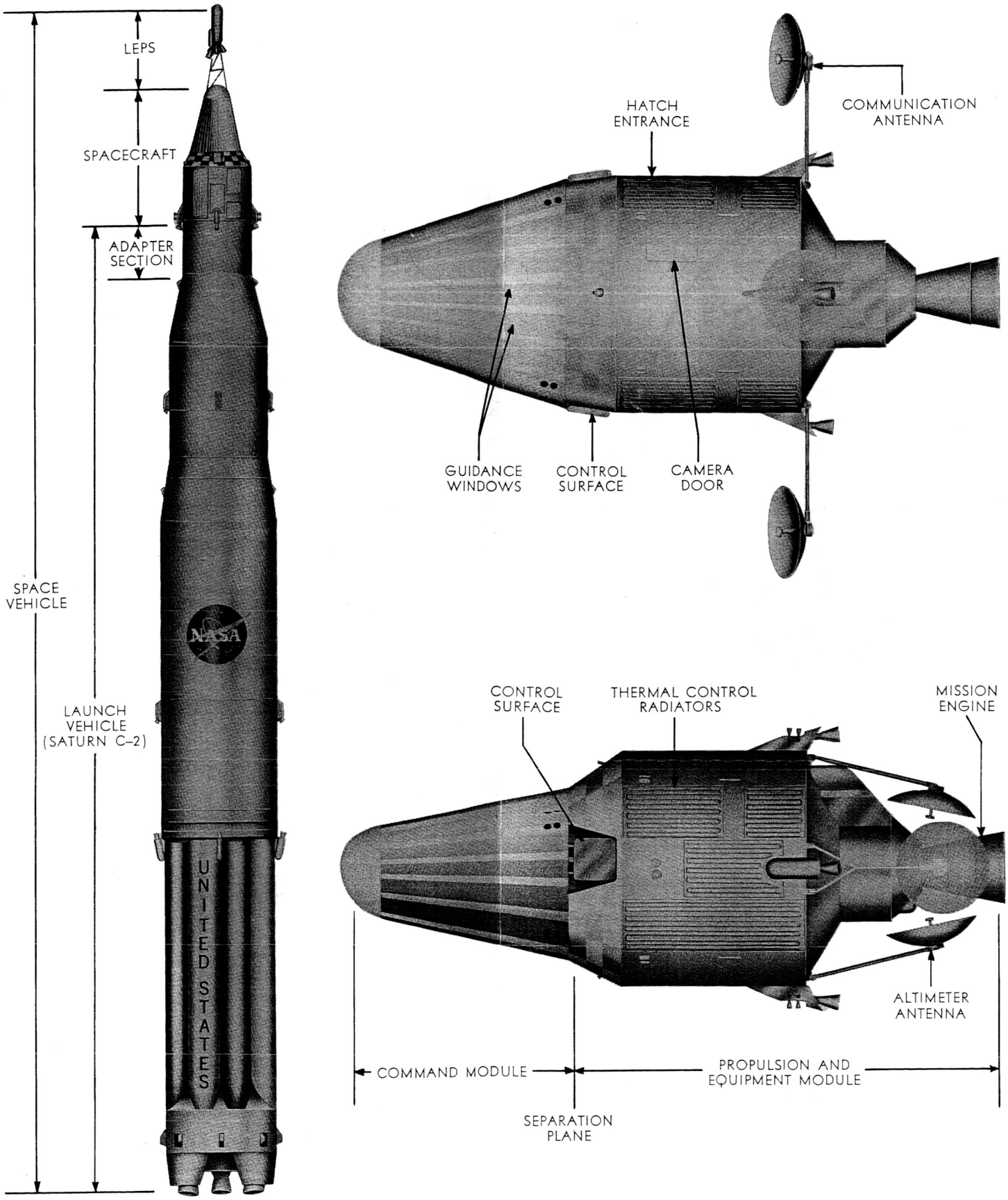

Fig. p-2. Model 410 Apollo Space Vehicle

#1

MISSION	EFFECTIVE GROSS WEIGHT (lb)	PROPULSION ΔV CAPABILITY (fps)	
		MISSION	VERNIER
CIRCUMLUNAR	15000	1830	525
LUNAR ORBIT	20820	6100	525
LUNAR TAKEOFF	22572	8600	200

VOLUMES (cu ft)	
COMMAND MODULE	350
MISSION MODULE	400
MISSION H_2 TANK	400
MISSION O_2 TANK	122

PROPULSION SYSTEM DATA

PURPOSE	TYPE	ISP. (sec)	THRUST (lb)
MISSION (1)	H_2—O_2 (ADV. LR115)	427	15600
VERNIER (4)	N_2H_4/UDMH–N_2O_4	315	300 EACH
ATTITUDE CONTROL (14+BACKUP)	N_2H_4/UDMH–N_2O_4	250–315	15 TO 50

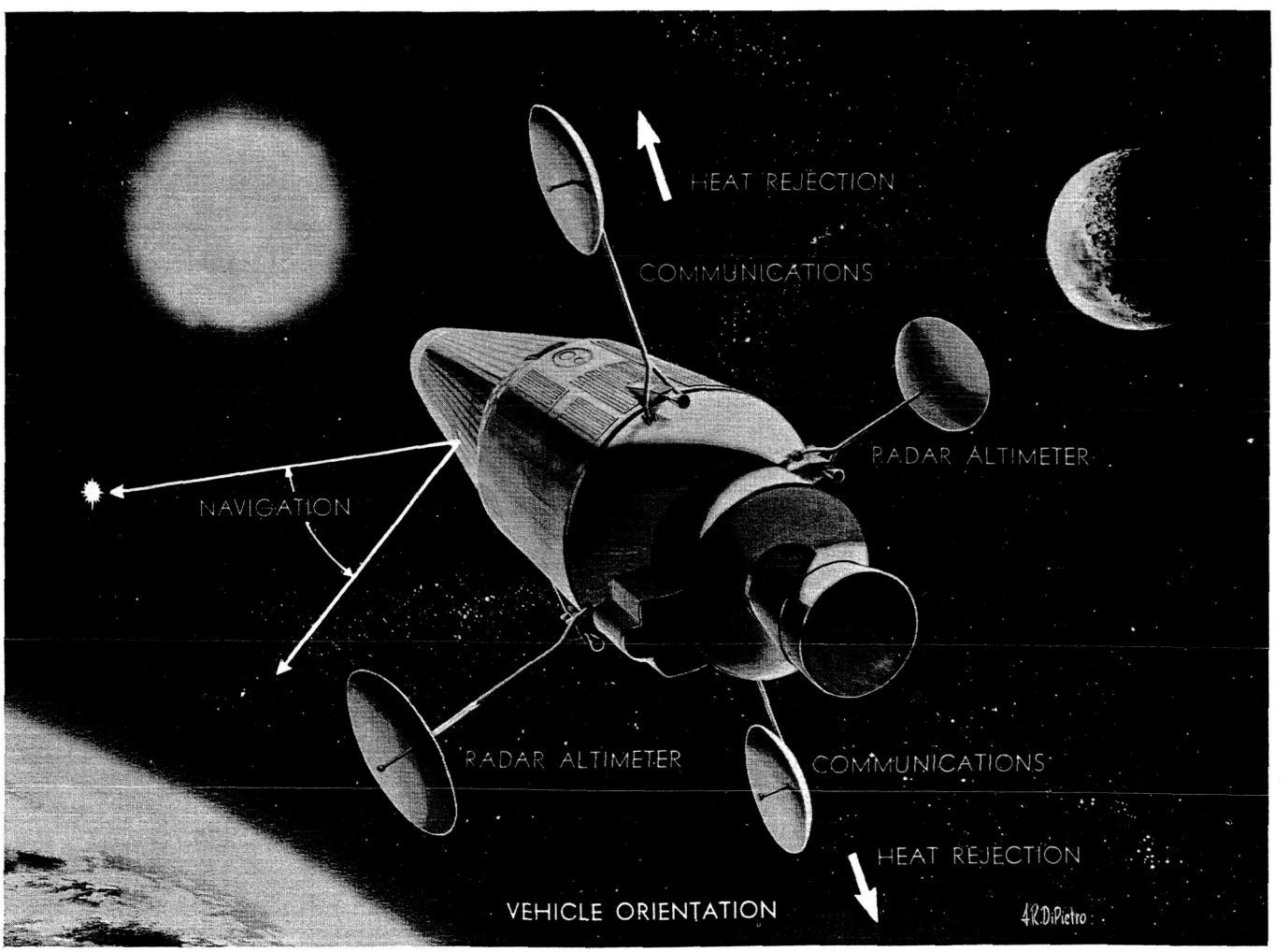

P-6 #2

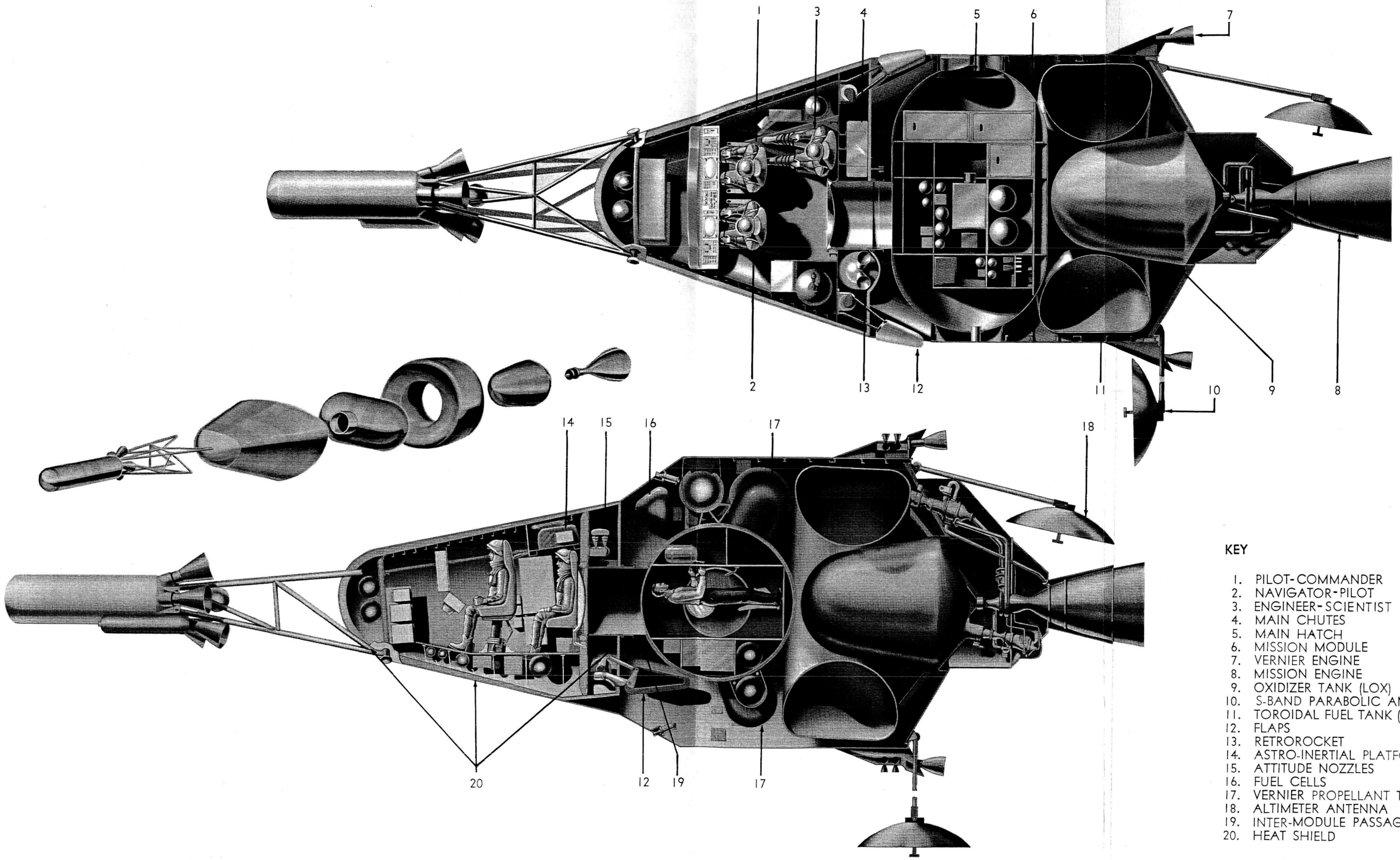

KEY

1. PILOT-COMMANDER
2. NAVIGATOR-PILOT
3. ENGINEER-SCIENTIST
4. MAIN CHUTES
5. MAIN HATCH
6. MISSION MODULE
7. VERNIER ENGINE
8. MISSION ENGINE
9. OXIDIZER TANK (LOX)
10. S-BAND PARABOLIC ANTENNA
11. TOROIDAL FUEL TANK (LH)
12. FLAPS
13. RETROROCKET
14. ASTRO-INERTIAL PLATFORM
15. ATTITUDE NOZZLES
16. FUEL CELLS
17. VERNIER PROPELLANT TANK
18. ALTIMETER ANTENNA
19. INTER-MODULE PASSAGE
20. HEAT SHIELD

Fig. p-3. Model 410 Apollo Inboard Profile

CONTENTS

CONTENTS

SUMMARY

Aerodynamic force and moment data have been developed for evaluation of various Apollo re-entry vehicles. This data, coupled with substantial NASA test data, has been used for comparative studies of the performance, heating and control of the Model 410, W-1, L-2-C and Mercury configurations and for generating design concepts and system requirements. Aerodynamic characteristics for normal re-entry and emergency abort conditions were derived from test data for similar configurations to estimate adequacy of analysis methods.

Estimates of moments and flap effectiveness were based on Newtonian analysis, with consideration of pertinent test results. Location of cg sensitivity of static stability to cg travel, and flap area requirements were discussed on the basis of those estimates. Reaction control requirements were also discussed briefly.

Re-entry dynamic stability of the Model 410 and Mercury type vehicles without controls was compared to indicate the relative merits of aerodynamic characteristics in damping oscillations and reducing angular accelerations.

Some aerodynamic effects not included in the analysis have been mentioned, with reference to future requirements for analysis and test data.

I. INTRODUCTION

Various aerodynamic characteristics of re-entry vehicles have been developed during the present study phase of the Apollo. These were required to evaluate performance characteristics of various configurations and to provide bases for various system and subsystem design requirements.

Hypersonic aerodynamic data necessary for re-entry performance, heating and control evaluation were obtained using Newtonian approximations and relevant test data. Transonic and subsonic data used for launch abort studies were obtained by methods developed in conjunction with Mercury data. A large amount of useful test data has been provided by NASA in formal reports and preliminary test data.

This report presents aerodynamic data for the Model 410, W-1, L-2-C and Mercury type (referred to herein as STG for brevity) configurations studies for the Apollo mission. This preliminary data, though useful for evaluation of configurations and during early design phases, will require verification and development through detailed test and analysis programs. Aerodynamic data curves for the M-1 configuration, which was included in the studies, have been presented and discussed in formal NASA publications and, therefore, are not contained in this report.

Static stability and control during re-entry are discussed, and estimates of cg locations, flap sizes, and reaction control requirements are made. The re-entry dynamic stability of two configurations without controls is also discussed. Aerodynamic data for emergency escape configurations are included.

Coefficients are referenced to the maximum cross-sectional area ($\pi\ d^2\ max/4$) and length of each vehicle, unless otherwise noted.

Aerodynamic heating analyses are presented in the Aerodynamic Heating Report, ER 12006. Characteristics of the parachute landing system appear in the Mechanical System Report, ER 12005. Dynamic control is discussed in the Guidance and Control Report, ER 12007.

II. METHODS

Hypersonic force and moment estimates for various configurations considered in this program have been obtained with the aid of Newtonian impact theory. Various comparisons with experimental data (Refs. 1 through 5) indicate the usefulness (and certain deficiencies) of the Newtonian method for preliminary design. Further comparisons have been made during this program, using unpublished test data from NASA-Langley, to confirm the adequacy of the impact theory for present body shapes and estimates of flap effectiveness at supersonic speeds.

The hypersonic data are presented here generally for a Newtonian stagnation-point pressure-coefficient of 2. This coefficient actually varies with Mach number and altitude for a dissociated gas, varying between 1.77 and 1.94 based on equilibrium real-gas properties during a typical re-entry. These differences, between the assumed and actual values, however, should have little effect on evaluating design concepts for the various configurations. The choice of coefficient affects the level of forces and moments; however, ratios, as lift to drag, and static trim angles remain unchanged, according to these Newtonian methods.

At hypersonic Mach numbers, where Newtonian calculations are considered to be most applicable, there remain many aerodynamic phenomena which cannot be accounted for in a Newtonian flow analysis. One of the limitations of Newtonian calculations on a blunt body is that when the local angle between a station on the afterbody and the free stream is small or negative, the Newtonian-predicted pressures may be too low. The higher pressures on the afterbody are induced by the nose (Refs. 2, 3 and 4) and can be calculated approximately for cylindrical afterbodies by blast-wave theory. The method described in Ref. 2, which essentially extends the range of applicability of blast-wave theory, yields rough predictions of pressure on slender axisymmetric afterbodies. The parameters which appear in Ref. 2 could probably be used to correlate the pressures on afterbodies much as the blast-wave parameter has been used to correlate data on cylindrical afterbodies (Ref. 3). Also, the real gas method of characteristic digital programs for axisymmetric bodies can be used to compute the bluntness-induced pressures on an approximately equivalent asymmetric body. However, induced pressure effects should be small on the windward side of the vehicles under consideration, since they fly at large angles-of-attack (Ref.).

For flight in the altitude range between about 150,000 and 250,000 ft (Fig. 3 of the Aerodynamic Heating Report) the inviscid flow in the

shock layer will be of a non-equilibrium or frozen nature. This occurs because the characteristic recombination reaction times for the dissociated and ionized gas are greater than the characteristic time for flow about the body. At some point on the body, then, the flow becomes of a non-equilibrium nature and, as it travels further along the body it freezes. Once the flow is frozen, it may be analyzed as a combination of perfect gases. Results for a sonic wedge-plate (Ref. 18) for equilibrium and frozen expansion about the corner, show that the frozen flow pressure may be an order of magnitude lower than the value computed assuming equilibrium dissociated flow. This is probably the largest possible size of the effect, and, again, it should be much less on the windward side of a vehicle at large angles-of-attack.

At very high altitudes, such effects as free molecule flow and shock-boundary layer interactions (Ref. 19) would also influence the pressures on the body. However, the vehicle does not maneuver much aerodynamically in these flight regimes so, for preliminary analyses, it has been assumed that these effects are negligible.

A suggested approach for evaluating flap effectiveness has been to compute the local flow around the body by the method of characteristics. An appropriate symmetrical representation of the body would be used, accounting for boundary-layer displacement and, if possible, non-equilibrium effects. This flow field would provide upstream conditions for determining the approximate pressures on the flap at various deflection angles. A procedure, used at NASA-Ames, computes the local impact pressures of stream tubes originating near the nose to correlate pitching-moment data. This "multilayer" approach to the inviscid solution might also be employed in conjunction with appropriate test data for evaluating flap pressures. All the real effects mentioned above will alter somewhat the present estimates of aerodynamic characteristics, but they should not greatly affect the general design evaluation and concepts. They will be evaluated using advanced analytic and testing techniques for the final design requirements.

The data presented herein are computed without corrections for friction drag. For a typical Model 410 re-entry trajectory, friction drag was estimated to be less than 3% of the total drag at altitudes below 400,000 ft and at zero angle of attack. At angles of attack near 35 deg, however, the friction drag may be 10 to 15 times larger (Ref. 7). The effect of these increments on the trajectory is small because the dynamic pressure and, therefore, the drag force is small. The maximum deceleration increments are of the order of 0.2 g acting for periods of about a minute during the rapid descent to 200,000 ft. The friction drag, therefore, does not affect L/D ratios important to evaluation trajectory calculations, although it must be included for actual

design trajectories. Where significant, base drag has been included in the data for the lower range of Mach numbers.

Subsonic data have been computed using semi-empirical methods developed from test data. The general background of these subsonic calculations is presented in the Appendix.

III. RE-ENTRY FORCE DATA

Outline sketches of various configurations recently evaluated during the study are presented in Fig. 1. Some reference axes are also indicated.

Force data for the Model 410 are presented in Fig. 2 through 4, as are the corresponding estimated data for W-1, L-2-C and STG configurations. Lift and drag coefficient variations with Mach number, derived for use in emergency abort studies, are presented in Chapter VI. Force data C_{Y_β} for the L-2-C configuration appear in Chapter IV.

A comparison of hypersonic characteristics pertinent to performance evaluation is tabulated below. The M-1 vehicle data (Ref. 1) is included in Fig. 1 and in Table 1.

The asymmetric vehicles (Model 410 and W-1) normally have angles of attack between $C_{L_{max}}$ and $(L/D)_{max.}$ For the Model 410 vehicle, the L/D ratio can be varied from 0.6 to 0.8 as the lift coefficient is modulated between 0.43 and 0.32 to obtain acceleration and heating control. The symmetric vehicles (L-2-C and STG) normally have high angles of attack in which the L/D ratio ranges between 0.2 and 0.6, and the lift is modulated between the same values. The Model 410, W-1 and L-2-C configurations obtain attitude control with flaps, while the STG configuration is trimmed solely by cg offset, and lift vector control is achieved by rolling with reaction jets.

For the L-2-C and STG vehicles, C_{L_α} is negative. This characteristic will later be indicated as having an adverse effect on dynamic stability. These vehicles also have less capability to change the resultant acceleration with lift modulation (Fig. 4), because of large resultant re-entry forces, primarily drag, which cannot be changed much by altering the angle of attack. The resultant force for L-2-C is only 34% greater at α = 90 deg than at α = 50 deg, while the Model 410 has a resultant force 62% greater at $C_{L_{max}}$ than at L/D_{max}, and 240% greater than at $C_L = 0$.

Also, the symmetric vehicles have a smaller flight corridor and maneuverable range because of these aerodynamic characteristics. Since they operate on the high drag side of the lift-drag curve, vehicles of the L-2-C type cannot use lift modulation for reducing maximum g forces. Modulating from $C_{L_{max}}$ toward $C_{D_{max}}$ increases the force vector, and therefore modulation should begin at $C_L <$

TABLE 1

Comparison of Hypersonic Aerodynamics

		Model 410	W-1	M-1	L-2-C	STG (Mercury)
$C_{L_{max}}$	α (deg.)	30	48	17	52	60
	C_L	0.43	0.58	0.36	0.52	0.46
	C_D	0.73	1.16	0.75	0.95	0.92
	L/D	0.58	0.50	0.48	0.55	0.48
	W/C_{D_A}	70	51	67	48	44
	W/C_{L_A}	121	102	139	87	92
$(L/D_{max}$	α (deg.)	13	26	8	52*	60*
	C_L	0.32	0.41	0.32	0.52	0.46
	C_D	0.42	0.51	0.59	0.95	0.92
	L/D	0.77	0.80	0.54	0.58	0.48
	W/C_{D_A}	122	117	85	48	44
	W/C_{L_A}	158	146	156	87	92
	S_{ref} (ft^2)	117	101	150	129.5	154
	W/A (psf)	51	59	50	46	40

Coefficients are referenced to $A = S_{ref}$ where $S_{ref} = \pi \frac{(d\ max)^2}{4}$ for each configuration. Data applies for trimmed conditions, except for the M-1 configuration. Fig. 1 shows reference axes.

*Taken at $C_{L_{max}}$; Angle-of-attack for STG is restricted to afterbody exposure $\alpha < 5$ deg.

$C_{L_{max}}$. With this lower initial lift, the vehicle penetrates deeper into the atmosphere so the acceleration is larger, even with subsequent modulation, than if the lift is held at its maximum value. This conflict for vehicles like L-2-C and STG does not exist for Model 410, since modulating Model 410 type vehicles from $C_{L_{max}}$ toward $C_{D_{max}}$ decreases the resultant force vector. These flight characteristics are discussed in the Trajectory Analysis Report.

IV. RE-ENTRY STABILITY AND CONTROL DATA

This chapter presents aerodynamic data and discussions of the static stability of Model 410 and other vehicles. Dynamic stability and control are discussed in Chapter V and in the Guidance and Controls report.

A. LONGITUDINAL

The Model 410 vehicle has certain static longitudinal stability characteristics similar to those of the W-1, M-1 and M-2 configurations. All have a semiconical profile with a spherical nose and a fineness ratio near unity. As for all re-entry vehicles, this geometry requires judicious compromises for Model 410 between aerodynamics, controls, structures and internal arrangement to achieve optimum stability characteristics during re-entry. The spherical nose results in large aerodynamic normal and axial loads forward, affecting trim and stability according to the axial and the vertical cg locations. The geometry of the nose can be adjusted to provide sensitive changes to trim and stability. The semicone provides large loads aft of the cg which result in basic stability of the vehicle. With appropriate pitch flaps, stability and control are maintained over the large range of angles of attack desirable for versatility in permissible re-entry trajectories. The objective is to obtain trim at $C_{L_{max}}$ (α = 30 deg) with the pitch flap fully retracted, and trim at $(L/D)_{max}$ (α = 13 deg) with the pitch flap aligned with the lower surface. This provides a high-lift attitude for the vehicle without a pitch flap for safety, and minimizes heat and air loads on the pitch flap for weight saving and improved reliability.

The hypersonic static stability typical of the supersonic flight regime for the basic geometry of Model 410 is indicated on the left side of Fig. 5. The basic shape refers to the spherical-nose, 18-deg semicone without flaps and without bottom flattening or nose tip-up. These pitching moment coefficient data are based on ℓ = 12.5 ft and, for convenience, a nominal reference area of 100 ft^2. The data are calculated with Newtonian methods. The basic shape is statically stable for cg locations forward of x/ℓ = 0.65 (measured from the nose) and trims at $C_{L_{max}}$ (α = 30 deg) for cg locations below z/ℓ = 0.11 (measured positive downward from the cone axis).

The hypersonic static stability for Model 410, aft flattened, is shown in Fig. 5. (Aft flattened refers to a geometric modification with the aft 20% ℓ of the cone a flat surface with zero incidence at α = 0.) This modification, while decreasing the stability, achieves the desirable large increase in the trim angle for a given cg location.

For example, with the cg at x/ℓ = 0.615 and z/ℓ = 0.08, the trim angle increases from about -15 degrees for the basic shape to +35 deg with aft flattened. It is obvious, however, that a more forward cg is required to maintain stability. Pitching moments with an 18-ft^2 pitch flap are shown for the cg at x/ℓ = 0.615 and z/ℓ = 0.0825 to illustrate the resulting improved stability and trim capabilities. Trim occurs at α = 35 deg with the flap fully retracted (δ = -35 deg) and at α = 9 deg with the flap aligned (δ = 0).

The pitch flap area of 18 ft^2 was estimated to provide trim from $(C_L)_{max}$ to $(L/D)_{max}$, with the flap limited, as previously mentioned, to no deflection outward relative to the aft skin line except for damping. This limitation is to minimize aerodynamic heating and flow separation complications during normal operation. A gap of about 2-1/2 inches is provided between the flap and the body, however, to allow some self-removal of the boundary-layer when the flap is extended for pitch damping. This flap has a span of 6 ft which is equal to the vehicle width at its bottom waterline with aft flattened, and a chord of 3 ft.

An alternate modification to the basic shape is nose tip-up for which the pitch characteristics are illustrated in Fig. 6. (5 deg tip-up refers to a geometric modification with the entire nose portion forward of station 50 tilted up 5 deg relative to the cone axis.) The 5-deg nose tip-up represents a minor geometric modification with strong effects on longitudinal control. With the cg at x/ℓ = 0.615 and z/ℓ = 0.088, the trim angle increases from about -15 degrees for the basic shape to +15 deg with 5-deg tip-up. The stability also increases, as indicated by the larger negative slope of the 5-deg tip-up curves, because the tip-up creates relatively larger load increments at the smaller angles of attack. These data include the effect of the axial and vertical cp displacements of the nose loads with tip-up.

Summarizing the modification effects, aft flattening greatly increases the basic trim angle of the vehicle while decreasing the stability. Nose tip-up increases the trim angle and stability. Aft flattening requires a more forward cg location and a vertical location nearer the axis. Appropriate geometric changes, therefore, coordinated with structural and internal arrangement studies, can be utilized to establish aerodynamic cg location requirements compatible with the vehicle capabilities, and to achieve control and stability over the desired 13- to 30-deg angle-of-attack range.

The results of a typical combination* of geometric modifications is shown on the right of Fig. 6 for the aft flattened as previously (20% ℓ) and with 5-deg nose tip-up forward of station 50. Data at the three axial cg locations are also presented for an 18-ft^2 pitch flap at various deflection angles (δ) relative to the cone axis. For a nominal cg location at x/ℓ = 0.635 and z/ℓ = 0.075, these data indicate that the vehicle with flap control is stable over the desired angle-of-attack range.

The flap deflections for trim are plotted in Fig. 7 for the three axial cg locations. The flap retraction at which the flaps would be ineffective for control, based on the Newtonian concept, is indicated to illustrate the margin of deflections available for pitch damping. This margin will be important in the dynamic analysis of the re-entry control because the re-entry vehicle without controls generally has little static stability.

Some preliminary typical estimates of allowable cg travel have been generated, based on the preceding pitching moment data for the vehicle with aft flattened and 5-deg tip-up. These are illustrated in Fig. 8 for several criteria. The solid boundary represents estimates of most allowable cg travel from the standpoint of aerodynamic static stability, while the dashed boundary is more conservative. Its selection would indicate that the cg should be slightly more forward and nearer the cone axis than the referenced position. The actual cg for the vehicle with its present internal arrangement lies within the solid boundary, 62.8% ℓ aft of the nose and 6.6% ℓ below the cone axis. During re-entry, the cg moves aft to 65.2% ℓ as ablation materials and propellants are consumed. Final selection of the nominal cg location and allowable travel will depend on aerodynamic data for the complete re-entry trajectory velocity-altitude boundaries and for the effects of modifications in vehicle geometry including those resulting from ablation.

Another aspect of longitudinal control is the proper alignment of the command module with the booster for the ascent flight. An angle of -5 deg (zero lift angle-of-attack for the command module) between the booster axis and the Model 410 command-module cone-axis has been selected to minimize bonding moments on the transition section at booster zero angle-of-attack. Asymmetric airloads on the

---

* A third possible geometric modification, employed on W-1, to increase stability, is an extension skirt aft on the bottom of the vehicle. This is essentially a fixed flap providing basic stability. Its merits have not been evaluated for Model 410, however.

transition section may be relieved by flow separation near the transition-command module junction at flight speeds near ascent maximum dynamic pressure, although this phenomenon possibly introduces transient buffeting. Possible modifications to the alignment and transition geometry are to be based on results of appropriate wind-tunnel tests.

Summarized longitudinal characteristics for W-1 are shown in Fig. 8 and 9. The axial location of the cg can be farther aft for W-1 than for Model 410 because of the larger pitch stability provided by the nearly flat bottom with its triangular extension skirt (Fig. 1). Also, for W-1, reasonable elevator angles are required to trim with substantial margin for pitch damping. The indicated allowable axial cg travel is comparable to that of Model 410, while the allowable vertical travel is larger.

Comparable data for L-2-C are presented in Figs. 10, 11 and 12. Generally, the aerodynamic characteristics of STG are similar to these data (Ref. 8). The present data were generated from NASA preliminary test data and application of the Newtonian theory. The vehicle is statically stable at angles of attack (referenced to a line normal to the axis of symmetry) larger than 60 deg. Pitch flaps for L-2-C are sized to obtain trim from 50- to 90-deg angles of attack. The vehicle is stable in this range (Fig. 10) for a 2% forward cg location (20% behind heat shield) which appears practical. The flap deflection required to trim at α = 50 deg is not significantly reduced by attempting to move the cg forward and, at the same trim, the L/D ratio would be slightly reduced (Figs. 11 and 12). Flap areas for trim at α = 50 deg are shown in Fig. 12a for δ_B = 90 deg; for a 6.6% flap area, cg shifts of 1-1/2% ℓ are tolerable for a nominal cg at 2% ℓ.

A 2% ℓ translation in the axial (z) direction changes the trim angle about 3 deg; the same translation vertically (x) changes it 20 deg. The flaps, then, can be used with reasonable deflection increments (about 12 deg) to compensate for errors in trim caused by the tolerable cg misalignments. Large increments, however, are required for L-2-C to trim between (C_L) max and (C_L) min. The travel ranges from zero to 78 degrees for the 6.6% flaps, or about five times the deflection required for the Model 410 pitch flap. (Figure 12B shows the results of calculations to confirm that the cg offset has little effect on L/D.)

Data (Ref. 8) show similar cg sensitivities for the STG vehicle, but it has reaction controls instead of aerodynamic controls. The vertical cg location must be closely controlled to eliminate propellant requirements of the reaction jets for possible pitch trim. The vertical cg sensitivity indicates that the nominal cg should be prescribed nearer

the cg required for $C_{L\ max}$, using roll modulation to control the direction of the lift vector during re-entry. The displacement depends on estimates of the cg tolerance or travel occurring during flight, and on trajectory requirements for C_L.

B. DIRECTIONAL

The basic Model 410 command module is slightly directionally unstable without side flaps for the cg at 0.635ℓ. The yawing moment coefficient C_n and stability C_{n_β} are shown in Fig. 13 for various angles of attack and sideslip.* Side-flaps are required to provide directional stability to the configuration, to trim for misalignments, and to provide yaw damping. Roll control is achieved with reaction jets instead of aerodynamic surfaces, thereby relieving flap system requirements and minimizing the aerodynamic roll-yaw coupling.

The side-flaps are sized to trim 2 deg of sideslip with a Newtonian flow-impingement angle of 20 deg. The trim angle capability can easily accommodate possible structural misalignments, and the impingement angle is a reasonable flap-heating criterion. For the area estimation, the additional conservative assumption was used that $C_{m_\beta} = +0.0013$ for the body alone. This stability occurs at angles of attack near 20 deg for a forward cg location near $62\%\ell$.

These criteria, with the calculated flap contributions to yawing moment (Figs. 14 and 15) (using a Newtonian coefficient of 1.5 for conservatism), require flaps with effective areas of about 3 ft^2 each for an axial cg location at $65\%\ell$. The physical areas, however, should be larger, depending on the aspect ratio of the flaps and the geometry of the vehicle, to guarantee flap effectiveness when they are partially blanketed by flow separation caused by shock-wave and boundary-layer interactions. Reference 1 provides experimental indications of the extent of the resulting pressure-losses on the flaps at the lower supersonic speeds. Considerations of these interactions, the effect of aspect ratio on the weight of the flaps and actuators and on interference with the mission module, lead to side-flap areas of 5 ft^2 each, with aspect ratios of 1.7.

---

* The directional stability is a function of both C_{n_β} and C_{ℓ_β}; as derived in NASA references, $(C_{n_\beta})_{eff} = C_{n_\beta} - C_{\ell_\beta} \propto \frac{I_z}{I_x}$.
The second term is particularly important at the high angles of attack required for the present mission. It has added significance because, for Model 410, C_{n_β} is nearly zero. Although its magnitude remains to be calculated for Model 410, C_{ℓ_β} is generally negative and its omission here may be a conservative procedure.

The side flaps are displaced downward from the cone centerline about 6 degrees (aft view) to minimize pitch coupling. Expected pitch coupling, however, will be controlled through the autopilot by appropriate pitch-flap corrections. Roll-moments introduced when the yaw flaps are differentially deflected are dependent on the direction of the relative velocity and will be controlled with the reaction roll-control system.

The side-flaps are normally aligned with the vehicle skin-line ($\delta = 0$) to provide a nominal static directional stability. The flaps may be deflected in or out differentially to provide directional control. For a trimmed side-slip angle of 7 deg (an extreme at least 3 times more than should be required), for example, the windward flap would be turned in -1 deg (parallel to the velocity vector), and the leeward flap turned out +6 degrees. Yaw damping is increased, as shown in Fig. 13 for static directional stability, by moving both side-flaps outward. Dynamic stability will be achieved by moving them outward differentially by appropriate autopilot commands. When the flaps are aligned with the cone surface ($\delta = 0$), C_{n_β} is slightly positive (directionally stable) at $C_{L_{max}}$ and increases as the angle of attack is reduced. The resulting increment in yaw stability is indicated by the data of Figs. 13 and 14. Individual flap moments are shown in Fig. 15.

The W-1 configuration is more unstable directionally without flaps (Fig. 16) than the Model 410 configuration, and the flap effectiveness appears more dubious. Increments in C_{n_β} as flap deflections were increased in NASA tests at Mach 6 of the NASA M-1, L-1, and L-4 configurations were compared with predicted increments, using Newtonian approximations. The L-1 and L-4 have physical characteristics similar to W-1; at positive angles-of-attack, essentially a flat-bottom is presented to the flow, and the flow must progress around a small-radius corner before impinging on the side-flaps. This corner causes flow separation and overexpansion which cancel the Newtonian approximation for the flow over the flaps. The comparisons between Newtonian predictions and test values showed that impact theory could not adequately estimate flap effectiveness at some angles of attack. For the M-1 vehicle, however, which is similar to the present Model 410 vehicle with a conical bottom, impact theory appears to offer satisfactory predictions of C_n (Ref. 1) at zero angle of attack and Mach numbers about 6. For the L-1 configuration, the pitching moment increments of the bottom flaps at angle of attack (M = 6) also are predictable with impact theory for $\alpha \sim 30$ deg and $\delta \sim 45$ deg. Based on these comparisons, the W-1 directional control could present exceptional difficulties which may not be predictable without further test data.

With the axis system defined for L-2-C in the NASA preliminary data, the z-axis is the axis of symmetry and is directed from the cg toward the heat shield. The L-2-C side flaps, therefore, control rotation about the roll axis. Side flap areas of $0.033S$ each provide sufficient trim and damping capabilities. For example, a flap deflection of 35 degrees trims 2 degrees throughout the angle of attack range, based on NASA test data. The L-2-C side flaps are 15% smaller than those of Model 410. Some NASA data for L-2-C is reproduced in Fig. 17 for reference.

C. REACTION CONTROLS

The Model 410 command module employs four pairs of reaction jets for three-axis control when approaching the earth's atmosphere. Two pairs with vertical axes control pitch, and the other two pairs with lateral axes control yaw. All of the jets, four simultaneously, are used for roll control. While the pitch and yaw control is transferred to aerodynamic flaps when the dynamic pressure becomes sufficient (2-g deceleration), the reaction jets maintain roll control throughout re-entry. This procedure offers the advantages of full utilization of the reaction system during re-entry and reduction of flap-area and flap-actuator requirements. Roll-yaw coupling is minimized. This procedure represents a saving in weight and an improvement in safety, particularly since the reaction system is dualized for high reliability.

An estimate of the maximum roll torque requirements is based on disturbing moments due to yaw-roll coupling induced by the side flaps ($C_{\ell} = 0.005$) and to an assumed axial misalignment (1 degree) of the vehicle. This roll control requires 1000 ft-lb of torque correction at maximum dynamic pressure; the correction is achieved by operating four 50-lb thrust reaction jets. The propellant requirement, assuming these types of disturbing moments were average for a typical re-entry trajectory and a propulsion specific impulse of 280 sec, is about 80 lb. Additional propellant is required for operation during the approach to the atmosphere. Based on dynamic calculations for this flight phase and the maximum thrust prescribed by roll requirements, the pitch and yaw jets provide 100 lb of normal and side forces with 20 lb of propellant available for each. These same jets provide 1000 ft-lb of roll-torque with 100 lb of propellant available.

The STG vehicle employs reaction jets for 3-axis control throughout re-entry. With four pairs of jets mounted forward between

the heat shield and the pressurized structure, each jet (using the NASA axis notation) has a yaw-moment arm of about 6 ft and pitch-roll moment arms of about 1 ft. If the jets were required to trim at maximum dynamic pressure during re-entry, as do the flaps of L-2-C, an impractical reaction thrust of over 25,000 lb would be required. It is, therefore, necessary to expect to trim only with cg offset and to relax the criteria for the pitch jets. Sizing the pitch and roll jets for an alternate criteria of angular acceleration of 2 deg/sec^2 in vacuum yields a thrust requirement of about 50 lb per nozzle. For a nominal operating time, approximately 75 lb of propellant each are required for pitch and yaw. For yaw, the 50-lb thrust nozzles provide an acceptable angular acceleration of about 18 deg/sec^2, and about 35 lb of propellant are required.

These reaction system requirements are based on preliminary criteria which must be re-evaluated through dynamic analyses.

V. DYNAMIC STABILITY OF RE-ENTRY BODIES WITHOUT CONTROLS

Re-entry is accomplished, under normal conditions, with the guidance and control system providing control and dynamic stability to assure that such re-entry effects as heating, normal and longitudinal accelerations and dynamic pressure are not excessive. However, for an emergency in which the guidance and control system and the control surfaces might be ineffective, knowing the dynamic performance of the re-entry vehicle without control is important for evaluating its safety.

The majority of all re-entry configurations is classed in either of two characteristic groups: (1) high drag and low L/D and (2) low drag and high L/D shapes. To evaluate the differences in dynamic behavior for aid in choosing a configuration, the dynamic performance of two vehicles, Model 410 and STG, each representative of a group, has been analyzed.

Considerable useful analyses and techniques concerning the re-entry dynamics have been reported in recent literature. The initial evaluation analyses employed consist of applying such investigative methods as are reported in Refs. 9 through 12, and introducing reasonable approximations to facilitate the solutions. More accurate investigations involving large re-entry angles of attack will require a 6-deg-of-freedom analysis with nonlinear aerodynamics. However, a general behavior of different re-entry bodies can be determined by several methods, assuming small re-entry angles of attack and linear aerodynamics.

These restrictions are less severe than they may first appear. For statically stable bodies, the initial re-entry phase is essentially independent of differences in aerodynamic characteristics (Figs. 18 and 19). The dominant factor is the time rate of change of dynamic pressure q, and the pitching and yawing moments are of secondary importance (as long as they are restoring). The effect of aerodynamic damping, lift and drag is negligible on the initial pitching or yawing motion of the re-entry body. For vehicles entering with a velocity of 36,000 fps, the oscillatory motion starts at about 1/3 of the re-entry angle of attack. If linear aerodynamics can be assumed in a range from + 10 to + 15-deg angles of attack (about zero-lift angle of attack), the actual re-entry angle of attack can vary from + 30 to + 45 deg while allowing reasonable accuracy with linear aerodynamics. Considering that, in the initial part of the oscillations, the relative importance of q rate remains valid, the re-entry angle of attack can possibly be extended to 45, or even 60 deg, with reasonable accuracy.

In the oscillatory part of the motion, maximum values of the accelerations or amplitudes and frequencies are of prime interest. Here the aerodynamic characteristics of the re-entry body gradually become more important to the behavior of oscillatory motion as the altitude and velocity decrease.

The angle of attack envelope can be expressed as

$$\frac{(\alpha_{max})_t}{(\alpha_{max})_{t=o}} = \sqrt[4]{\frac{(M_\alpha / I_y)_{t=o}}{(M_\alpha / I_y)_t}} \exp\left[-\frac{1}{2}\int_{t=o}^{t}\left(-\frac{M_q + M_{\dot\alpha}}{I_y} + \frac{L_\alpha}{mV}\right)dt\right]$$

This expression is convenient to use if the histories of the above parameters are known for a nominal non-oscillatory re-entry trajectory and it can be assumed that the oscillatory motion has a negligible effect on the nominal trajectory. The term under the fourth root is determined almost completely by the time rate of change of the dynamic pressure q. The exponential term expressing the effect of aerodynamic damping is close to unity in the initial part of the re-entry. However, as the re-entry continues, this term either decreases rapidly approaching zero if $-\frac{M_q + M_{\dot\alpha}}{I_y} + \frac{L_\alpha}{mV} > 0$, or increases if $-\frac{M_q + M_{\dot\alpha}}{I_y} + \frac{L_\alpha}{mV} < 0$, becoming increasingly dominant as the re-entry progresses. The sign of this exponential term results in either a converging or diverging oscillatory motion.

The dynamic oscillatory performance for the re-entry vehicles Model 410 and STG has been determined using the non-oscillatory or static re-entry trajectories shown in Fig. 20.

The initial dynamic performance of Model 410 and STG is very similar with respect to the maximum angle of attack envelopes (Figs. 18 and 19). However, about 60 sec later, when the aerodynamic characteristics become more important, the behavior of the two bodies is very different. While the α max envelope of the Model 410 configuration is converging, the STG α max envelope is diverging. The main contributary factor to this divergence is the large negative lift-curve

slope of the STG configuration. The damping terms for both configurations are approximately the same. For the assumed cg location, C_{m_q} = -0.133 and C_{m_q} = -0.1903, respectively; $C_{m_{\dot{\alpha}}}$ = 0 for Mach numbers exceeding 4.

Figures 21 and 22 show the time histories $\dot{\alpha}$ max and ω_n (frequency of oscillations in cps). The differences in the dynamic re-entry characteristics between the two configurations are more apparent in these time histories. When these oscillations are translated into the normal accelerations experienced by the two re-entry bodies, the differences become more obvious. As shown in Fig. 23, there is a large difference between the normal accelerations of each vehicle relative to the body-axis system. The maximum normal accelerations of the order of 2 g per radian of α re-entry for the Model 410 configuration are not large, however, when compared to the maximum longitudinal accelerations.

The normal accelerations are oscillatory with the frequency reaching about 2 cps. The effect of these oscillatory normal accelerations on a human will be different from his reaction to the only slightly oscillatory but considerably larger longitudinal accelerations. The total accelerations (or rather decelerations) for both types of configurations will be of approximately the same magnitude.

To illustrate the sensitivity of the normal accelerations to the direction of the reference axis system, another set of accelerations are shown (Fig. 23) for the same cases, except the accelerations are related to an axis system normal to the flight path. There is very little difference between the maximum normal accelerations for the Model 410 re-entry vehicle if a slightly different axis system is used. The STG vehicle, however, shows a significant sensitivity to the axis system employed. This results from the total force for the STG configuration very nearly coinciding with the vehicle axis of symmetry and, therefore, the normal forces or accelerations along an axis perpendicular to this axis are always very small. However, since the longitudinal force or acceleration for the STG is significant and the oscillatory angles of attack never become very small, the projection of this force on an axis perpendicular to the flight path are considerably larger. This sensitivity should be examined when the effects of the direction of acceleration on parts of the human body are considered. However, the direction of the total force varies considerably with angle of attack for a Model 410 type vehicle and, therefore, is not too sensitive to small changes of the axis system to which the accelerations are referred. The large changes in the direction of the total force for this type of vehicle are offset by the relatively smaller amplitudes of the oscillations, as compared to the STG-type re-entry vehicle. Referred to the flight-path axis, the normal accelerations of the two re-entry body configurations do not differ significantly.

The accelerations shown are for the center of gravity. All other locations in the re-entry vehicle will be subjected to accelerations which will be the vectorial sum of the total accelerations due to the motion of the cg and the motion about the cg. In the Model 410 configuration for points aft of the cg, the normal accelerations will always be additive. This is an addition because, at points on the trajectory where the oscillatory displacement of the cg is maximum relative to an average nonoscillatory trajectory, the normal velocity will be zero and the acceleration maximum (during a cycle). Since the acceleration is maximum, the lift force and, consequently, the angle of attack are also maximum. Since it must be a restoring angle of attack, the parts of the body aft of the cg describe a larger amplitude than the cg and, therefore, experience a larger maximum acceleration. However, for re-entry bodies of the size under consideration, the additional maximum normal acceleration will be about one g or less. For locations forward of the cg, the normal accelerations will be subtractive and of the same magnitude. The maximum longitudinal accelerations due to the motion about the cg will be about 2.5 g (each g in this discussion is expressed per radian of re-entry angle of attack) and will be substractive for points aft of the cg and additive for points forward of the cg. A similar but more complicated condition exists for points above or below the cg. The main result of the accelerations from the motion about the cg will most likely be the adverse effects of the additional oscillatory accelerations on the human occupants.

In summary, there are no significant differences in the dynamic performance of the emergency re-entry for both types of re-entry vehicles. Although the oscillations of the Model 410 configuration are converging, while those of the STG are diverging during the second part of the re-entry trajectory, the maximum total accelerations are approximately of the same magnitude. The normal oscillations, if the axis system sensitivity is considered for the STG configuration, should be of the same order of magnitude for both re-entry vehicles. The oscillatory nature of the accelerations produced by the normal motion of the cg and the rotary motion about the cg should be recognized, because the effect on the human body of such oscillatory accelerations will be different from the comparatively larger, constant direction, longitudinal accelerations. The magnitude and direction of the oscillatory accelerations will be different for different parts of the body and different locations of the crew members relative to the cg. A more detailed 6-deg-of-freedom investigation is necessary to obtain more exact solutions of this problem, although methods used in this investigation are considered sufficient for a preliminary analysis.

VI. ABORT AERODYNAMIC AND STABILITY DATA

This section presents aerodynamic and stability data for several vehicles with the abort configurations which include a tower containing emergency escape rockets. Discussion of the abort phases of flight, including results of studies utilizing this data, is presented in the Trajectory Analysis Report ER 12003. The present data is for power-off flight conditions. Data computed for W-1 is assumed to apply for Model 410, because the geometries of the two vehicles are essentially the same.

Figure 24 compares Mercury data with subsonic calculations for the exit and escape configurations. The method of calculation for this subsonic regime is described in the Appendix. The comparisons show generally satisfactory calculated results. With the tower, however, the subsonic aerodynamics are too complex beyond 10 deg angles-of-attack for adequate analysis. Figure 25 similarly compares the supersonic regime. Here the calculations are in agreement, except at the lowest Mach numbers, to about 20-deg angles-of-attack.

Figures 26 through 29 illustrate effects of tower length, tower ballast and body flare on aerodynamic parameters applicable to the Model 410 and W-1 escape configurations. The tower length is measured from the forward end of the tower to the nose of the vehicle. Ballast is assumed to be at the forward end of the tower. The benefits of the forward cg movement as the tower length is increased are largely cancelled by the increased destabilizing moments of the tower. Tower ballast and body flare introduce undesirable weight penalties to achieve static stability, and the vehicle flaps cannot control the vehicle during abort. Possibilities for dynamic control are discussed, as mentioned previously, in the Trajectory Analysis Report ER 12003. The data for $M = 1.3$ were generated for abort studies at q max condition during ascent. They show static stability and trim near 10 deg angle-of-attack for a specific tower length and ballast.

Figures 30 through 35 present data for the L-2-C escape configuration. The lift and drag data of Figs. 30 and 31 were developed using cone data jointly with Mercury test data which are included for comparison.

VII. REQUIREMENTS FOR FURTHER ANALYSIS AND EXPERIMENT

The discussions and data of Refs. 1 to 6 and 13 to 16, for example, clearly show the requirements of final design for more erudite methods of analysis, and for specific test data, in particular at the hyper-velocities. However, ground facility test data which accurately duplicates all the anticipated re-entry conditions will be impossible to obtain. Only a judicious combination of tunnel, flight test and analytical techniques can yield a thorough understanding of the aerodynamic characteristics of the vehicles. Matching modified Newtonian and Prandtl-Meyer pressures and slopes (Ref. 4) yields more accurate pressure distributions downstream of the sonic point on spherical nose caps than ordinary modified Newtonian results. Method of characteristics solutions, employing digital computers can also assist in understanding the flow field. (Martin has a real gas equilibrium characteristics program applicable to symmetric bodies at zero angle of attack and is presently developing a method for computing the flow field about as asymmetric bodies at angle of attack). Such effects as shock-boundary layer interactions, flow separation, flow about control surfaces, and base pressures are typical phenomena which must be studied, both analytically and experimentally, in developing aerodynamic characteristics of the re-entry vehicle. Further analyses should include the effects of finite chemical reaction times (non-equilibrium and frozen flow effects) on the flow field, since it is anticipated that the contributions due to these effects may be large, especially on the afterbodies of the re-entry vehicles.

Wise utilization of appropriate government and contractor test facilities, including free-flight and wind-tunnel tests, is necessary to obtain basic data which the analyses will augment. (Martin has shock-tube facilities (Ref. 17) and a hot-shot (M=12 to 24) hypersonic wind-tunnel which can provide research data useful to the Apollo program.) The complete test program is discussed in terms of applicable facilities in ER 12012, Test Program report.

In particular, it is necessary to obtain stability data for the command module at supersonic and hypersonic speeds to establish the requirements for cg location and allowable cg travel, and to determine complete dynamic characteristics. Flap effectiveness and hinge moments must be evaluated, particularly at conditions where multiple-shock and boundary layer effects are important, to optimize the flap control system for minimum weight and maximum effectivity. Pressure distributions on the flaps and on the body must also be determined with an experimental basis to refine structural design.

Roll-control system requirements will be determined using analog simulation which includes aerodynamics of the vehicle with flaps. Other simulation for the re-entry oscillations, predicting possible amplitudes and accelerations during re-entry, will be undertaken. (Six-deg-of-freedom programs have been developed at Martin for such studies.) These types of analyses, together with the experimental data, will lead to refinements which improve the aerodynamic configuration by indicating appropriate changes in body shape, flap size and locations, and cg location.

VIII. CONCLUSIONS

Some specific conclusions for the Model 410 configuration are:

(1) The lift and drag characteristics provide for deceleration control with a wide corridor. For angles of attack from 13 to 30 deg, C_L varies from 0.32 to 0.43 while L/D varies from 0.73 to 0.58. Zero lift is at a -5-deg angle of attack.

(2) With a pitch flap area of 18 ft^2 the vehicle can be trimmed to achieve attitude control over the desired angle-of-attack range. Trim occurs at $C_{L_{max}}$ with the flaps retracted and at (L/D) max with the flaps extended to the skin-line. Variations in external geometry, such as aft flattening and nose-tip, are available to adjust the design trim and stability with appropriate changes in internal arrangement to properly locate the cg.

(3) Side flaps, of 5 ft^2 area each, provide directional stability and damping and trim capabilities.

(4) The forward-facing cone geometry provides damping of pitch and yaw oscillations during emergency re-entry without controls. The angular accelerations are not excessive.

(5) The escape configuration is statically unstable. Ballast in the tower and thrust vector control during the separation are typical means for improving dynamic stability during abort operations.

IX. REFERENCES

1. Sarabia, M. F., "Aerodynamic Characteristics of a Blunt Half-Cone Entry Configuration at Mach Numbers from 3 to 6," NASA TM X-393, October 1960. CONFIDENTIAL

2. Chernyi, G. G., "Effect of Slight Blunting of Leading Edge of an Immersed Body on the Flow Around It at Hypersonic Speeds," NASA TT F-35, June 1960, UNCLASSIFIED

3. Van Hise, V., "Analytic Study of Induced Pressure on Long Bodies of Revolution with Varying Nose Bluntness at Hypersonic Speeds," NASA TR R-78, 1960. UNCLASSIFIED

4. Traugott, S. C., "Some Features of Supersonic and Hypersonic Flow About Blunted Cones," Research Memorandum RM-64, The Martin Company, March 1960. UNCLASSIFIED

5. Frank, J. L., Green, K. H. and Hofstetter, R. V., "Measurements of the Flow Over Blunt-Nosed Bodies at Mach Numbers from 2.5 to 3.5," NASA TM X-367, May 1960. CONFIDENTIAL

6. Henderson, A., Jr., "Investigation of the Flow Over Simple Bodies at Mach Numbers of the Order of 20", NASA TN D-449, August 1960. UNCLASSIFIED.

7. Schmidt, J. F., "Laminar Skin-Friction and Heat Transfer Parameters for a Flat Plate at Hypersonic Speeds in Terms of Free-Stream Flow Properties", NASA TN D-8, September 1959. UNCLASSFIED

8. "Project Apollo, STG Study Progress Report", NASA Space Task Group, 15 March 1961. CONFIDENTIAL

9. Frederick, H. R., and Dore, R. L., "The Dynamic Motion of a Missile Descending Through the Atmosphere", Journal of Aeronautical Science, Vol. 22, No. 9, September 1955. UNCLASSIFIED

10. Allen, M. J., "Motion of a Ballistic Missile Angularly Misaligned With the Flight Path Upon Entering the Atmosphere and Its Effect Upon Aerodynamic Heating, Aerodynamic Loads, and Miss Distance", NACA TN 4048, 1957. UNCLASSIFIED

11. Chapman, D. R., "An Approximate Analytical Method for Studying Entry into Planetary Atmospheres", NACA TN 4276, 1958. UNCLASSFIED

12. Sommer, S. C., and Tobak, M., "Study of the Oscillatory Motion of Manned Vehicles Entering the Earth's Atmosphere", NACA Memo 3-2-59A, 1959. UNCLASSIFIED

13. Phillips, W. H., "Research on Blunt-Faced Re-entry Configurations at Angles of Attack Between 60° and 90°", USAF-NASA Joint Conference Report Compilation, Part I, April 11-14, 1960. CONFIDENTIAL

14. Creager, M. O., "An Approximate Method for Calculating Surface Pressures on Curved Profile Blunt Plates in Hypersonic Flow", NASA TN D-71, September 1959. UNCLASSIFIED

15. Dennis, D. H. and Edwards, G. G., "The Aerodynamic Characteristics of Some Lifting Bodies", USAF-NASA Joint Conference Report, Part I, April 11-14, 1960. CONFIDENTIAL

16. Seiff, A., and Whiting, E., "The Effect of the Bow-Shock on the Stability of Blunt-Nosed Slender Bodies", USAF-NASA Joint Conference Report, Part I, April 11-14, 1960. CONFIDENTIAL

17. Chapin, S. G. and Heyman, R. J., "Performance Characteristics of a Chambered Buffered Shock Tube", Hypervelocity Techniques Symposium, IAS, Denver, Colorado, October 20-21, 1960. UNCLASSIFIED

18. Whalen, R. J., "Visions and Inviscid Non-Equilibrium Gas Flows", IAS Paper No. 61-23, January 23-25, 1961. UNCLASSIFIED

19. Hayes, W. D., and Probstein, R. F., "Hypersonic Flow Theory, Academic Press", New York 1959. UNCLASSIFIED

APPENDIX

AERODYNAMIC COEFFICIENTS IN SUBSONIC FLOW

Empirical methods have been developed for estimating subsonic aerodynamic coefficients for studying emergency abort flight conditions for the Apollo vehicles. The emergency escape configurations which are similar for each of the vehicles, utilize and escape rocket supported on a tower extending forward from the manned re-entry command module. The module in the escape attitude is a modified forward-facing cone or semicone. The methods, therefore, are based on developing equations expressing aerodynamic forces on cones and cylinders for appropriate application to cone-cylinder representations of the actual escape configurations. The basic equations are presented in this Appendix with an indication of their empirical foundations.

1. Cones

From Newtonian theory, the normal force coefficient of a cone of semivertex angle θ at angle of attack α is $C_n = \cos^2\theta \sin 2\alpha$.

Analysis of some applicable subsonic test data of which the most completed are those of the Mercury capsule, showed that, for subsonic flow, the above equation represents the normal force coefficients in an α-range from zero to $(90 - \theta)$ degrees if used in the form

$$C_N = 0.9 \cos^2\theta \sin 2\alpha \qquad (1)$$

referred to the base area.

For a frustrum of a cone, C_N is reduced by the factor $\left(1 - \frac{r_f^2}{r_b^2}\right)$ where r_f and r_b are the radii of the frustrum.

The axial force coefficient of a cone at zero angle of attack is given by the equations

$$C_x = C_{D_o} = (.5) \sin\theta \quad \text{for} \quad \theta = 0 \text{ to } 50 \text{ deg} \qquad (2)$$

$$\text{and } C_x = C_{D_o} = 2.22 \sin\theta - 1.32 \quad \text{for} \quad \theta = 50 \text{ to } 90 \text{ deg} \qquad (3)$$

These equations are based on test data such as summarized in "Fluid Dynamics Drag" by S. Hoerner. Results from equation (2) were also successfully checked with Mercury test data. Equations (2) and (3) do not include base drag.

To determine angle-of attack effects on the axial force coefficient C_x, the following considerations were made:

(1) For angles of attack smaller than Θ (Fig. A-1), the axial force, which will not change significantly, will be a maximum.

(2) At an angle of attack of about $(90 - \Theta)$ deg, the axial force will be nearly zero. It is assumed that the positive x- component of the lower-side pressure cancels the negative x-component of the upper-side negative pressure.

Between the two selected points at $\alpha = \Theta$ and $\alpha = (90 - \Theta)$ degrees, a linear dependency may be assumed, as represented by the function $C_x = C_{D_o} \cos\left(\frac{90^\circ}{90^\circ - \Theta}\right)$ (Fig. A-1).

2. Cylinders

The subsonic normal force coefficient of a cylinder is

$$C_N = \left[0.5 + 0.1\sqrt{\ell/d}\right] \sin^2\alpha \qquad (4)$$

in a range from $\ell/d = 1$ to 10. This equation is based on test data and referenced to the plan area $\ell \cdot d$. The axial force coefficient of the blunt cylinder face (flat plate) is

$$C_x = (0.9)\cos^2\alpha \text{ based on } \pi d^2/4 \qquad (5)$$

where α is the angle of attack of the cylinder center-line.

3. Base Drag

The base drag coefficient has been investigated by several authors (cf. e.f., Hoerner, "Fluid Dynamics Drag"). For cylindrical bodies, C_D base = 0.22 to 0.25. Bodies with boat tail have a base drag smaller than 0.22; conical bodies show a slightly larger base drag. The base drag decreases with $\cos\alpha$, and its contribution to the axial force of a body changes with $\cos^2\alpha$. Thus, the axial force coefficient of a body, due to base drag, will approximately be

$$C_{x_{base}} \approx 0.25 \cos^2\alpha \qquad (6)$$

Equations (1) through (6) were used to recalculate subsonic test data of the Mercury exit configuration, represented by a frustrum of a cone plus a cylindrical forebody. The drag increment due to cylinder-cone interference and the skin friction drag was not considered in the recalculation. The results of the calculations agree favorably with test data (Fig. 24). Calculation procedures based on these equations have, therefore, been applied to obtain subsonic aerodynamic data for the Apollo configurations.

ILLUSTRATIONS

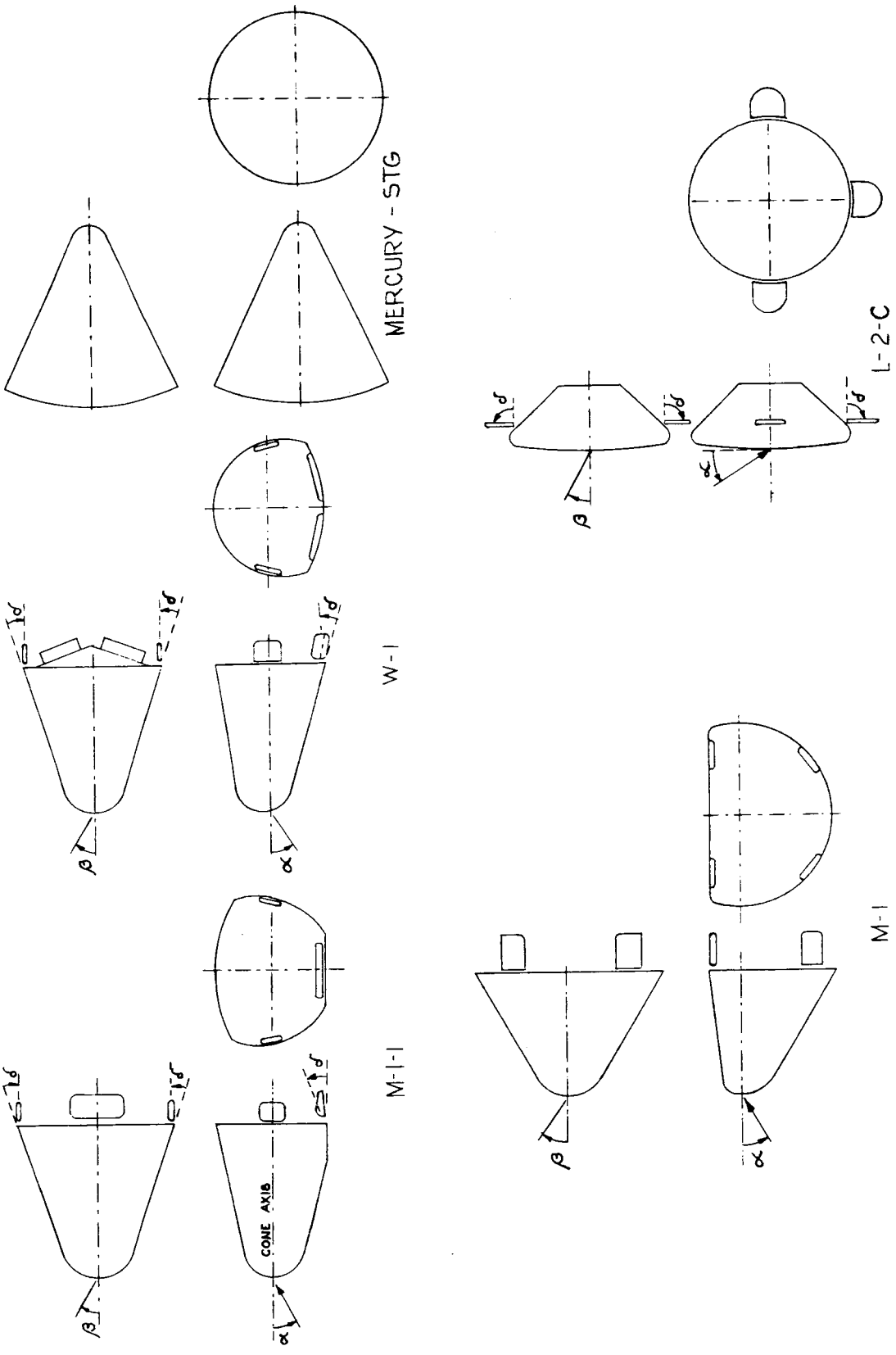

Fig. 1. Re-entry Configuration Outlines

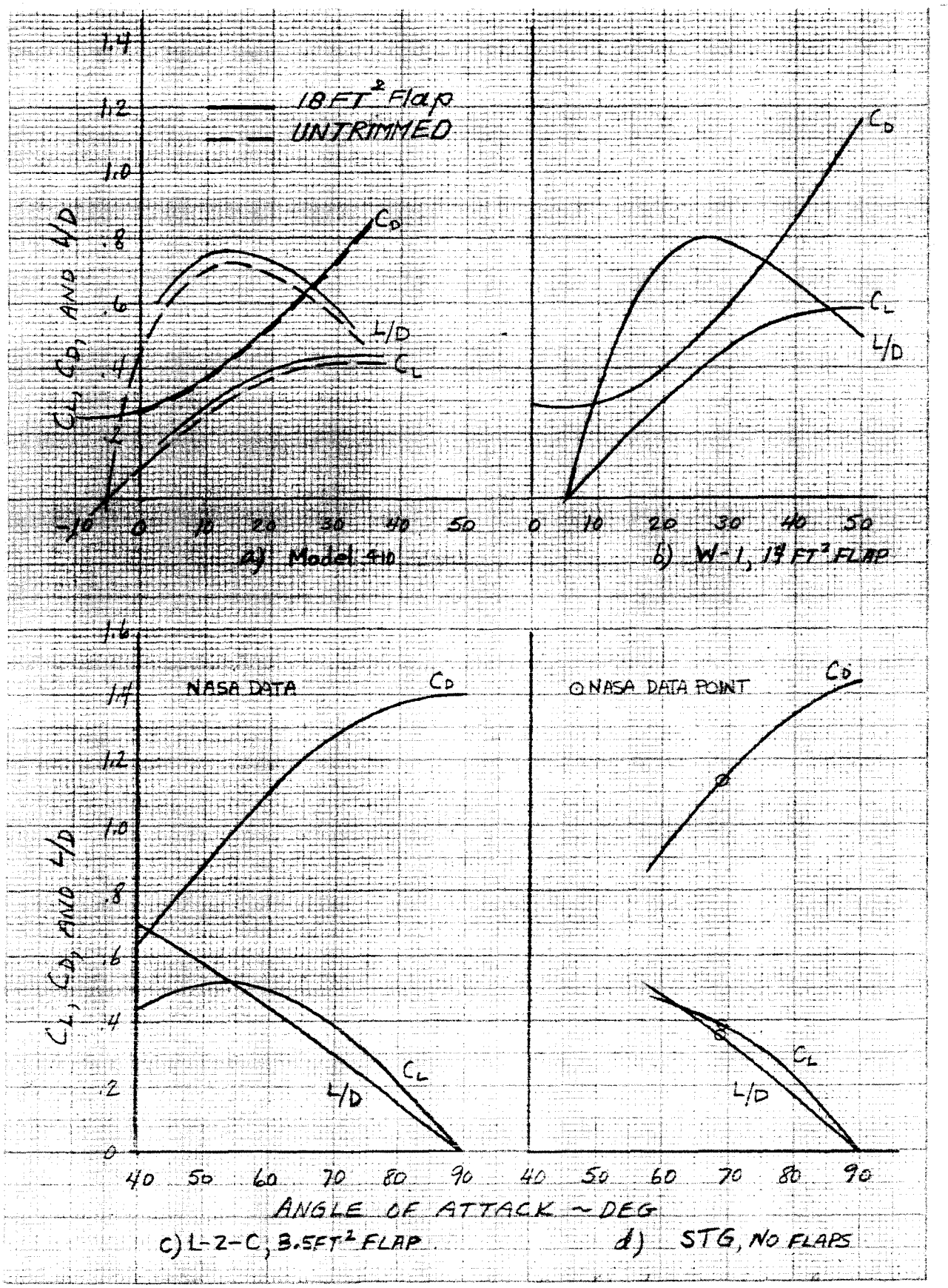

Fig. 2. Hypersonic Lift, Drag and Lift-Drag Ratio for Four Configurations

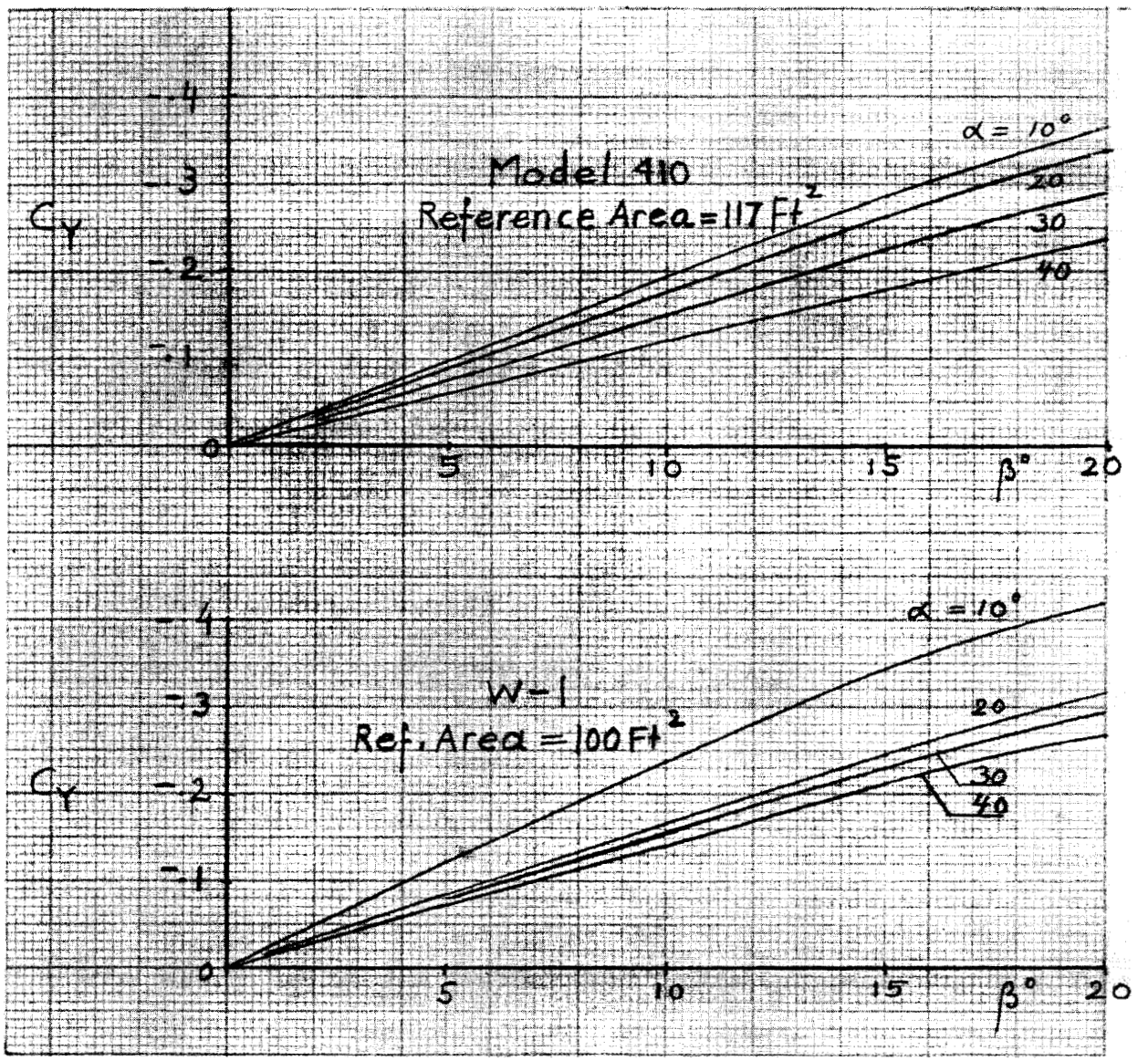

Fig. 3. Hypersonic Side Forces for Model 410 and W-1

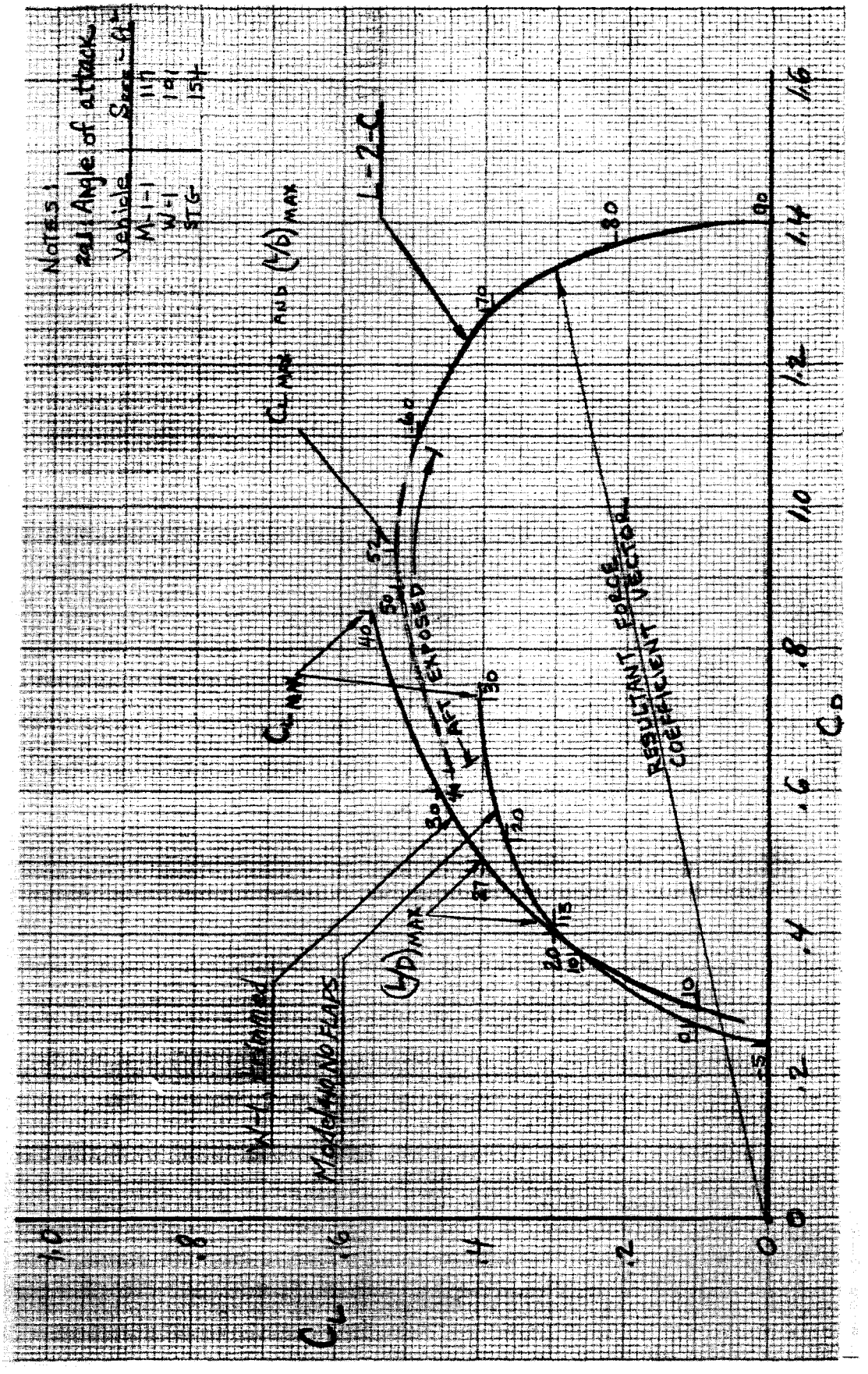

Fig. 4. Lift-Drag Curves for Model 410, W-1 and L-2-C Vehicles

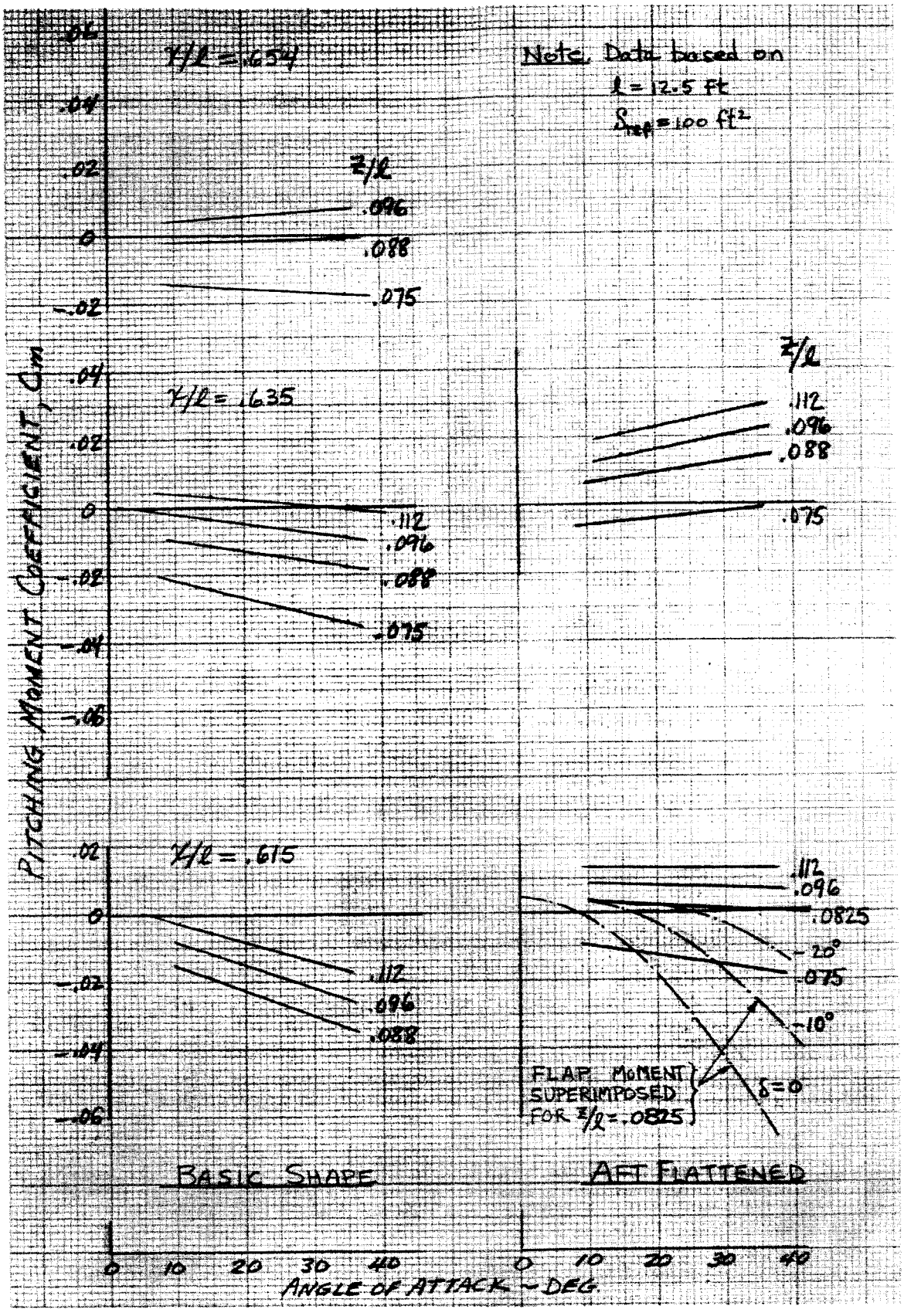

Fig. 5. Pitching Moments for Model 410, Basic and Aft Flattened

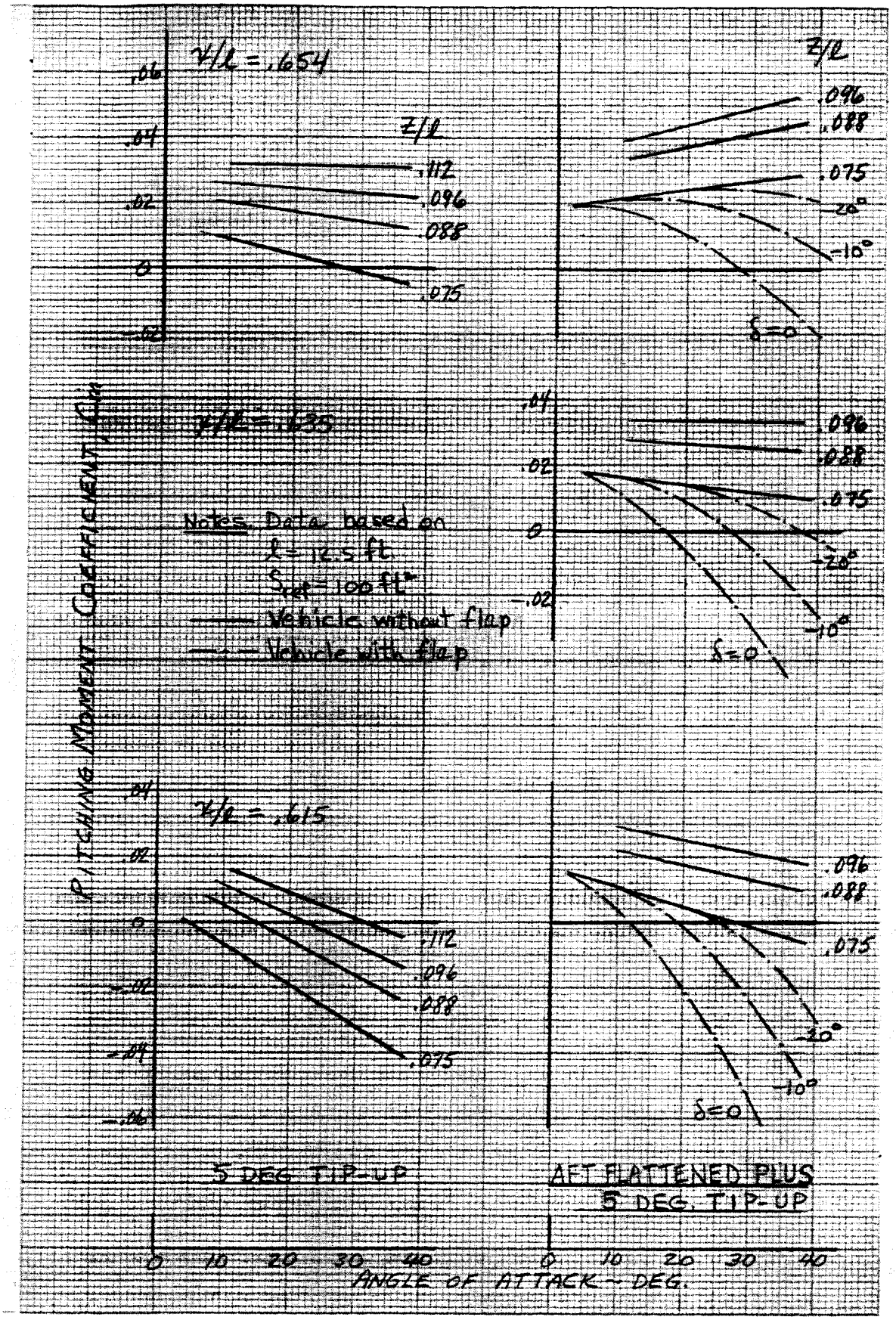

Fig. 6. Pitching Moments for Model 410, 5 degrees Tip-Up and Aft Flattened Plus 5 degrees Tip-Up

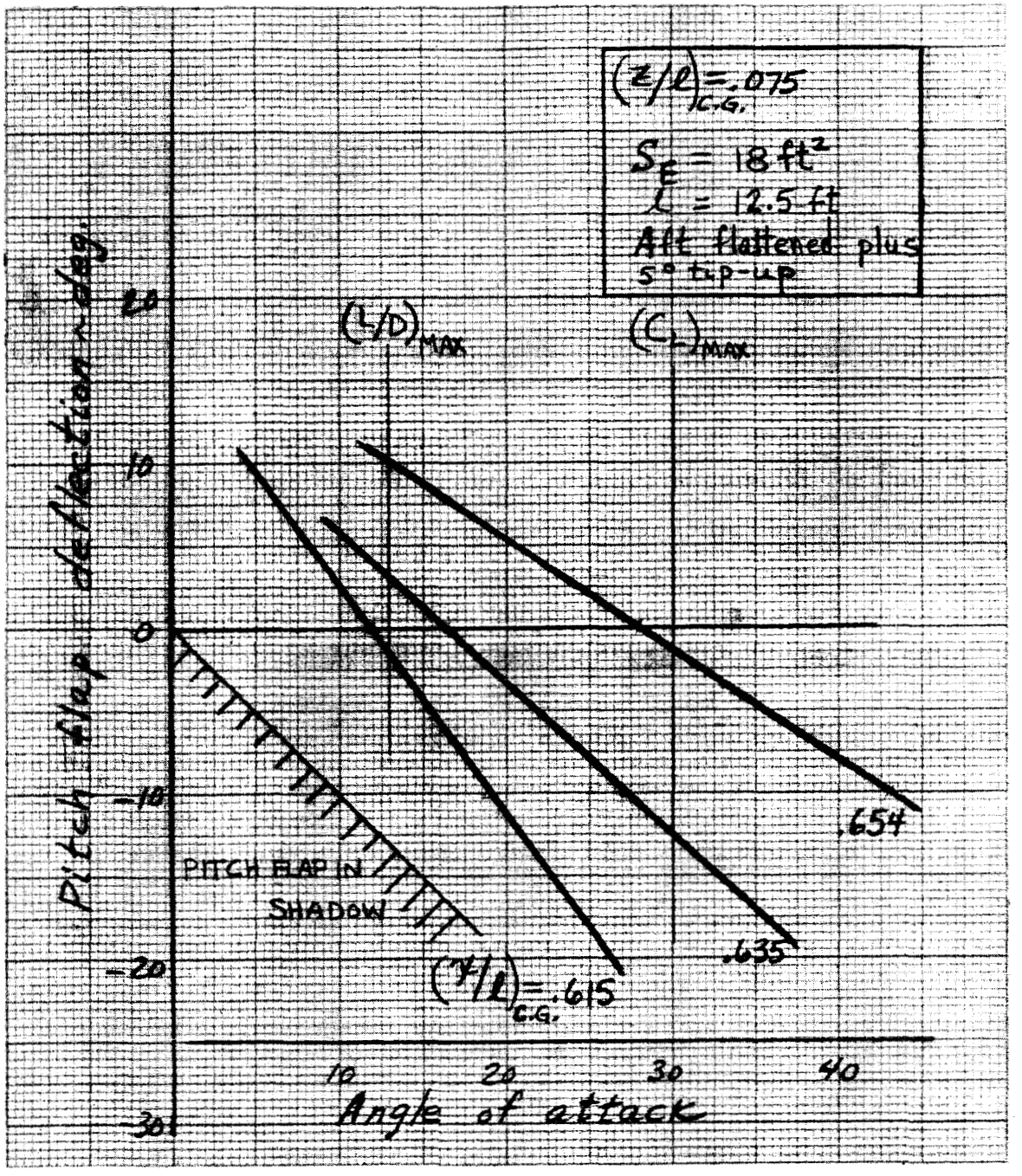

Fig. 7. Pitch Flap Deflection Required to Trim Model 410

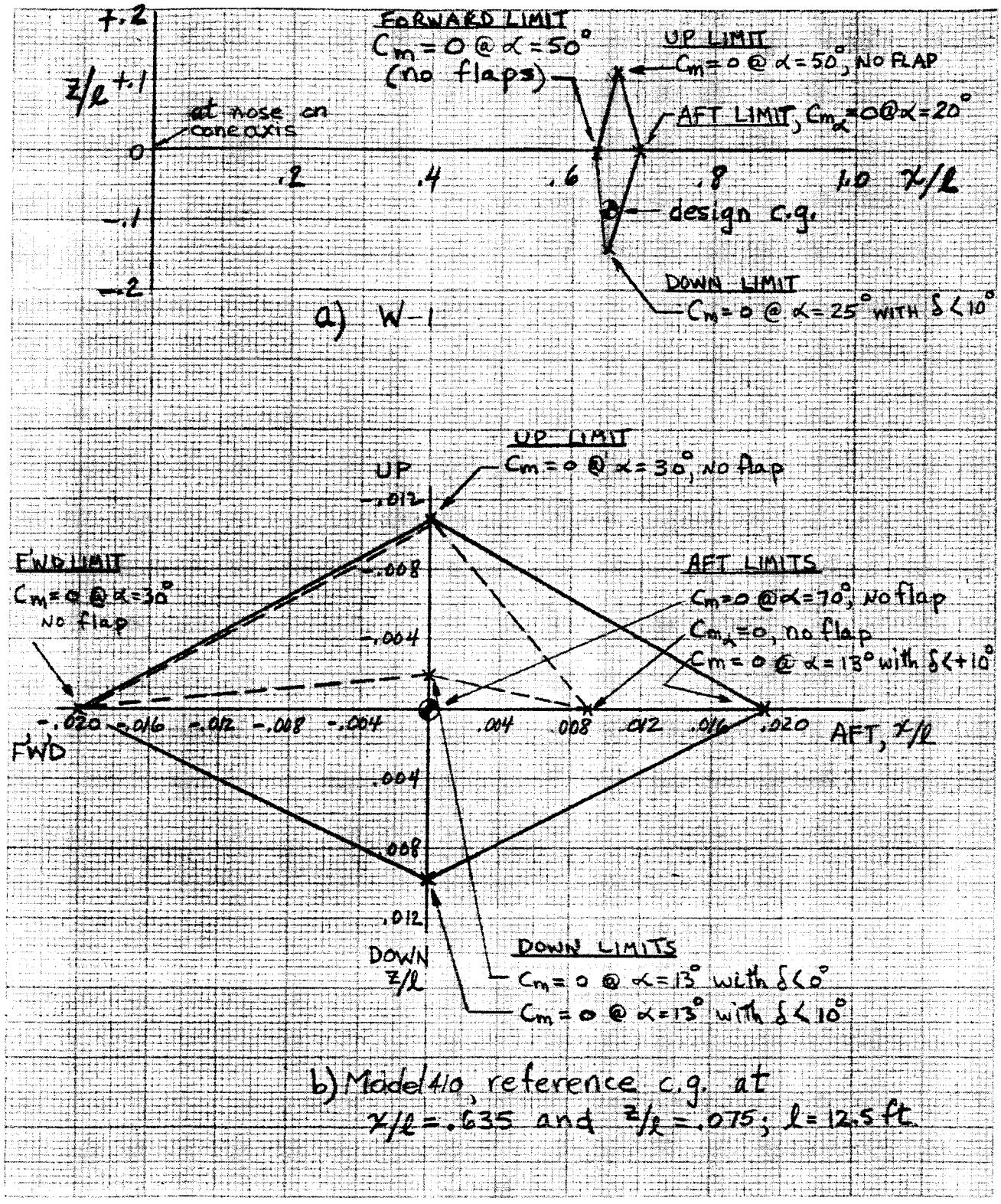

Fig. 8. CG Limits for W-1 and Model 410

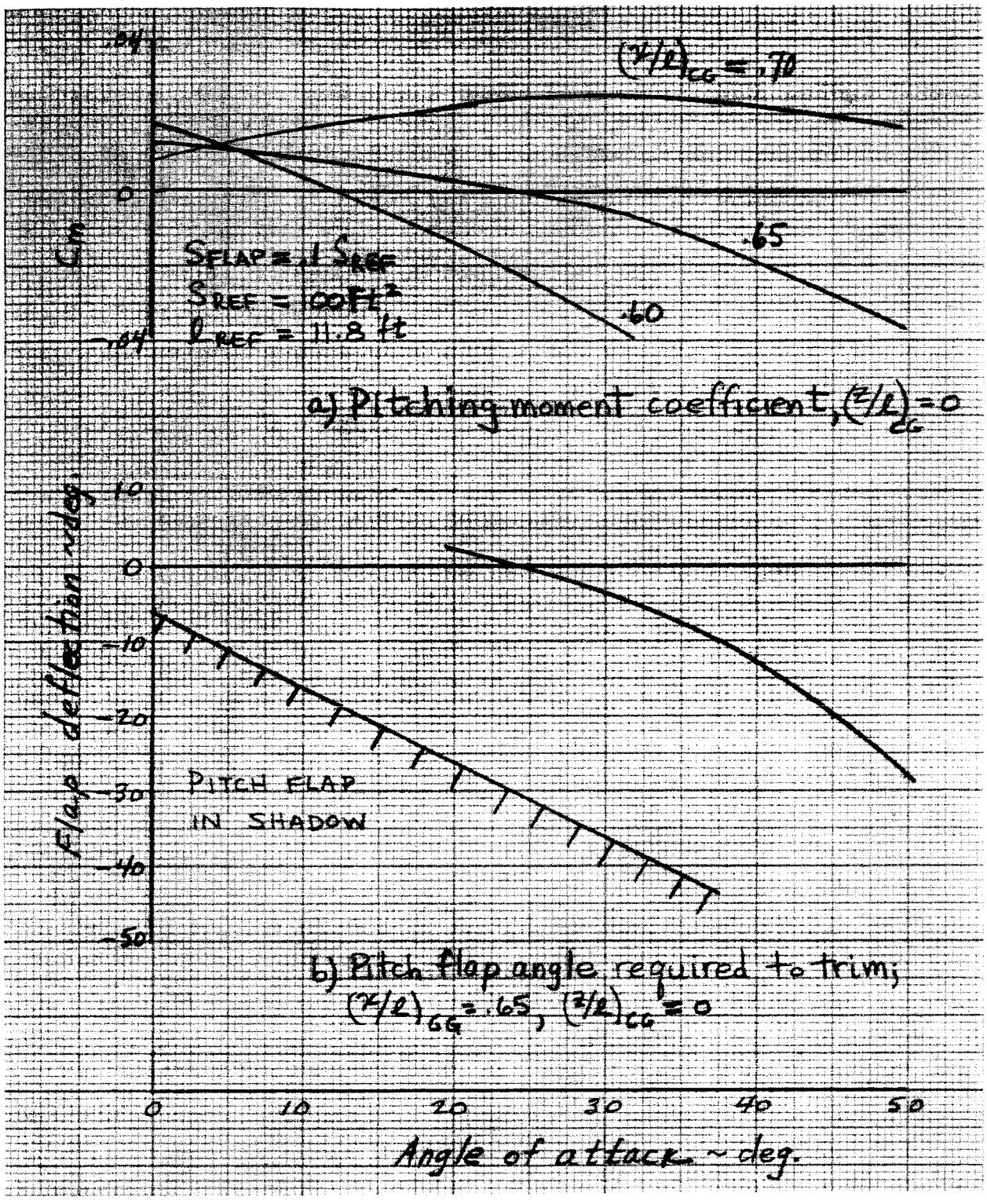

Fig. 9. Longitudinal Control and Pitch Flap Deflection Required to Trim W-1

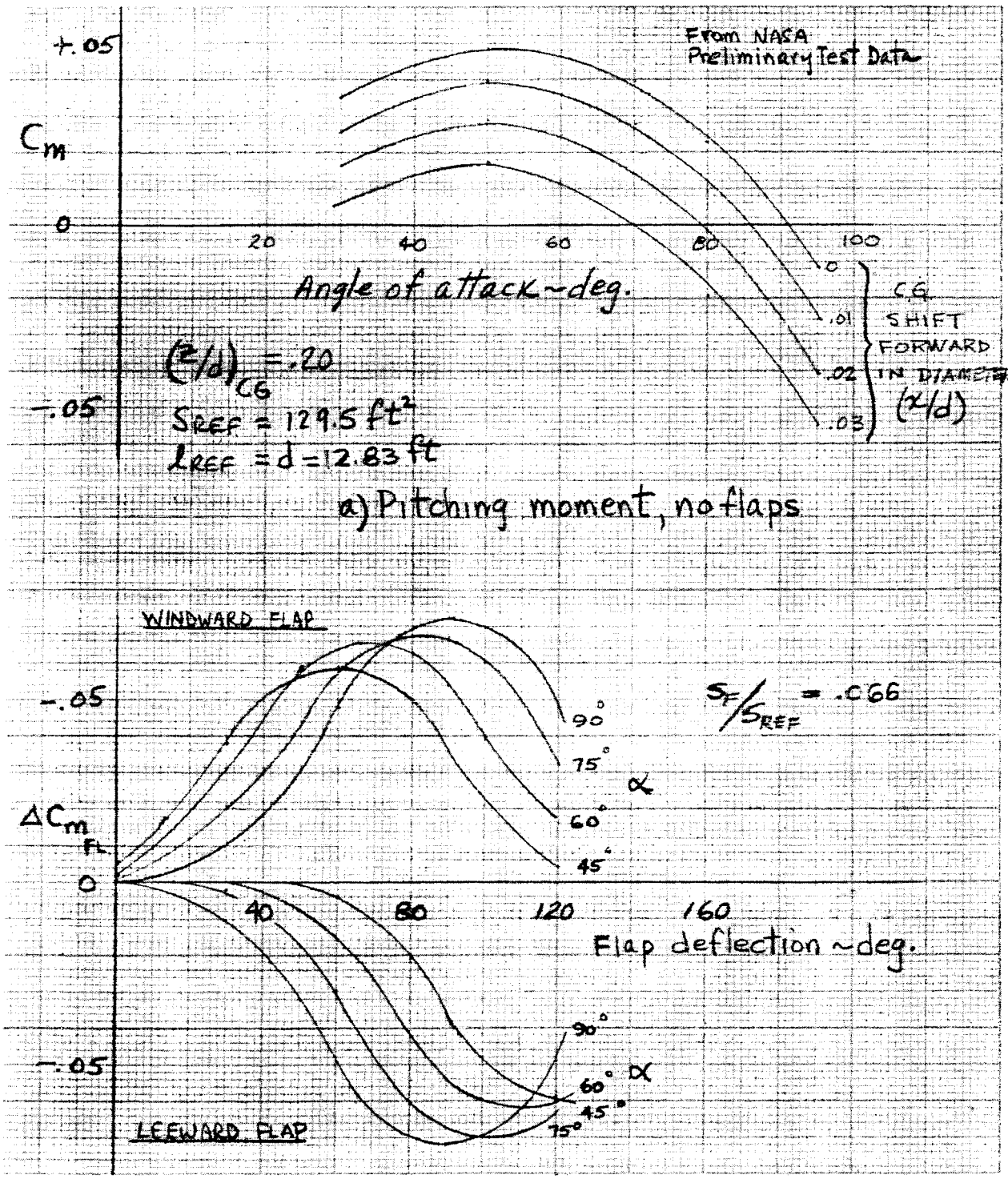

Fig. 10. L-2-C Longitudinal Control

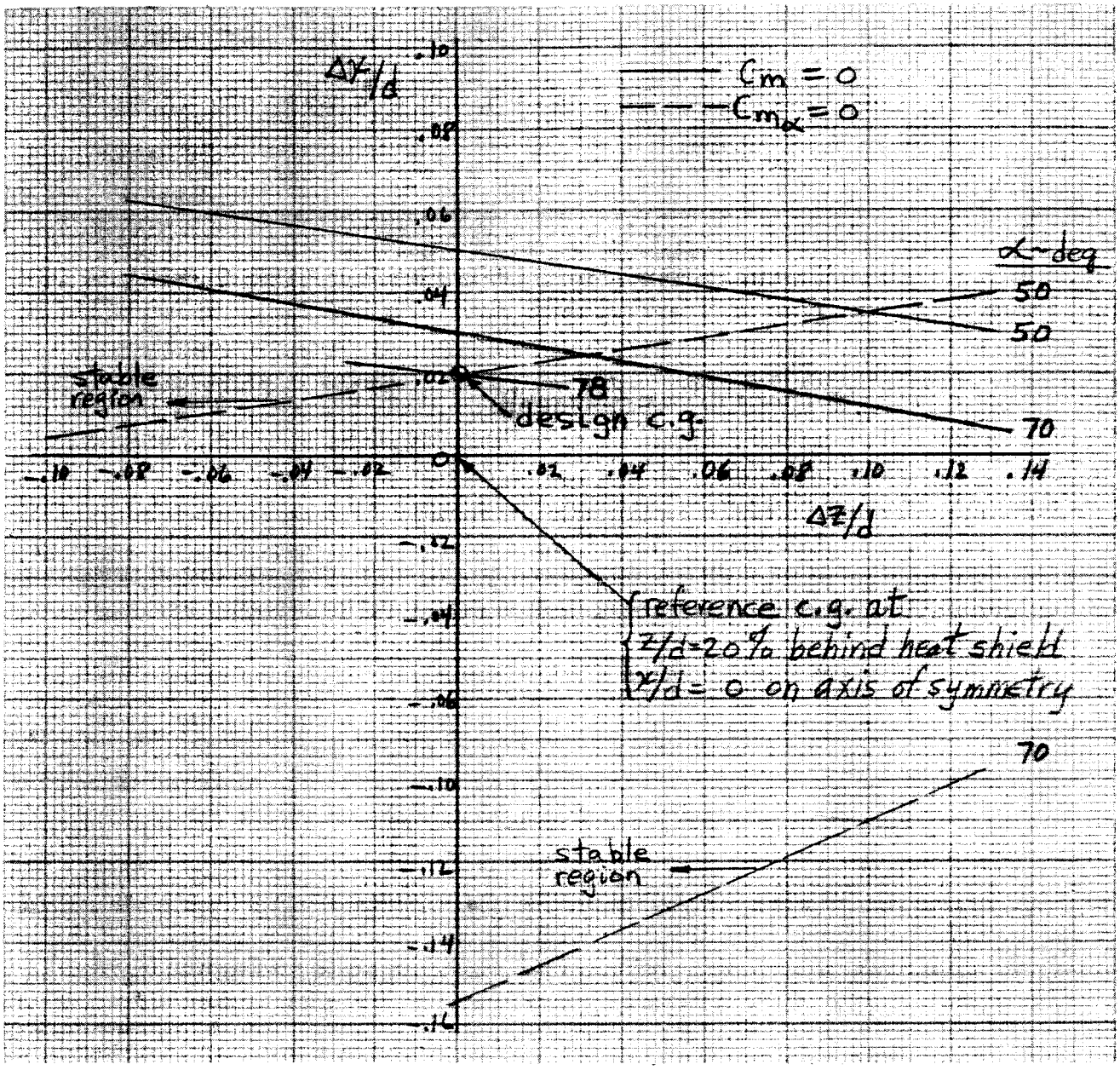

Fig. 11. Effect of CG Location on Longitudinal Characteristics of L-2-C

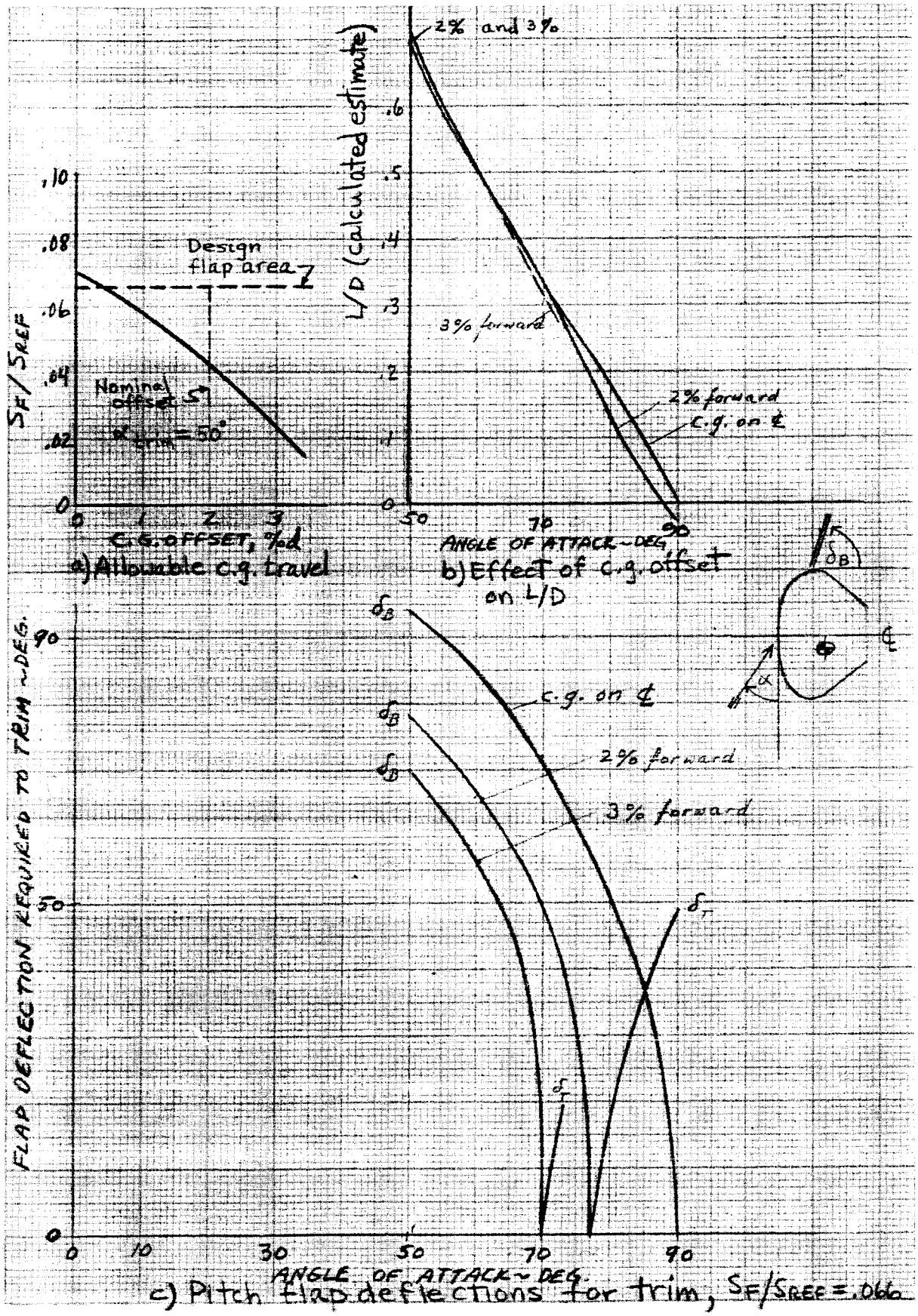

Fig. 12. L-2-C Longitudinal Control Characteristics

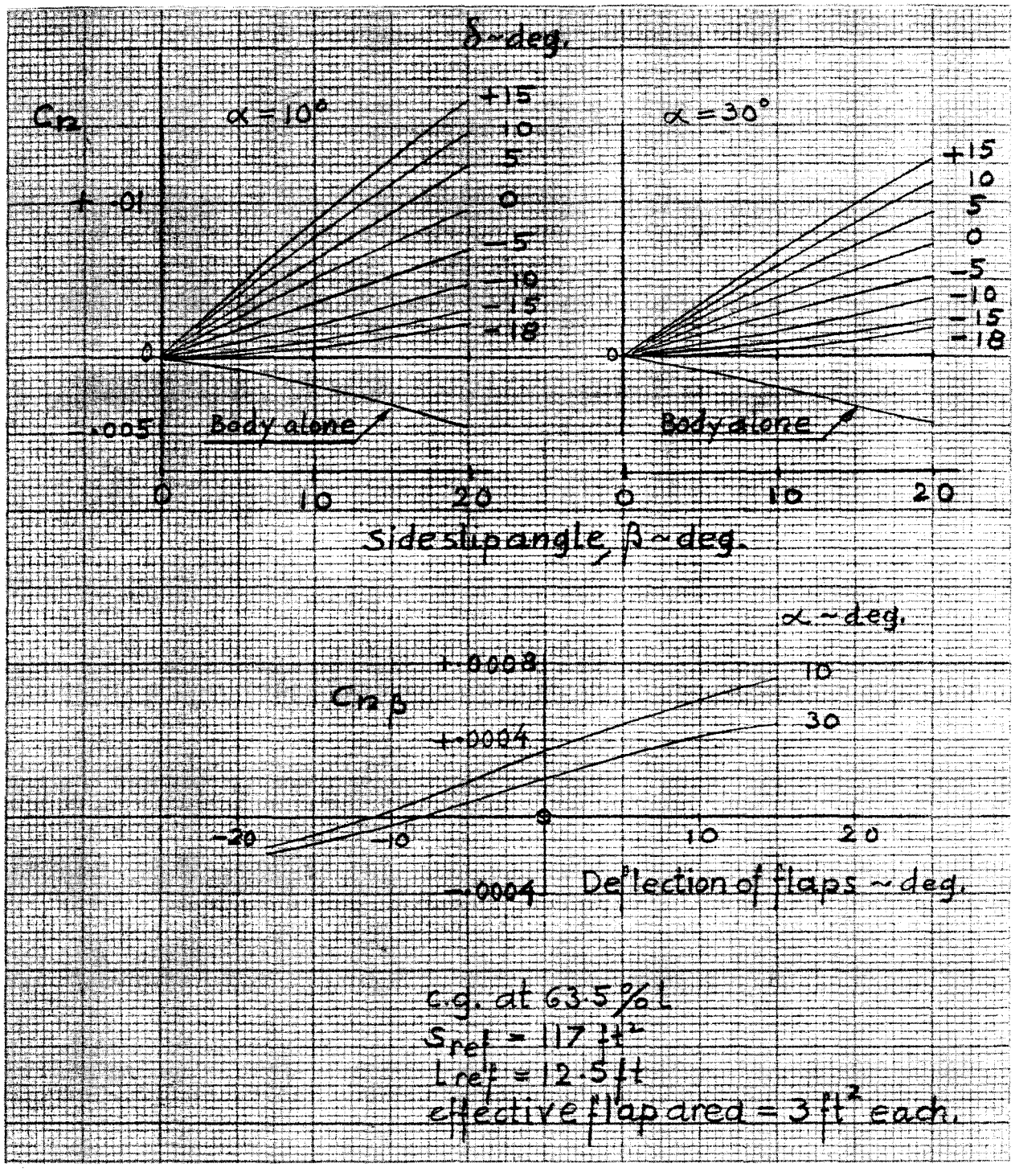

Fig. 13. Directional Stability of Model 410, Body Alone and with Flaps Equally Deflected

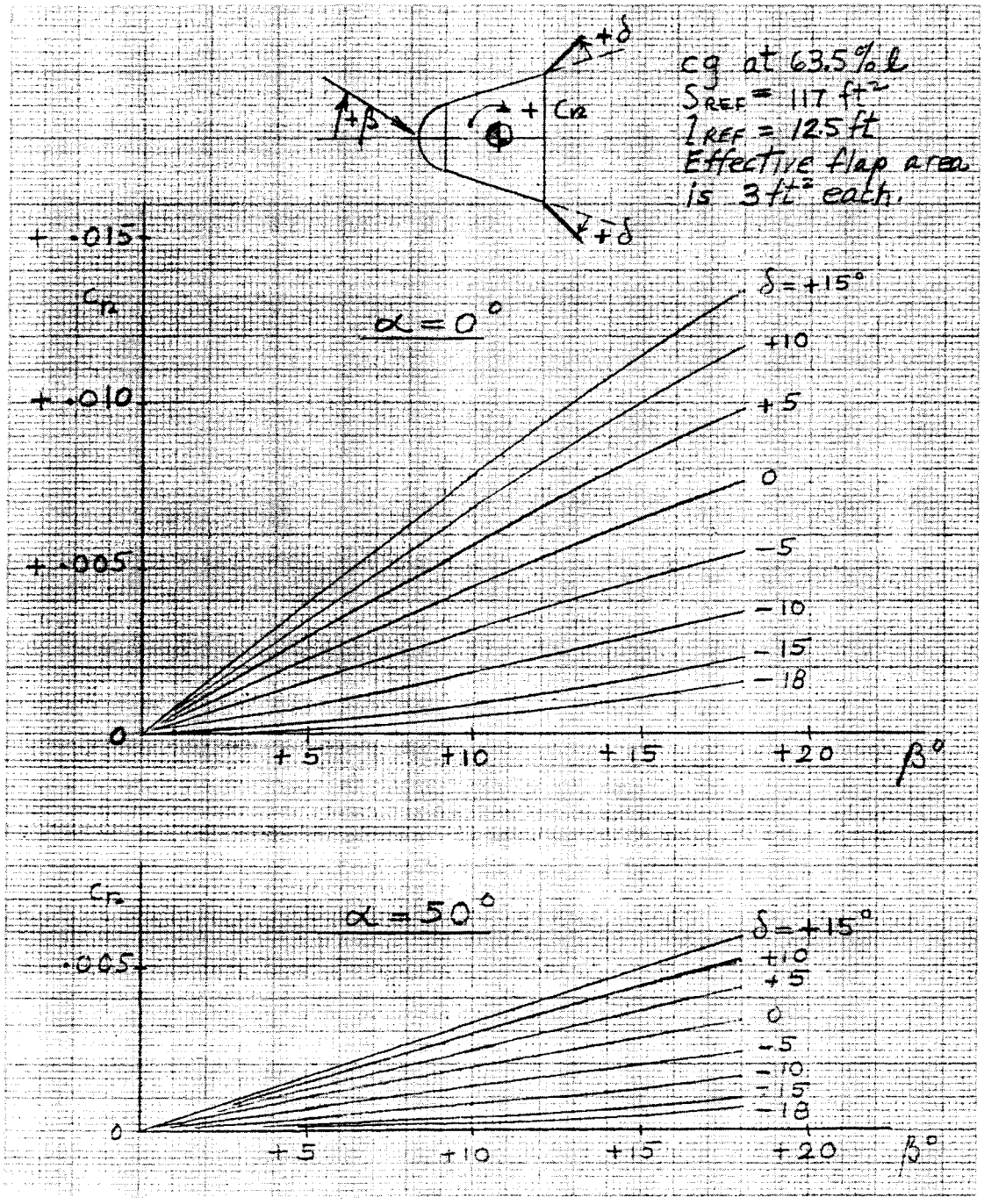

Fig. 14. Model 410 Yawing Moment Coefficients of Side Flaps, Equally Deflected

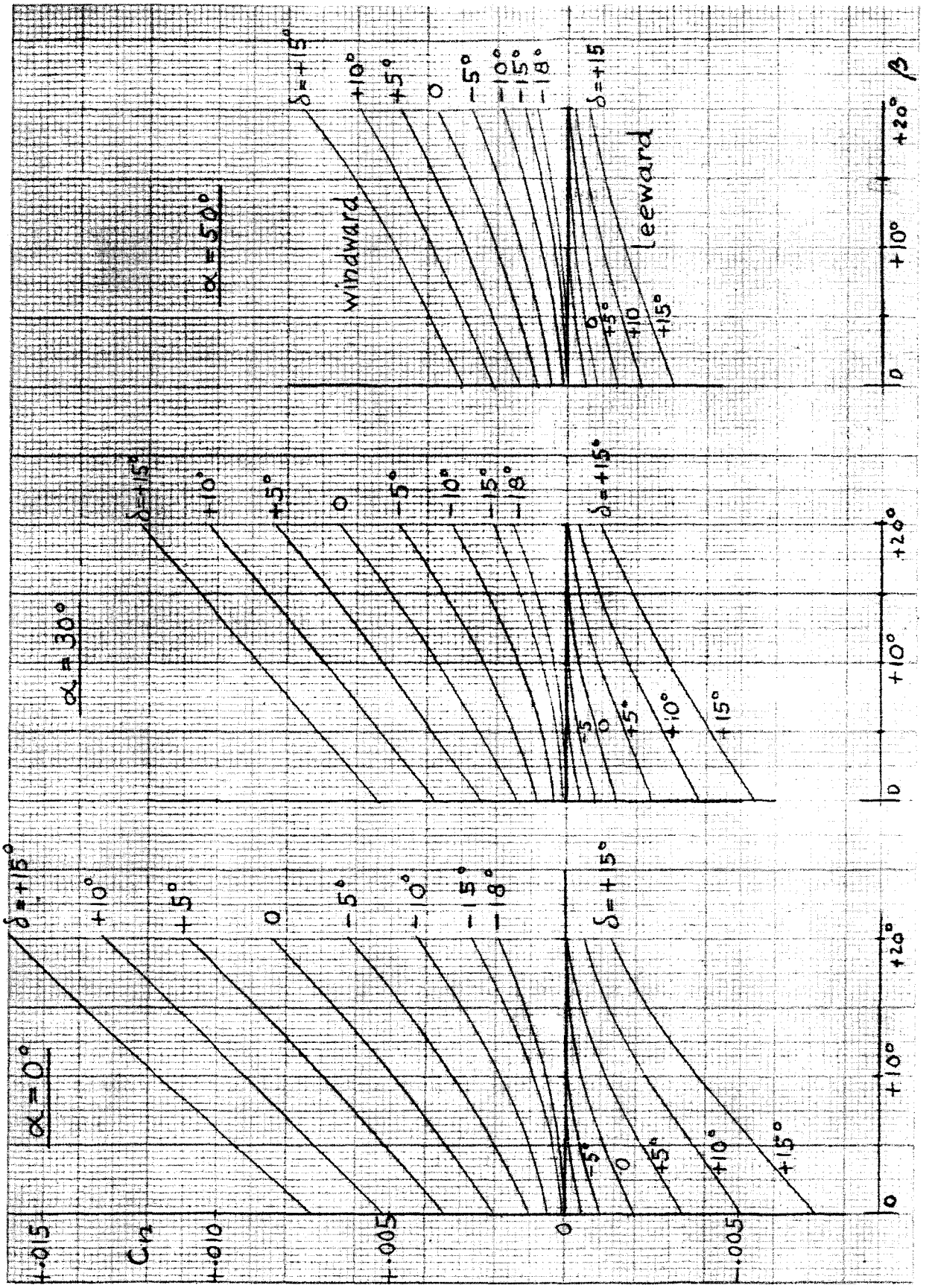

Fig. 15. Model 410 Yawing Moment Coefficients of Side Flaps, Individually Deflected

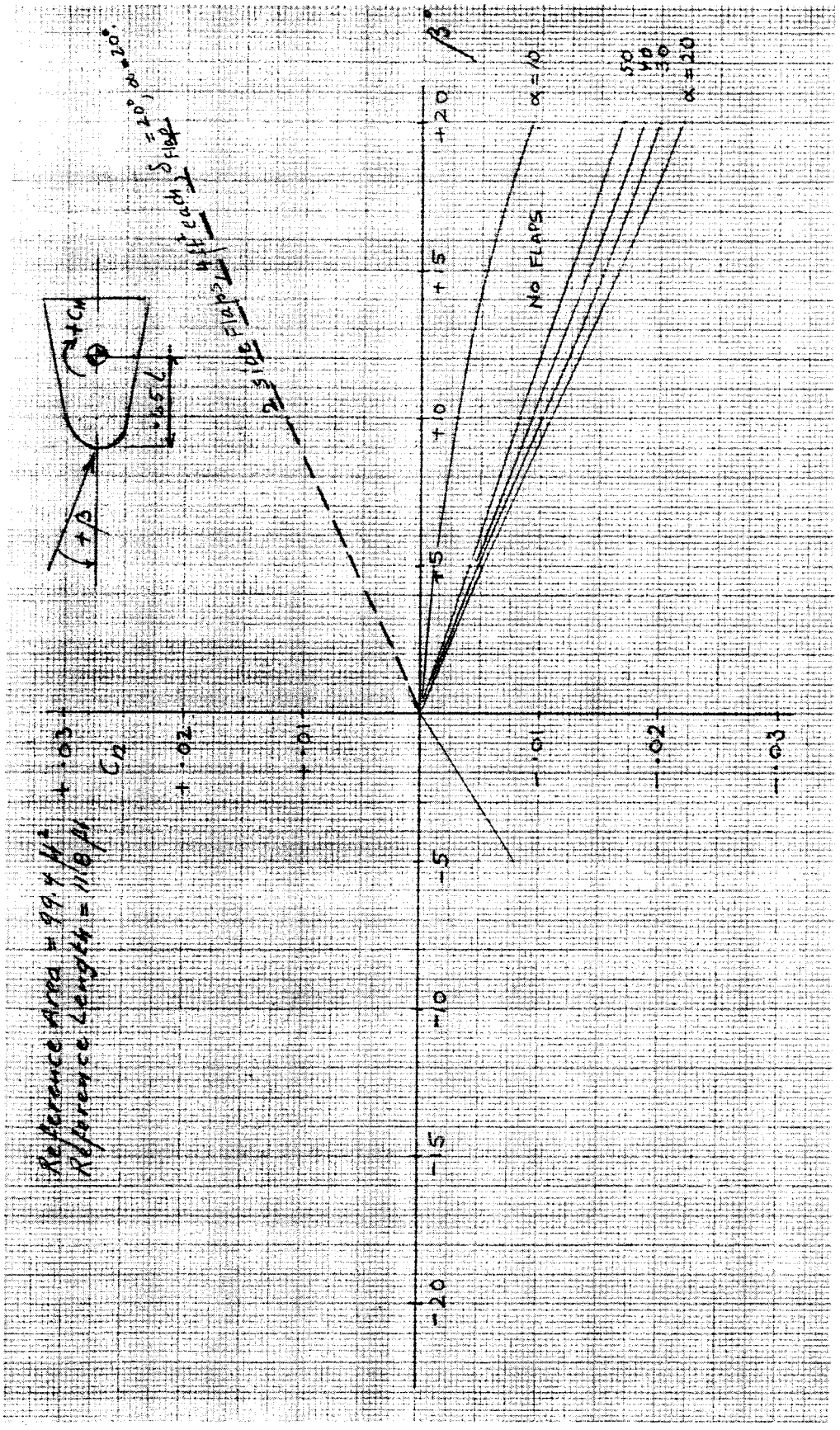

Fig. 16. Directional Characteristics of W-1

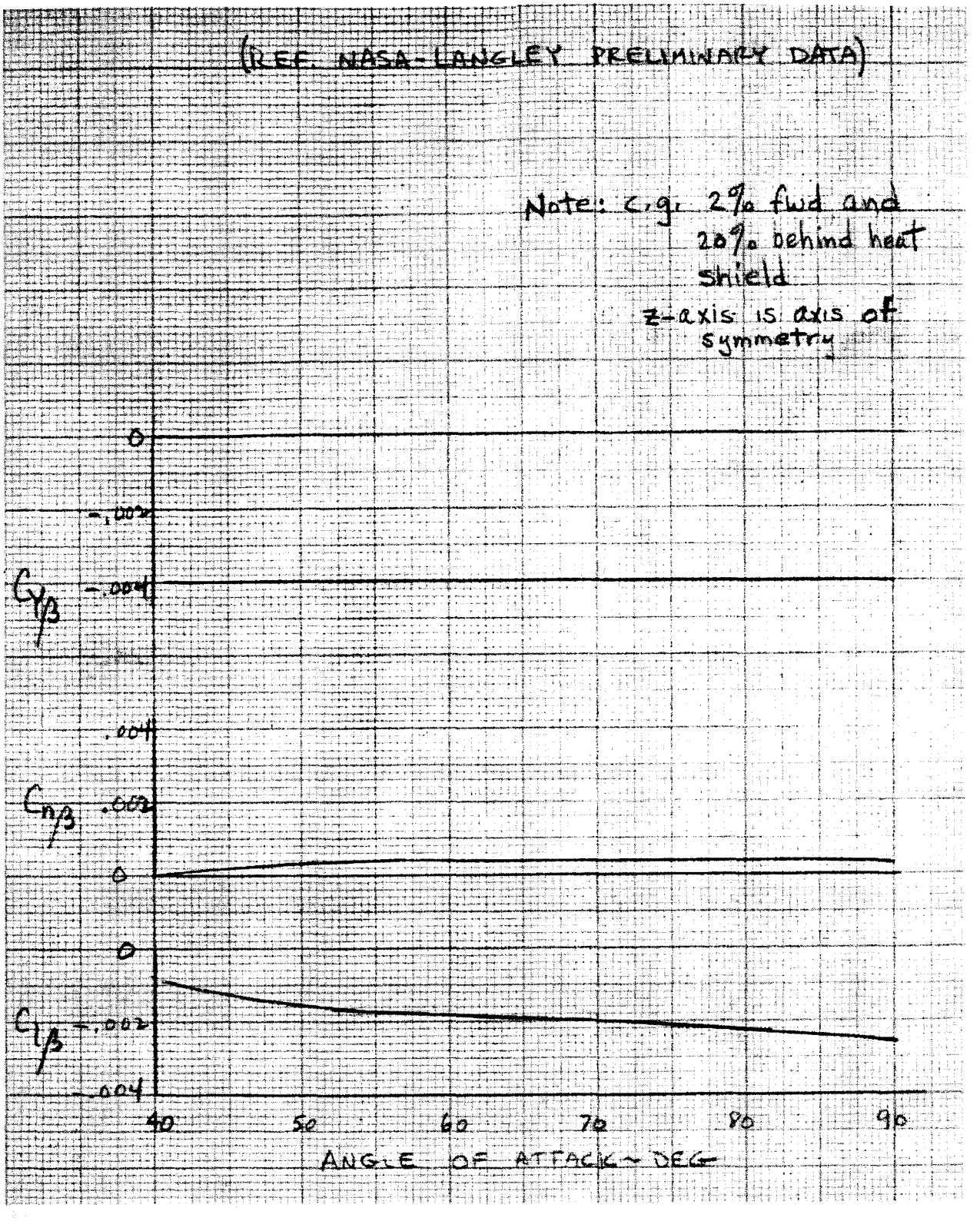

Fig. 17. C_{y_β}, C_{n_β} and C_{l_β} for L-2-C

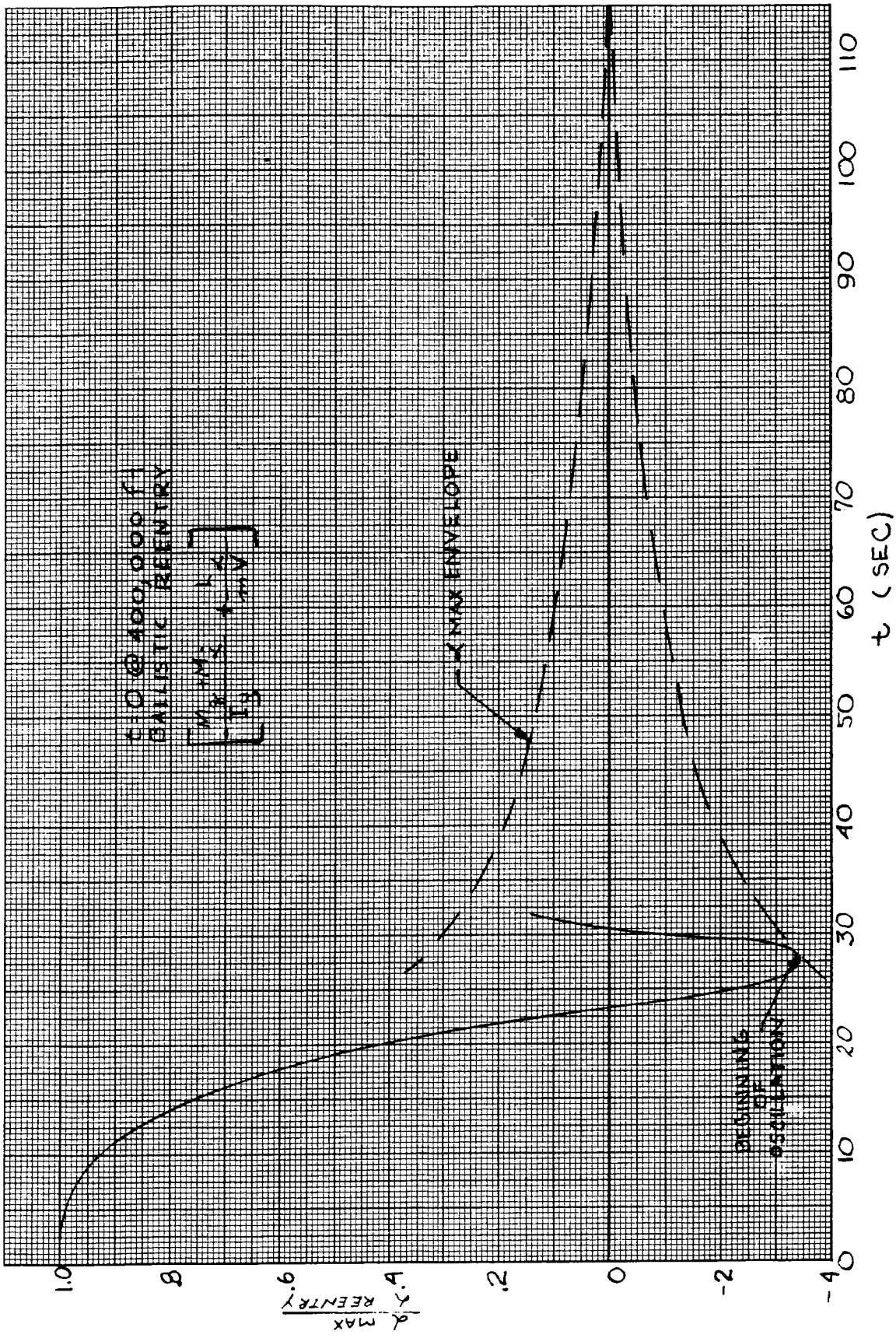

Fig. 18. Maximum Re-entry Angle of Attack Envelope, Model 410 Re-entry Vehicle

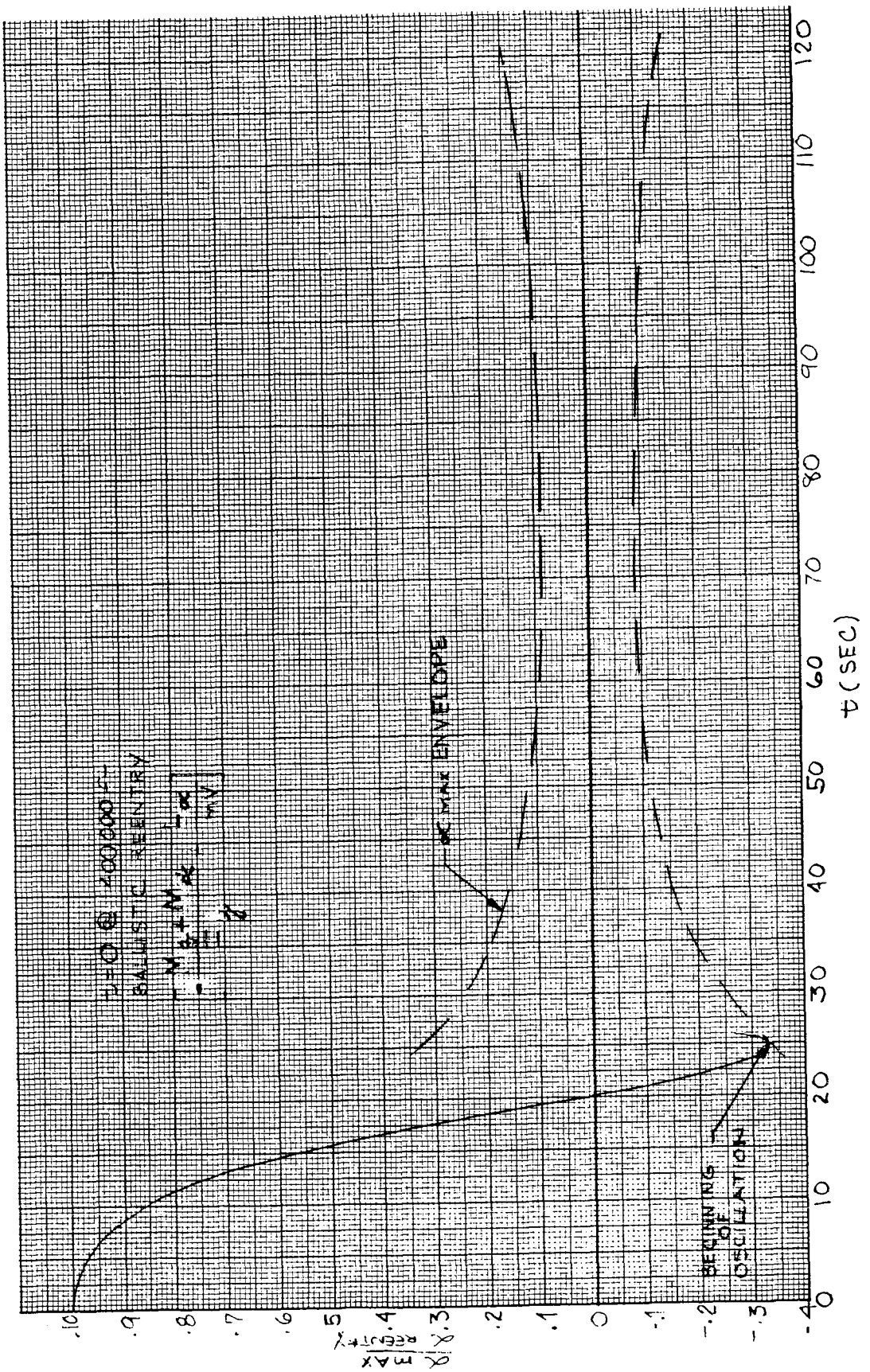

Fig. 19. Maximum Re-entry Angle of Attack Envelope, Mercury Re-entry Vehicle

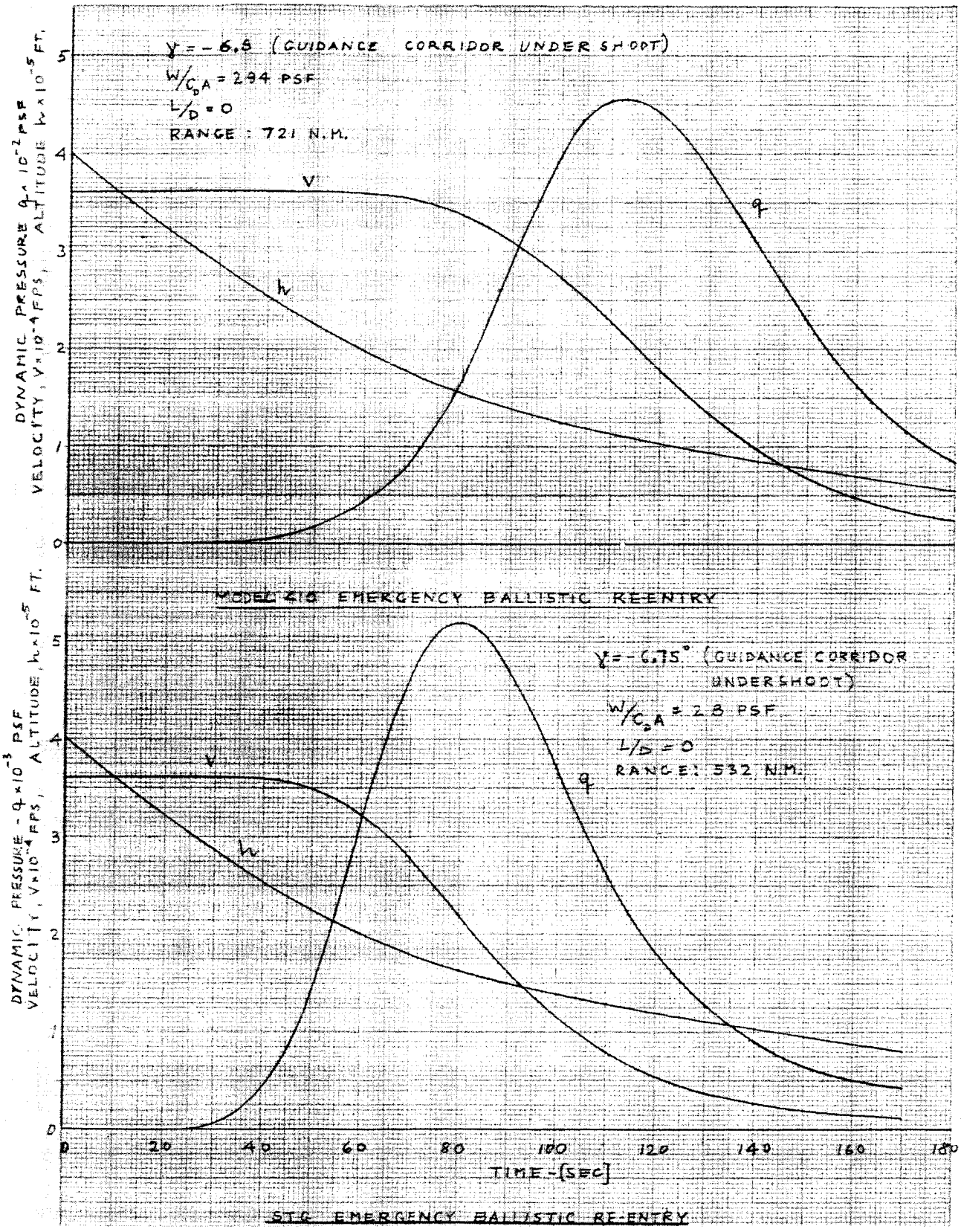

Fig. 20. Emergency Re-entry Trajectories for Model 410 and STG

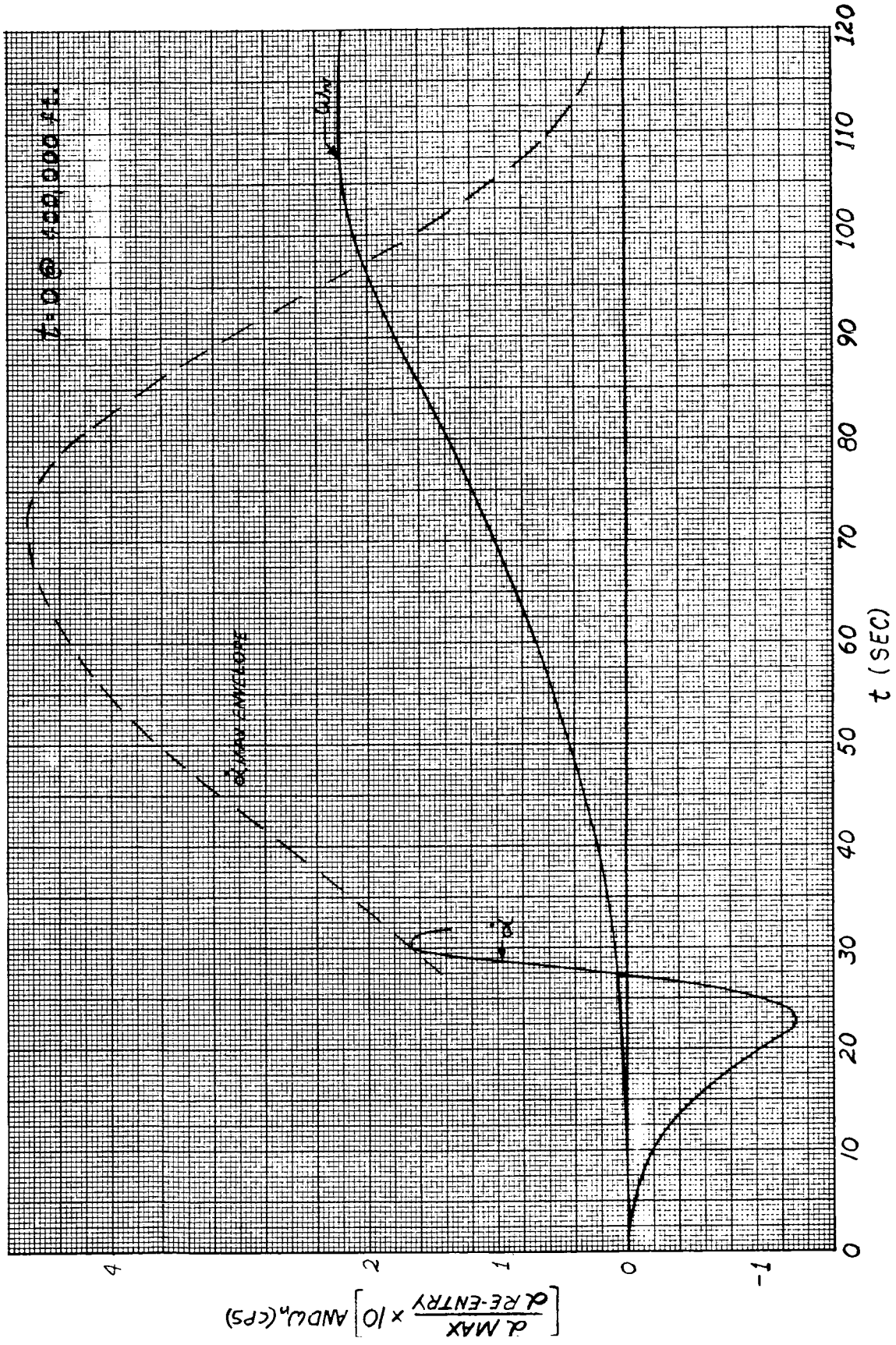

Fig. 21. Dynamic Motion of Model 410 Re-entry Vehicle

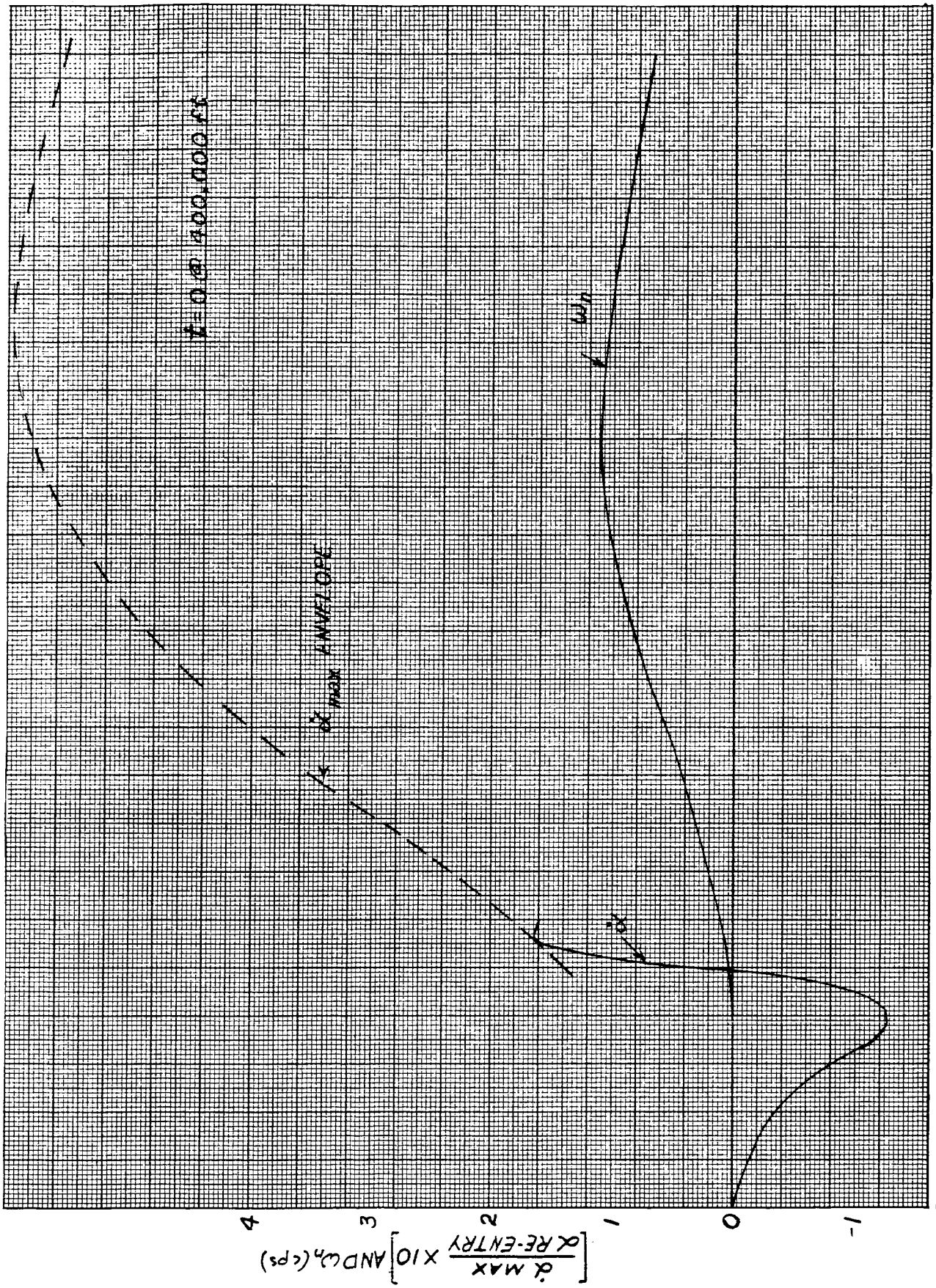

Fig. 22. Dynamic Motion of Mercury Re-entry Vehicle

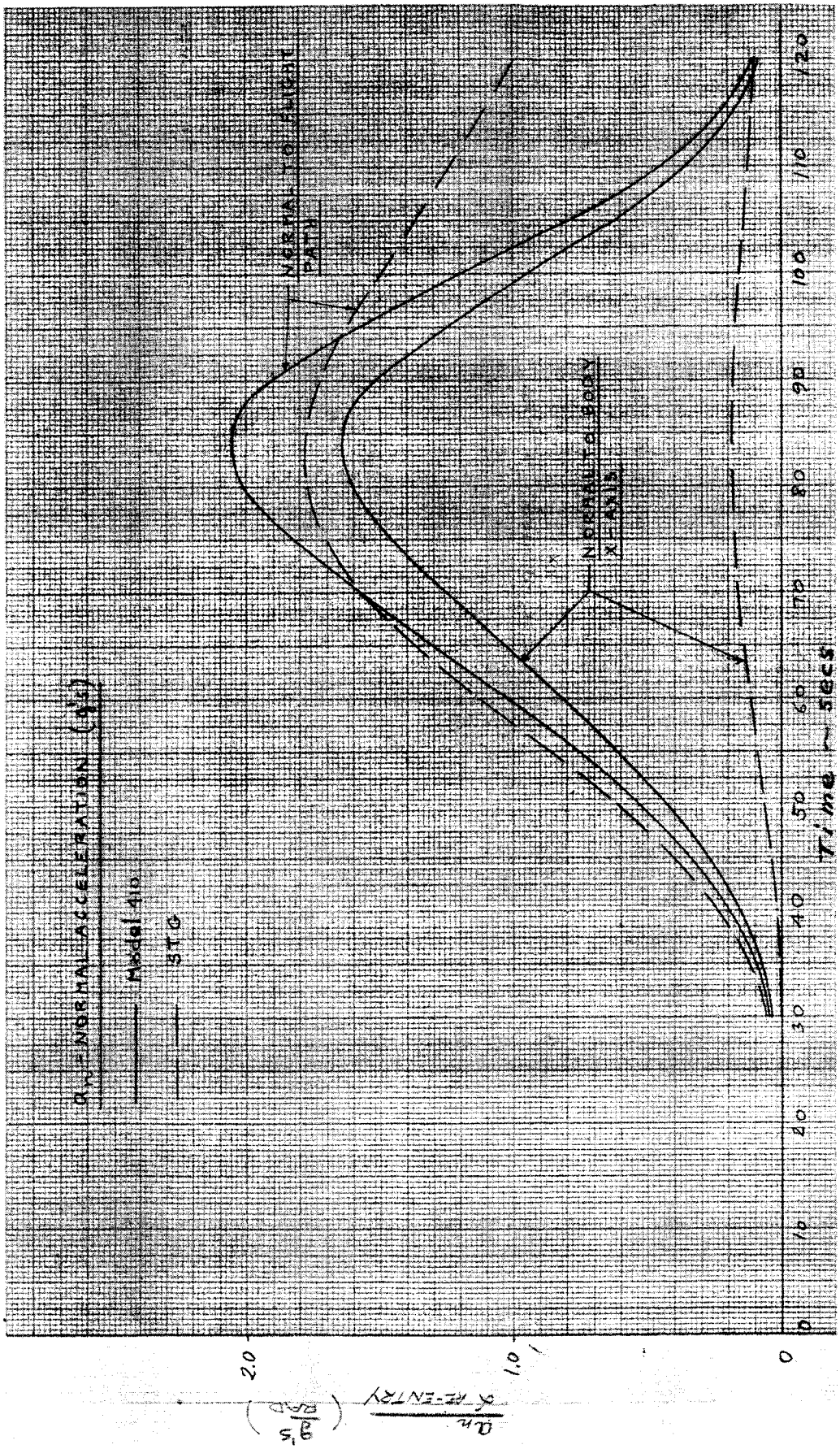

Fig. 23. Maximum Normal Acceleration Envelopes

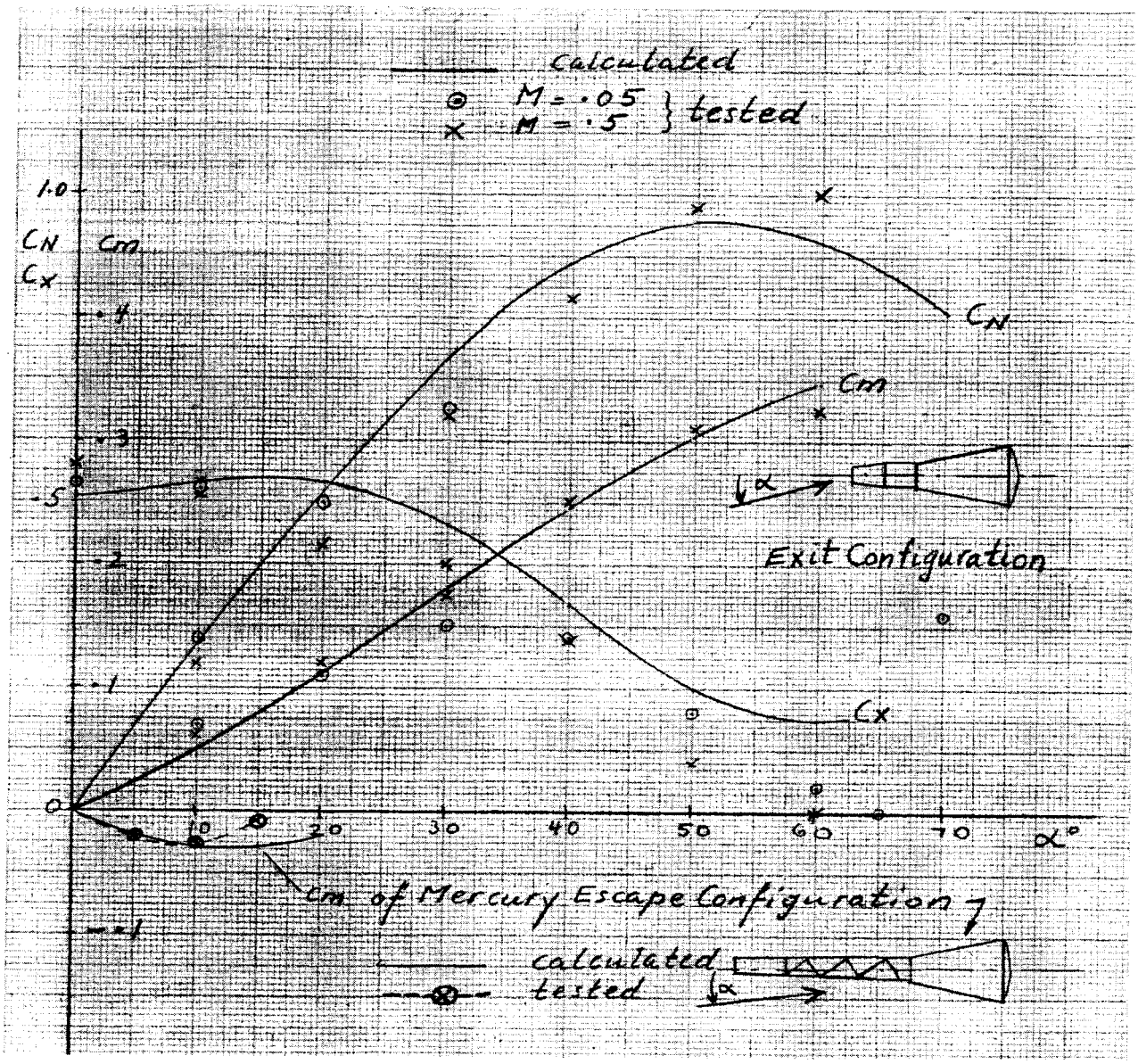

Fig. 24. Subsonic Data for the Mercury Exit and Escape Configurations Including Comparison with Calculated Results

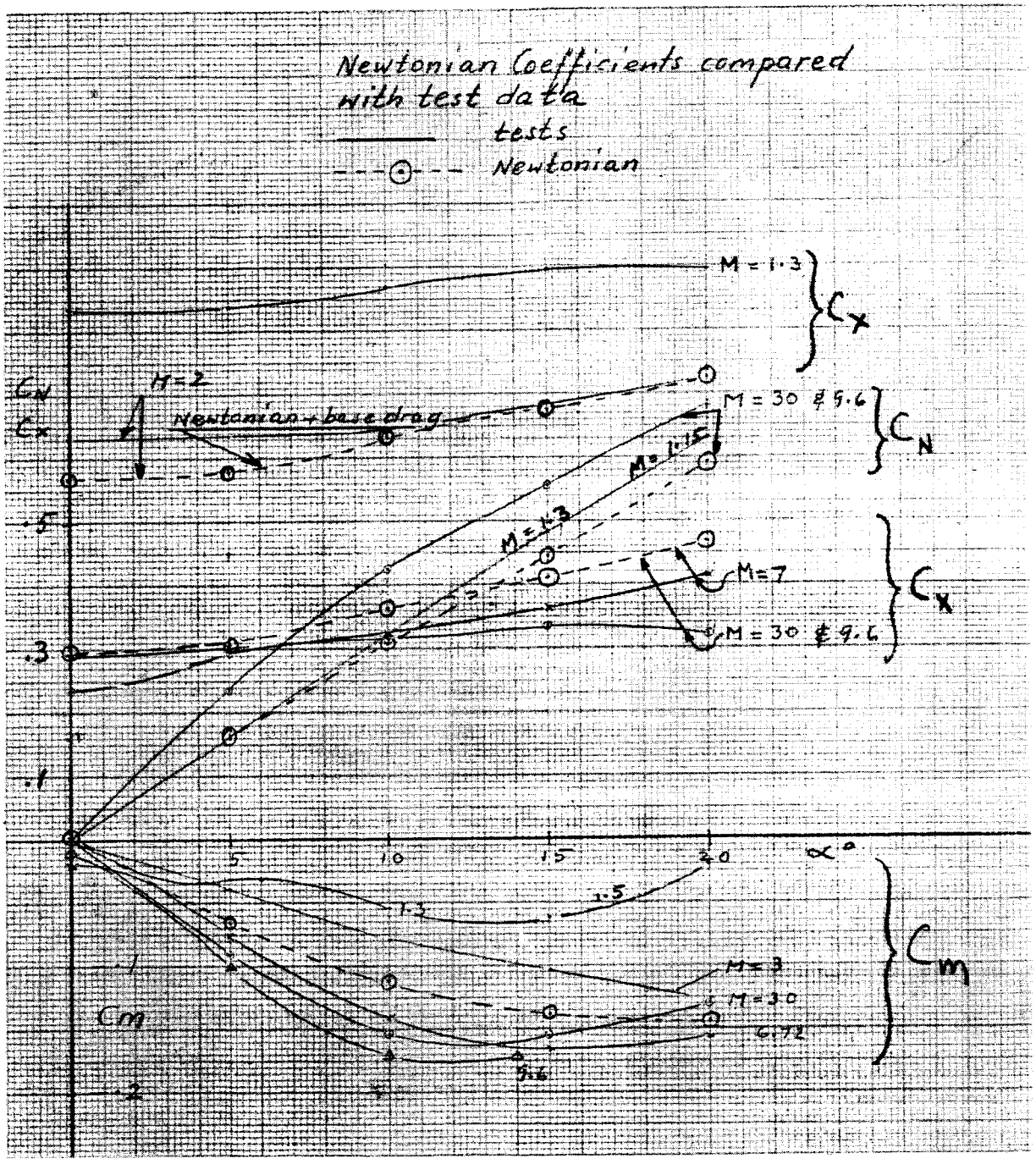

Fig. 25. Subsonic Data for Mercury Escape Configuration Including Comparison with Calculated Results

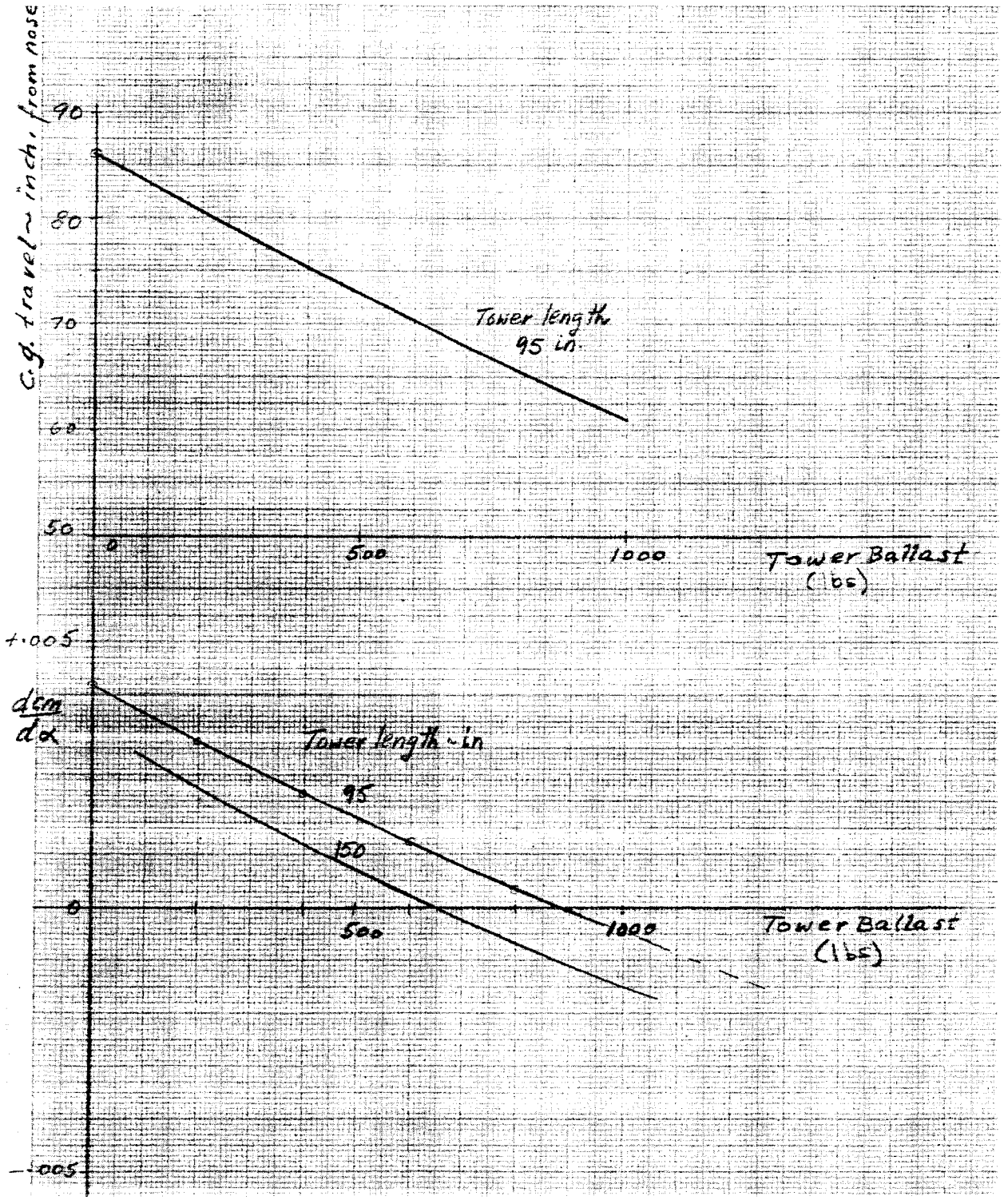

Fig. 26. Effect of Tower Ballast on Subsonic of Model 410 and W-1 Escape Configurations

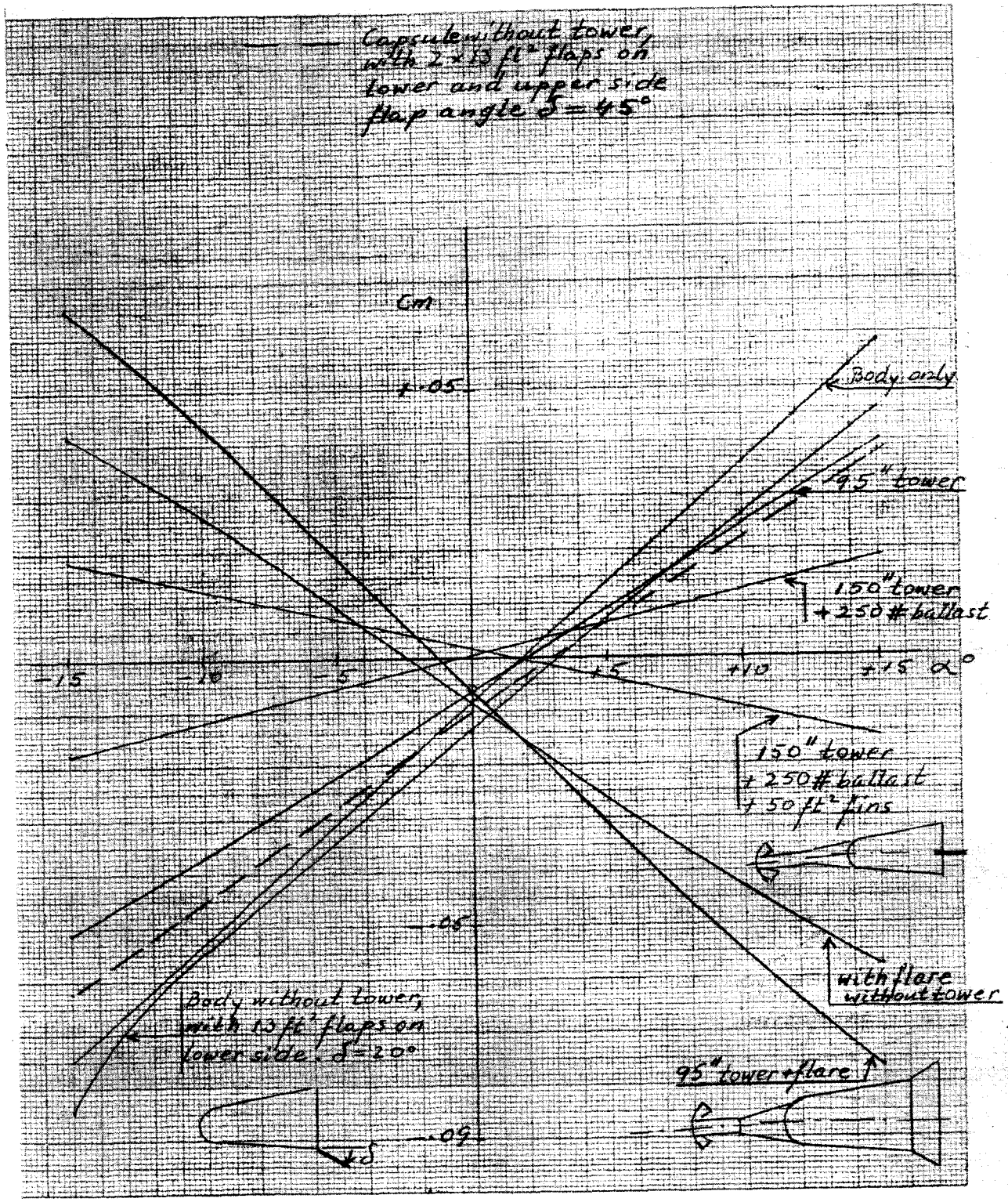

Fig. 27. Subsonic Stability Data for Model 410 and W-1 Escape and Exit Configurations

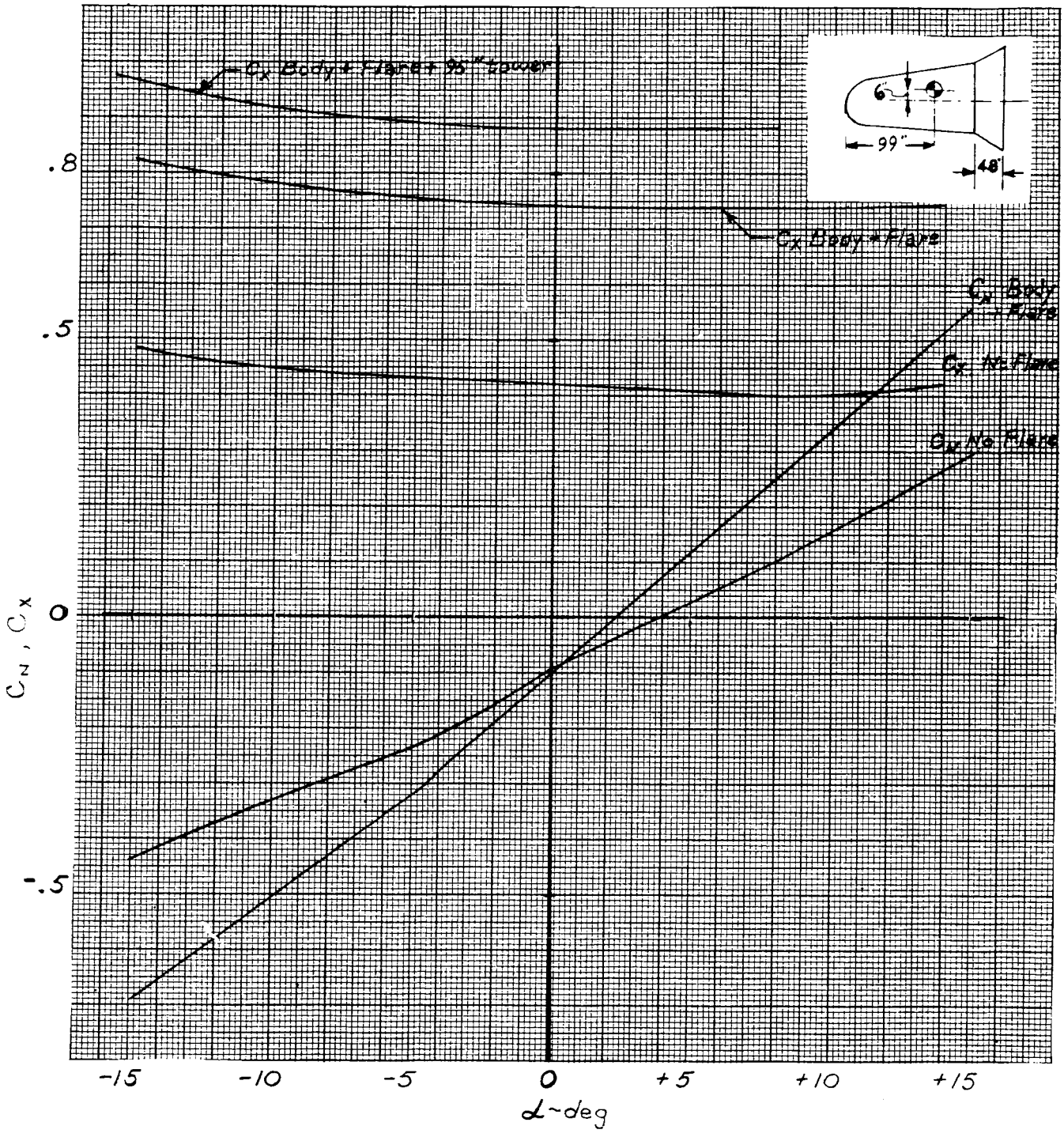

Fig. 28. Subsonic Axial and Normal Force Data for Model 410 and W-1 Escape Configurations

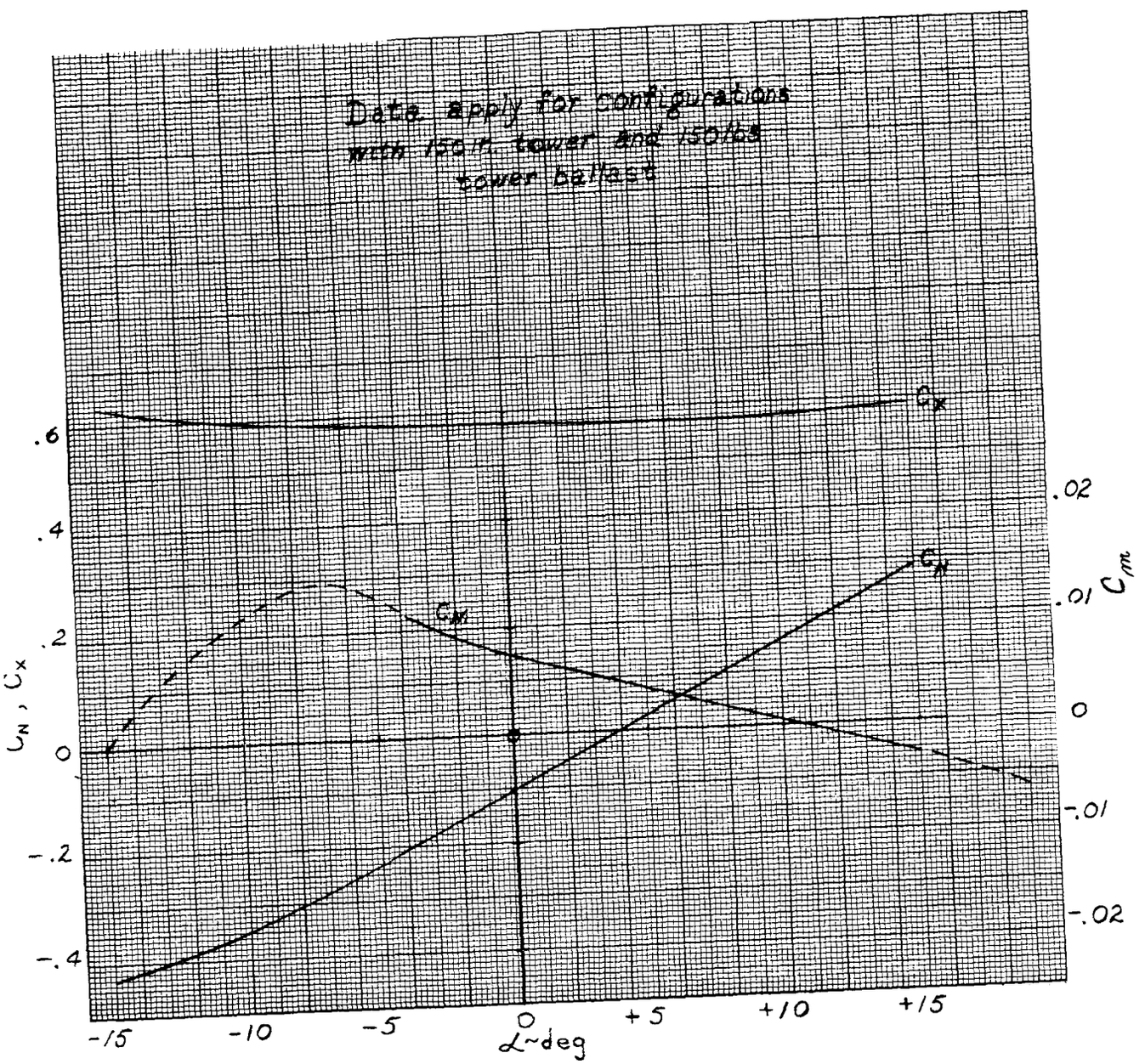

Fig. 29. Mach 1.3 Aerodynamic Data for Model 410 and W-1 Escape Configurations

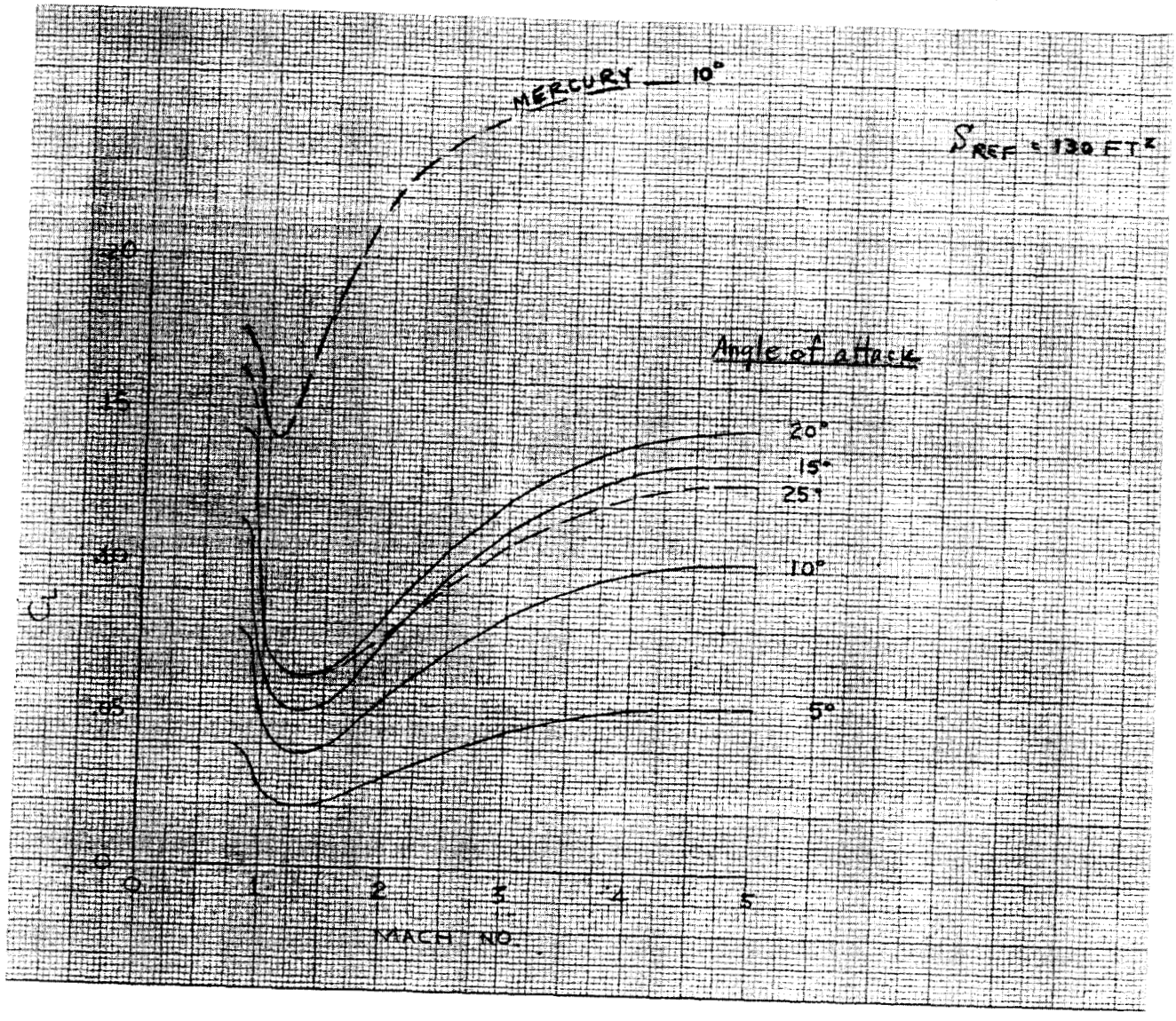

Fig. 30. Lift Coefficients as Functions of Mach Number and Angle of Attack for L-2C Escape Configuration

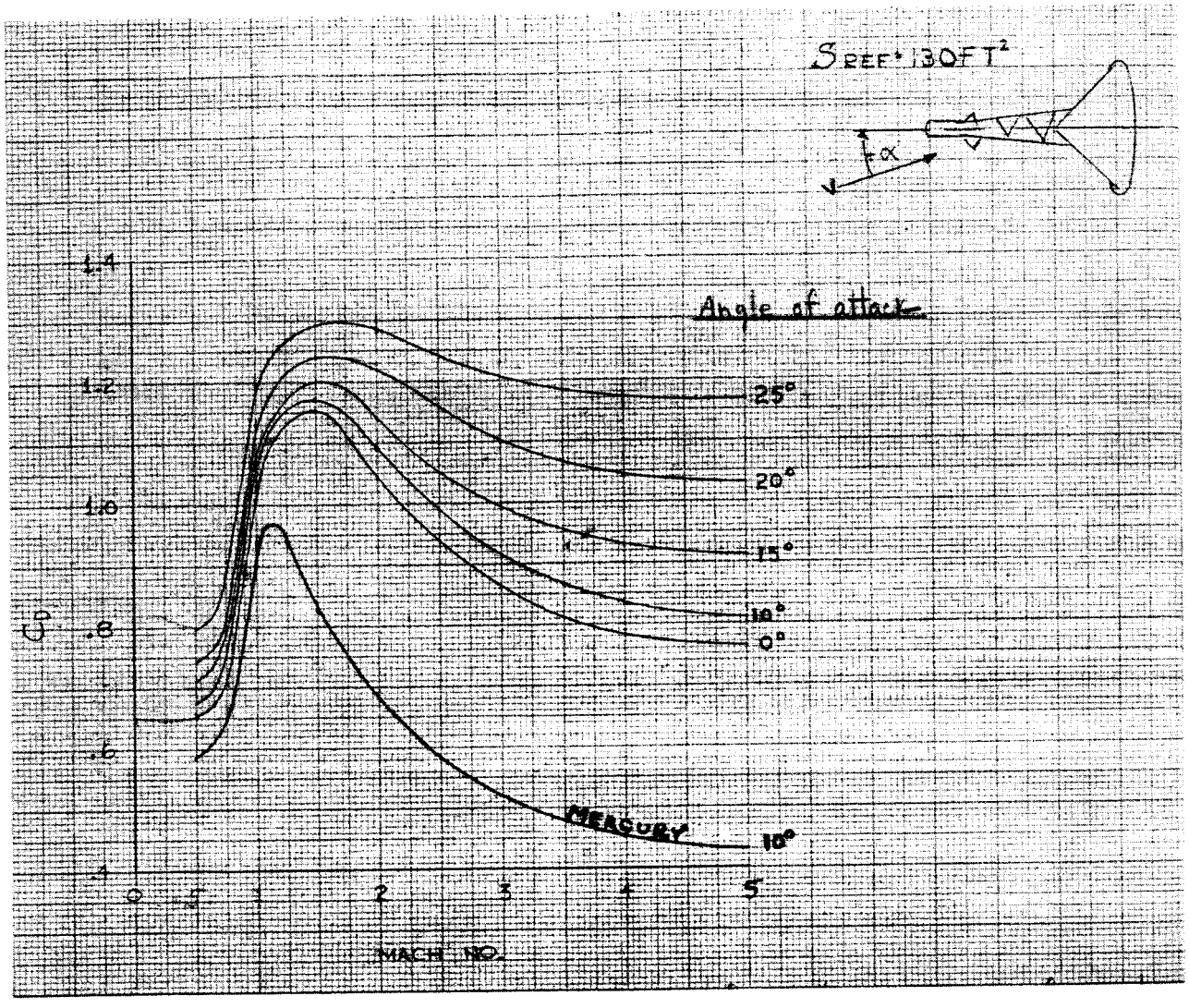

Fig. 31. Drag Coefficients as Functions of Mach Number and Angle of Attack for L-2C Escape Configurations

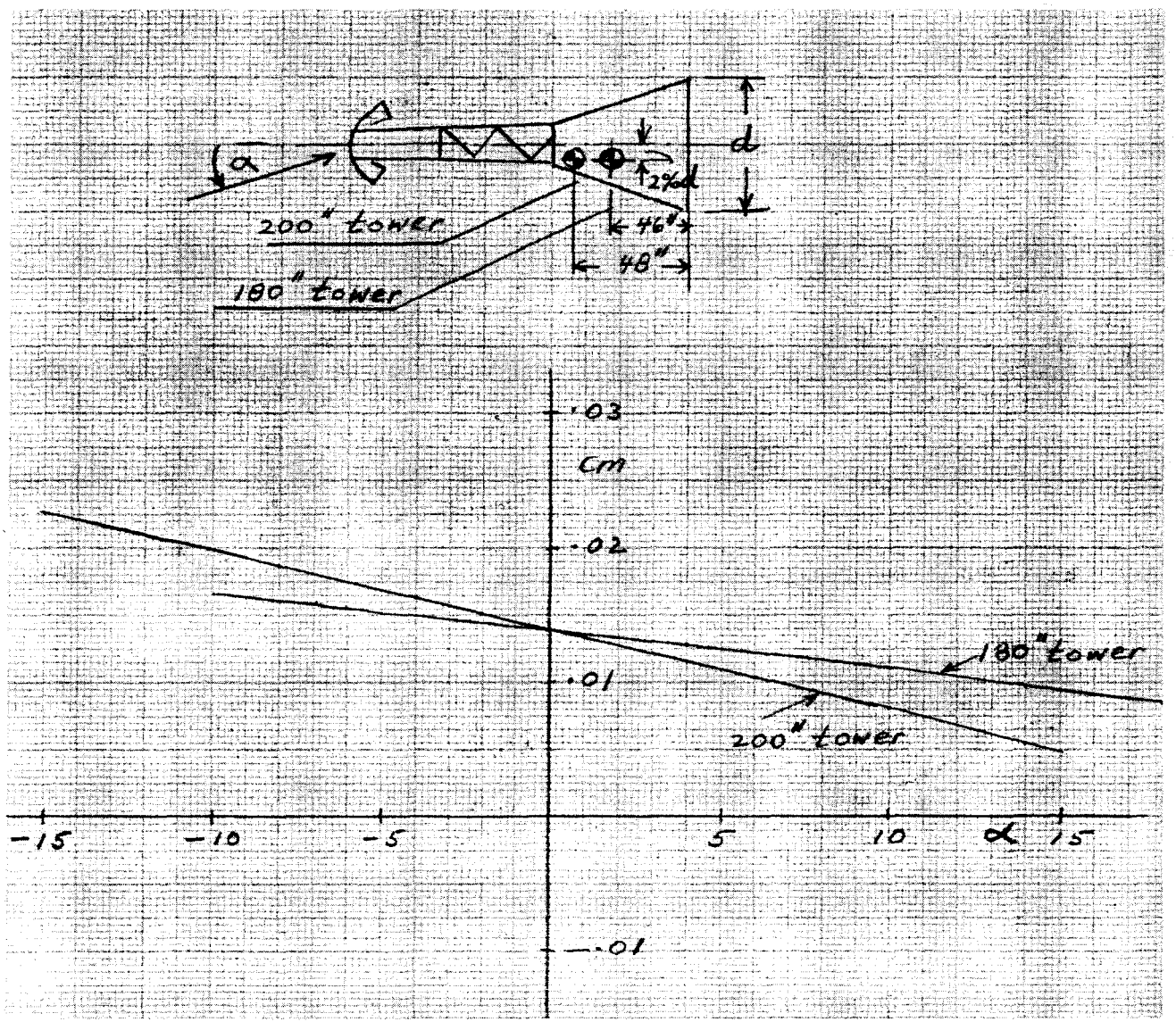

Fig. 32. Subsonic Stability Data for L-2C Escape Configuration Without Tower Ballast

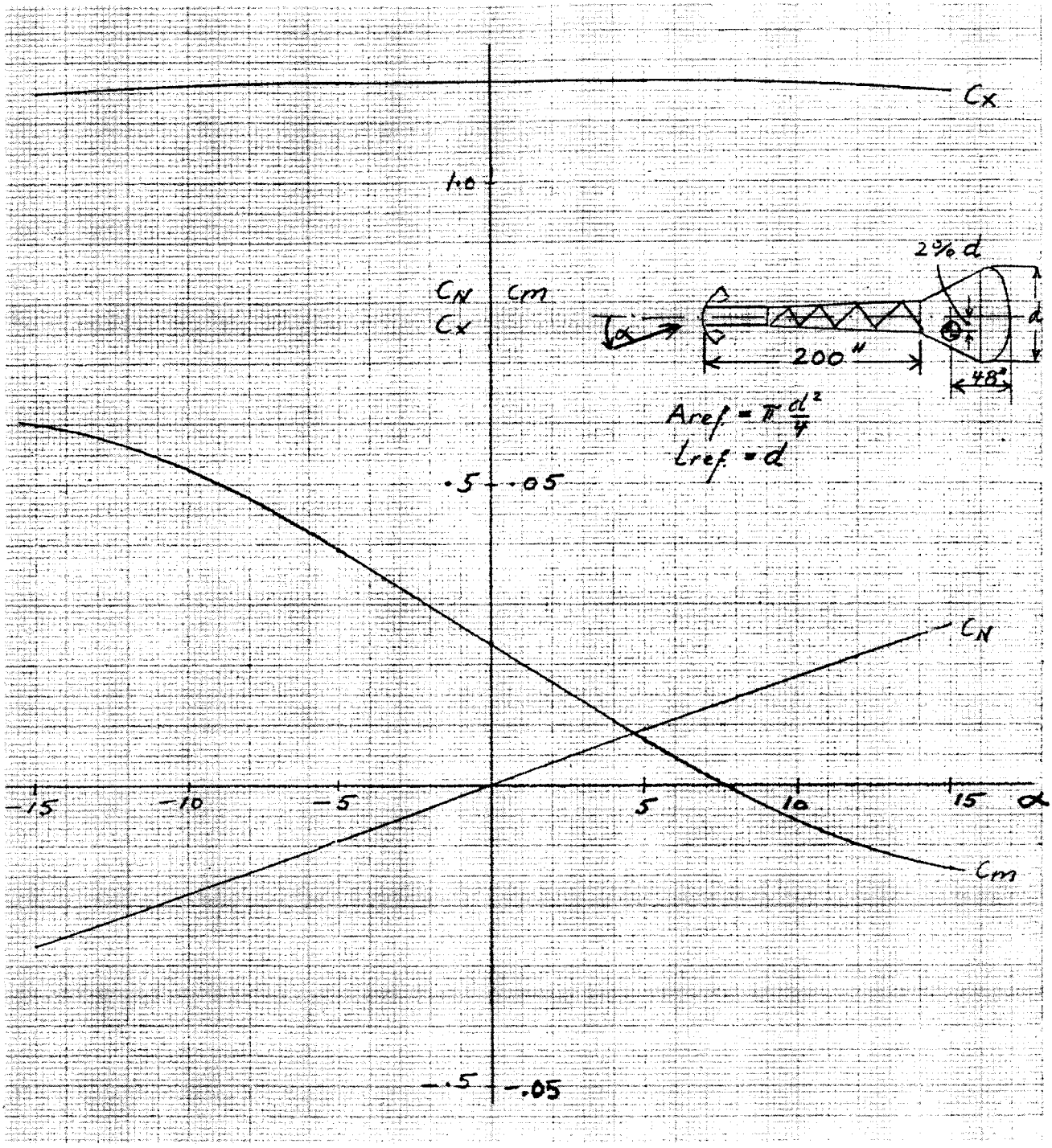

Fig. 33. Mach 1.3 Aerodynamic Data for L-2C Escape Configuration with 200-Inch Tower

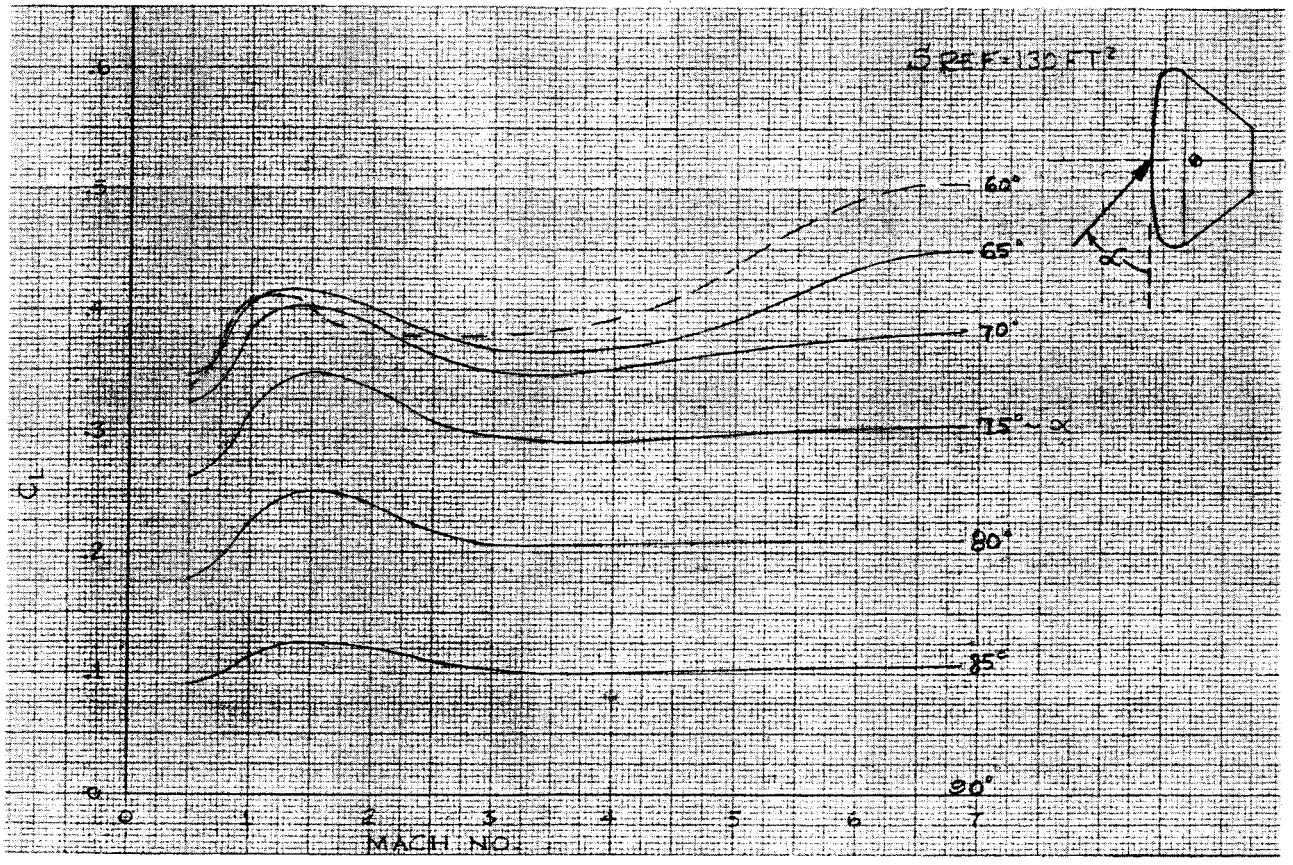

Fig. 34. Lift Coefficients as Functions of Mach Number and Angle of Attack for L-2C Re-entry Configuration

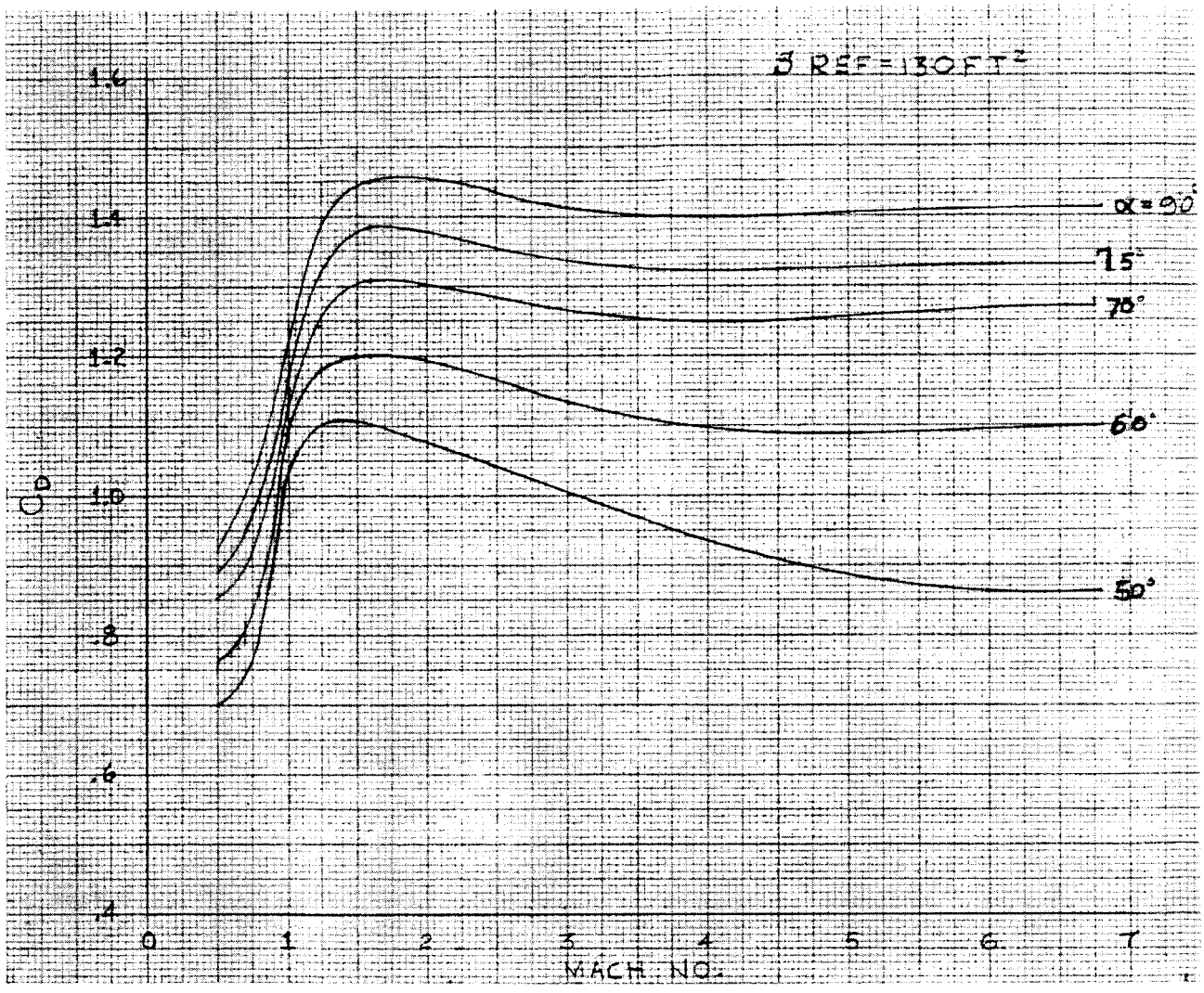

Fig. 35. Drag Coefficients as Functions of Mach Number and Angle of Attack for L-2C Re-entry Configuration

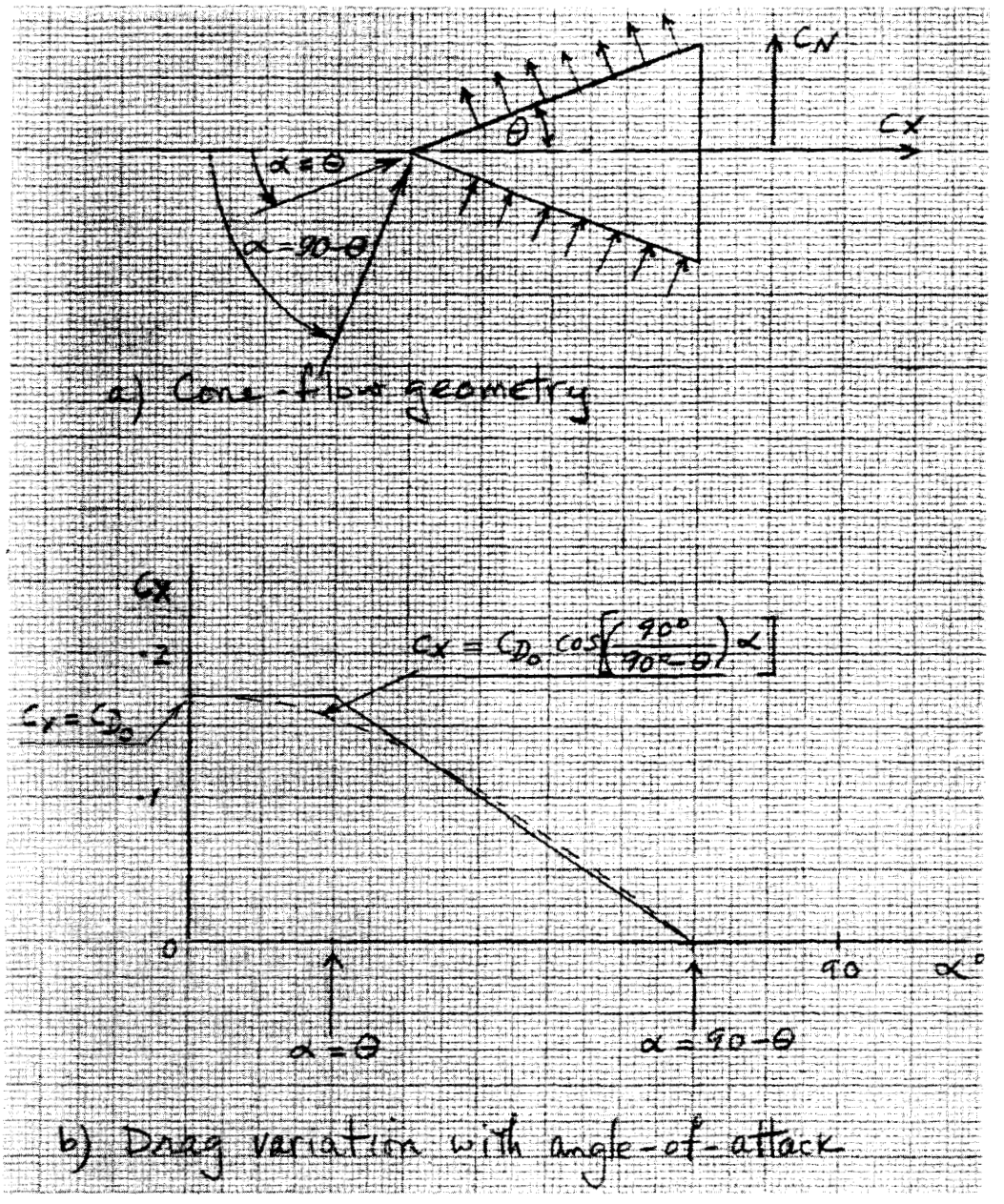

Fig. A1. Geometry and Drag for a Cone in Subsonic Flow

THE FINAL REPORT of The Martin Company's Apollo design feasibility study comprises the following publications:

System and Operation	ER 12001
Support	ER 12002
Trajectory Analysis	ER 12003
Configuration	ER 12004
Aerodynamics	ER 12017
Mechanical Systems	ER 12005
Aerodynamic Heating	ER 12006
Guidance and Control	ER 12007
Life Sciences	ER 12008
Onboard Propulsion	ER 12009
Structures and Materials	ER 12010
Instrumentation and Communications	ER 12011
Space Environment Factors	ER 12018
Test Program	ER 12012
Fabrication and Quality Assurance	ER 12013
Program Management	ER 12014
Business Plan	ER 12015
Preliminary Specifications	ER 12016